MISCELLANEOUS PAPER GL-82-10

THE EFFECTS OF END PLATENS, METHOD OF LOADING, AND SPECIMEN SIZE IN MONOTONIC TRIAXIAL $\bar{R}$ TESTS

by

Herbert V. Johnson

Geotechnical Laboratory
U. S. Army Engineer Waterways Experiment Station
P. O. Box 631, Vicksburg, Miss. 39180

September 1982

Final Report

Prepared for Office, Chief of Engineers, U. S. Army
Washington, D. C. 20314

Under CWIS 31145

Unclassified

SECURITY CLASSIFICATION OF THIS PAGE *(When Data Entered)*

REPORT DOCUMENTATION PAGE

READ INSTRUCTIONS BEFORE COMPLETING FORM

1. REPORT NUMBER: Miscellaneous Paper GL-82-10

2. GOVT ACCESSION NO.:

3. RECIPIENT'S CATALOG NUMBER:

4. TITLE *(and Subtitle)*: The Effect of End Platens, Method of Loading, and Specimen Size in Monotonic Triaxial $\bar{R}$ Tests

5. TYPE OF REPORT & PERIOD COVERED: Final report

6. PERFORMING ORG. REPORT NUMBER:

7. AUTHOR*(s)*: Herbert V. Johnson

8. CONTRACT OR GRANT NUMBER*(s)*:

9. PERFORMING ORGANIZATION NAME AND ADDRESS:
U. S. Army Engineer Waterways Experiment Station
Geotechnical Laboratory
P. O. Box 631, Vicksburg, Miss. 39180

10. PROGRAM ELEMENT, PROJECT, TASK AREA & WORK UNIT NUMBERS: CWIS 31145

11. CONTROLLING OFFICE NAME AND ADDRESS:
Office, Chief of Engineers, U. S. Army
Washington, D. C. 20314

12. REPORT DATE: September 1982

13. NUMBER OF PAGES: 122

14. MONITORING AGENCY NAME & ADDRESS*(if different from Controlling Office)*:

15. SECURITY CLASS. *(of this report)*: Unclassified

15a. DECLASSIFICATION/DOWNGRADING SCHEDULE:

16. DISTRIBUTION STATEMENT *(of this Report)*:
Approved for public release; distribution unlimited.

17. DISTRIBUTION STATEMENT *(of the abstract entered in Block 20, if different from Report)*:

18. SUPPLEMENTARY NOTES:
Available from National Technical Information Service, 5285 Port Royal Road, Springfield, Va. 22151.

19. KEY WORDS *(Continue on reverse side if necessary and identify by block number)*:

Dams
End platens
Foundations
Liquefaction (soil)
Method of loading
Monotonic $\bar{R}$ tests
Pore pressure
Rate of loading
Sands
Specimen size

20. ABSTRACT *(Continue on reverse side if necessary and identify by block number)*:

The purpose of this research was to investigate the effect of changing certain test parameters associated with establishment of the critical void ratio using the monotonic triaxial $\bar{R}$ test. The parameters investigated include the effect of specimen size, method of loading (ramp or step function), and end platens. The parameters which are usually held constant in the routine performance of critical void ratio determinations were investigated to determine their effect on the critical void ratio curve ($\bar{e}_f$ curve) which is
(Continued)

DD FORM 1 JAN 73 1473 EDITION OF 1 NOV 65 IS OBSOLETE

Unclassified

SECURITY CLASSIFICATION OF THIS PAGE *(When Data Entered)*

20. ABSTRACT (Continued).

used to predict the liquefaction potential of a cohesionless material.

The principal material used in this investigation was an Ottawa sand (Banding sand). A reference $\bar{e}_f$ curve was developed and compared to the previous established $\bar{e}_f$ curve using Banding sand as determined by Castro. Test procedures and triaxial equipment were calibrated against Castro's established curve. The parameters mentioned above were individually varied in the test program to determine what effect they had on the $\bar{e}_f$ curve. The effect was determined by the relative vertical movement of the curve.

The test program consisted of five test series. Two series were tested using lubricated end platens of the type described by Rowe. Other series were conducted using conventional ends platens. Specimen sizes were 1.4 inches in diameter or 2.8 inches in diameter. Load was applied axially either by a pneumatic system or by dead weights in the form of step or ramp loadings. All series were isotropically consolidated.

The critical void ratio relationships resulting from the five test series were compared to the reference $\bar{e}_f$ curve. It was concluded based on insignificant movement of critical void ratio curves that end platens, specimen size, and method of loading do not influence the critical void ratio determination.

PREFACE

The investigation reported herein was conducted by the U. S. Army Engineer Waterways Experiment Station (WES) for the Office, Chief of Engineers, U. S. Army, under CWIS project 31145, "Liquefaction Potential of Dams and Foundations."

Mr. Herbert V. Johnson, Soil Mechanics Division (SMD), Geotechnical Laboratory (GL), WES, conducted the research under the general supervision of Mr. Leroy C. McAnear, Chief, SMD, and Dr. William F. Marcuson III, Chief, GL.

COL Nelson P. Conover, CE, and COL Tilford C. Creel, CE, were Commanders and Directors of WES during the conduct of this research and preparation of this report. The Technical Director was Mr. Fred R. Brown.

CONTENTS

CONVERSION FACTORS, U. S. CUSTOMARY TO METRIC (SI)
UNITS OF MEASUREMENT

U. S. customary units of measurement used in this report may be converted to metric (SI) units as follows:

Multiply	By	To Obtain
cubic feet	0.02831685	cubic metres
inches	2.54	centimetres
pounds (force)	4.448222	newtons
pounds (force) per square inch	6894.757	pascals
square inches	6.4516	square centimetres

THE EFFECTS OF END PLATENS, METHOD OF LOADING, AND SPECIMEN SIZE IN MONOTONIC TRIAXIAL $\bar{R}$ TESTS

PART I: INTRODUCTION

Background

1. Many structural failures are due to a phenomenon known as liquefaction.* In 1964 earthquake-induced ground vibration caused numerous foundation failures via liquefaction in Niigata, Japan. In the province of Zeeland in Holland, on the shores of the straits between numerous islands of that province, a large number of flow slides have occurred which, in many cases, have breached dikes and caused inundation of lowlands. Further, numerous flow slides, induced by monotonically (steadily) changing stresses, have occurred along the Mississippi River.

2. Liquefaction takes place when a soil experiences a tremendous reduction in shear strength due to an increase in pore fluid pressure. This has been qualitatively understood for a number of years, but recently new advances have been presented to evaluate quantitatively the potential for a mass of cohesionless soil to experience this phenomenon. One such advance--a concept presented by Castro (1969) and Casagrande (1979) to evaluate liquefaction potential--is based upon establishing the critical void ratio.

3. The critical void ratio is understood to be that void ratio at which a saturated cohesionless soil can undergo deformation or actual flow, under static monotonic loading without volume change. In general, critical void ratio is expressed as a function of effective confining pressure. That is, as effective confining pressure increases, the critical void ratio decreases. For void ratios less than the critical value, at a given confining pressure, the cohesionless material will

---

* Definitions are given for selected soils terms and symbols are listed and defined in Appendix D, "Notations and Definitions."

tend to dilate, while for void ratios greater than the critical value, contraction and liquefaction can occur.

4. The critical void ratio is determined in the laboratory from the stress-controlled monotonically loaded triaxial $\bar{R}$ test.

Purpose

5. The goal of this research was to investigate the effect of changing some of the test parameters associated with establishment of the critical void ratio using the monotonic triaxial $\bar{R}$ test. The parameters investigated included the effects of specimen size, method of loading (ramp function or step function), and end platens. The parameters which are usually held constant in the routine performance of critical void ratio determinations were investigated to determine their effect on the critical void ratio curve ($\bar{e}_f$ curve) which is used to predict the liquefaction potential of a cohesionless material.

Scope

6. The scope of this investigation included reproducing in the laboratory the known $\bar{e}_f$ curve for Ottawa sand (Banding Sand) as previously established by Castro (1969). Test procedure and triaxial equipment were calibrated as closely as possible, against Castro's test procedure and triaxial equipment. (The material test procedure and triaxial equipment used by Castro are given in Appendix A.) The factors mentioned above were individually varied in the test program to determine what effect they had on the critical void ratio curve as compared to the known (reference) curve.

PART II: REVIEW OF PREVIOUS AND RELATED WORK

End Platens

7. If the engineering behavior of a material is to be determined in the laboratory, it is essential to know all three principal stresses and their directions and all three principal strains and their directions in the laboratory soil test program. No test currently in use fully satisfies these requirements, partly because of the relationship between stress, strain, and volume change inherent in soil as an engineering material, and partly because of the mechanical problems posed even by apparently simple boundary conditions (U. S. Army Engineer Waterways Experiment Station 1970).

8. The most widely used stress-strain test in the field of soil mechanics is the cylindrical compression test. The mechanical simplicity of applying loads and axially measuring deformation and the ease in forming the specimen (or trimming a so-called cylindrical undisturbed sample taken from the ground) make the triaxial compression test the most convenient test; however, both from the engineering and the scientific point of view the test has certain limitations.

9. A major limitation of the triaxial test is that the stresses and strains are not uniform throughout the soil specimen. This limitation results partially from nonuniform density distribution of the material (i.e., heterogeneity). However, the limitation is primarily due to the boundary conditions which are represented by end platens and a rubber membrane surrounding the specimen. The use of rigid (regular) end platens (on which shear stresses as well as normal stresses can develop) is considered the principle in this case.

10. At the specimen ends, it is postulated that stress concentration is due to the Poisson effect (U. S. Army Engineer Waterways Experiment Station 1976a). That is, as a material is axially compressed it also tends to expand laterally. If lateral strain is prevented or even partially restricted at the ends by friction between the specimen and end platen, stress concentrations will result and an additional unknown

nonuniform shear stress distribution will be active at the ends of the specimen. Several attempts have been made to solve this problem either theoretically or experimentally.

11. Perhaps the first to undertake a theoretical study of the problem was Filon (1902). He analytically evaluated stress distribution in compression test cylinders using series functions. His work was based on an assumption that implied that no radial movement of boundary points on the restrained surface would occur. Balla (1960) presented analytical results based on the assumption that platen roughness is a function of coefficient of friction between the end platen and specimen. Additional analytical work was done by Pickett (1944) and D'Appolonia and Newmark (1951).

12. Experimental work by Taylor (1941) on the development of the triaxial test for soil found that if a sample had a length-to-diameter ratio in the range of 1.5 to 3.0, the effect of end friction on strength was negligible. On the basis of this work, triaxial specimens have generally been standardized at a length-to-diameter ratio ranging from 2.0 to 2.5 and the effects of end restraint have been discounted (U. S. Army Engineer Waterways Experiment Station 1976a). Taylor's research was conducted using drained sand and undrained clay. His emphasis was primarily on evaluating strength as affected by end restraint.

13. Work done by Shockley and Ahlvin (1960) at the U. S. Army Engineer Waterways Experiment Station showed variations in sample density due to nonuniform volume change. That is, pore water migrates within a specimen as different strains induce different tendencies to volume change, resulting in redistribution of void ratio. Other investigators have indicated similar results (Ellis and Holtz 1959 and Bishop et al. 1960).

14. Thus, intertwined with the recognition of stress concentration at the platen/specimen interface and coupled with the expanded use for the triaxial test (not only for strength measurements but for stress-strain and pore pressure measurements) a new impetus was generated to develop a frictionless end platen.

15. As far as can be determined, Rowe and Barden (1964) were

among the first investigators to try low-friction platens. They used greased rubber membranes between the soil specimen and the end platens. Tests were conducted using Mersey River sand. Four-inch-diameter* by four-inch-high drained specimens were tested utilizing the low-friction ends. Comparative tests were made on 4-inch-diameter by 8-inch-high specimens with regular ends. The result of their investigation showed that low-friction end platens permitted high volumetric and axial strains at failure and yielded lower strength than those specimens tested with regular platens.

16. Raju, Sadasivan, and Venkataraman (1972) conducted comparative tests using lubricated and nonlubricated end platens. The tests were accomplished using drained sand and end platens of the type described by Rowe and Barden. Raju found that the use of lubricated ends resulted in uniform stress and deformation conditions in the specimens.

17. Other investigators have indicated similar conclusions (Duncan and Dunlop 1968, Lee and Seed 1964, Barden and McDermott 1965, and Roy and Lo 1971). Still others (Olson and Campbell 1964 and Bishop and Green 1965) conclude that the use of regular ends with a length-to-diameter ratio of 2.0 and lubricated ends with a length-to-diameter ratio of 1.0 results in about the same strength; however, the general consensus seems to be that using lubricated ends results in much more uniform distribution of stress, strain, and volume change.

18. Still Kirkpatrick, Seals and Newman (1974), using lubricated and nonlubricated ends, conducted further tests to evaluate stress distributions under drained conditions. Stress gages were used with the test program. The stress gages were placed between the specimen and platens and the normal stress distribution that resulted was analyzed. Their work indicated that the distribution of axial normal stress at the ends of a specimen varied depending on the restraint offered by the platens to lateral deformation. Lubrication allowed uniform distribution of normal stress with uniformity improving as the strain

---

* A table of factors for converting U. S. customary units of measurement to metric (SI) units is presented on page 3.

increased. For the nonlubricated specimens, significant nonuniformity occurred and became more severe as the strain increased.

19. A number of investigators have evaluated friction resistance, using "frictionless" ends, in terms of lubricant type, lubricant thickness, membrane thickness, grain size, and prolonged consolidation. Lee and Seed (1964) concluded that frictional resistance (sliding resistance) is a function of all these items. They stated that the smaller the grain size, the smaller the amount of friction that develops and that the greater the thickness of rubber membrane and lubricant (grease), the less friction that develops. Prolonged consolidation time results in higher friction at the end platens. For clays, consolidation may require several days and this effect may be significant. For sands, the time period is considerably shorter and the effect of consolidation time can be negligible. Among the popular lubricants, high vacuum silicone grease is most effective; i.e., under high consolidation pressure regular silicone grease tends to squeeze out.

Method of Loading

20. The literature review indicates that only two methods of stress-controlled monotonic $\bar{R}$ loading have been studied. They are load applied in incremental steps (step function) and continuously applied load (ramp function).

21. Torrey (1981) evaluated the effect of method of loading in monotonic $\bar{R}$ testing. Torrey concluded from his testing that method of loading, as shown by comparative positioning of the $\bar{e}_f$ curves (Figure 1), does affect the critical void ratio determination. He reasoned that incremental loading of specimens as opposed to continuous loading allowed the specimen to readjust during the 1-minute loading intervals. He further reasoned that small additional strains developed during the adjustment period and this allowed the sand particles to be pushed to a "fine edge" before structural failure. When failure did occur, he thought perhaps the flow structure as hypothesized by Casagrande had been reached, thus developing a higher pore pressure

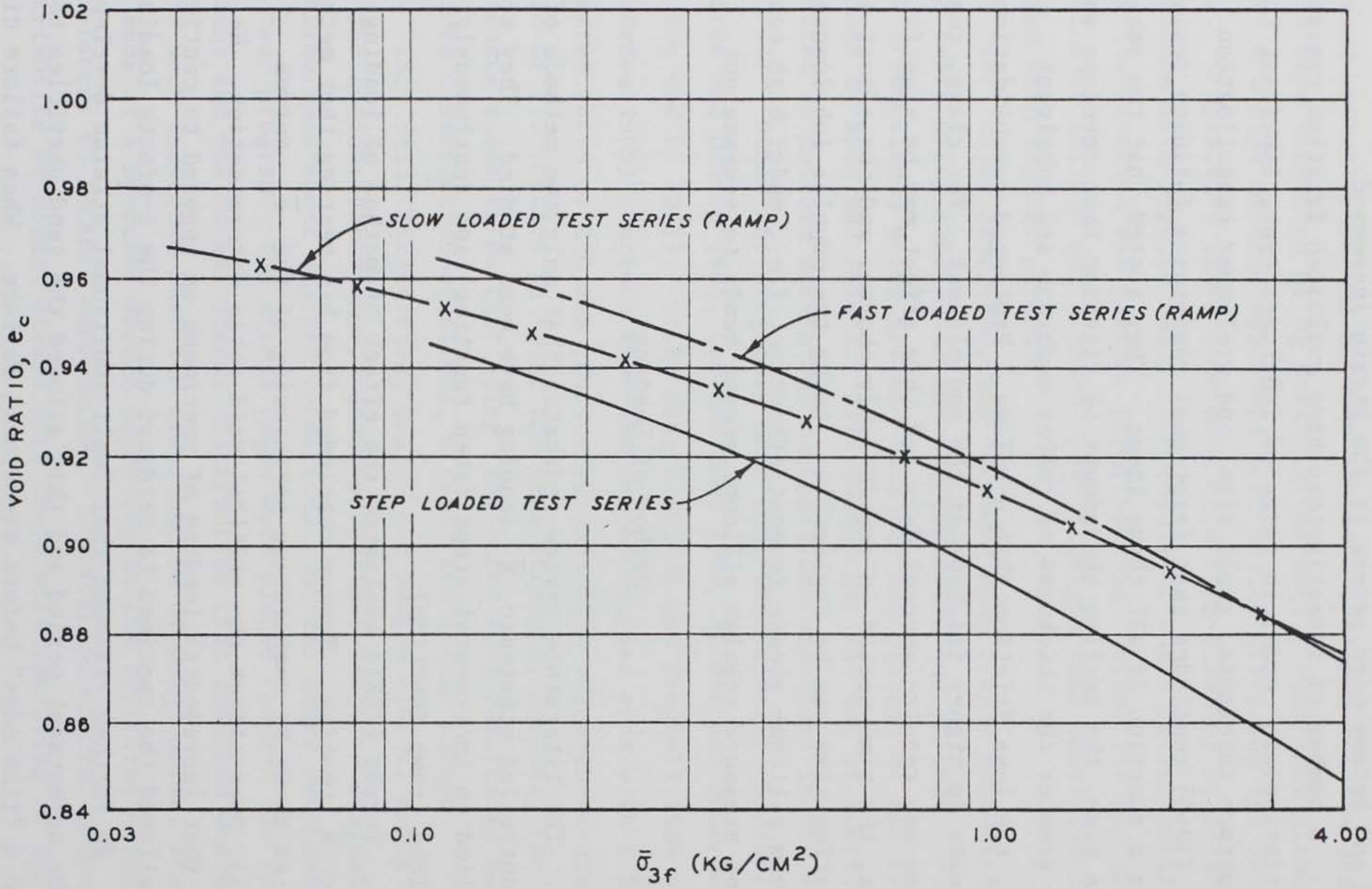

Figure 1. Development of critical void ratio curve showing influence of method of loading as determined by Torrey (after Torrey 1981)

response and a lower positioned $\bar{e}_f$ curve. He further stated that, with continuous ramp loading, adequate development of a flow structure may be impeded by increased nonuniformity of stresses and strains within a specimen.

22. Three series of tests were conducted by Torrey. Evaluation of effects were based on the relative positioning of the critical void ratio curve. The critical void ratio curve, $\bar{e}_f$, developed from the incrementally loaded series served as the standard to which others were compared. The two ramp function series consisted of loads being applied at very fast (2016 lb/min) and at very slow (0.025 lb/min) rates. The standard series consisted of several load increments to peak deviator stress applied at 1-minute intervals. A pneumatic loading system with volume booster supply was used. All series were anisotropically consolidated (K_c = 0.5). Test specimens were reconstituted to low density, using Carrollton Bend sand (a Mississippi River point bar sand). Size of specimens were 1.4-inch diameter by 3.5-inch height. Relative density after consolidation ranged from 15 percent to about 48 percent. Carrollton Bend sand is fine, uniform, and tends to be angular. Its D_{10} is 0.077 mm. Initial effective confining pressures ranged from 0.5 to 4.7 kg/cm^2.

Specimen Size

23. Intuitively one would think that specimen discontinuities, density variations, grain size segregation in placement, and boundary condition effects would be factors that would influence the effects of specimen size. Certainly building a specimen by any present-day reconstitution procedure leaves something to be desired. It seems reasonable that density and gradation variations do occur in the specimens and that the larger the specimen, the greater the probability these nonuniformities will exist. But it also seems reasonable that boundary effects would be more severe for smaller specimens.

24. Limited work has been conducted to determine the effect of specimen size on the liquefaction susceptibility of a specimen. Durham

and Townsend (1973) are the only known investigators to evaluate specimen size effect under monotonic loaded $\bar{R}$ tests. Several investigators, including Wang (1972) and Vernese and Lee (U. S. Army Engineer Waterways Experiment Station 1977), have studied the effect of specimen size under cyclic loading.

25. Durham and Townsend conducted triaxial tests on 1.4- and 2.8-inch-diameter specimens of Reid Bedford sand. The specimens were anisotropically consolidated and controlled-stress loaded. As shown by Figure 2, results of their work indicate that specimen size has a negligible influence on liquefaction susceptibility. The sections in Figure 2 delineate the responses of a liquefiable material.

26. Under cyclic loading, Wang, and Vernese and Lee also tested 1.4- and 2.8-inch-diameter specimens. The specimens had relative densities of about 55 to 60 percent and were tested at an initial effective confining pressure of about 1.0 kg/cm^2. Wang found (Figure 3) that if failure occurred in 10 cycles of loading or less, both sizes exhibited the same liquefaction resistance. If failure occurred in 100 cycles or more, 1.4-inch-diameter specimens were 5 to 10 percent stronger than 2.8-inch-diameter specimens. On the other hand Vernese and Lee concluded that specimen size has no effect on liquefaction resistance at any cycle. Results of their work are shown in Figure 4.

27. In summary, the literature seems to indicate that specimen size has no effect on liquefaction susceptibility. For cyclically loaded specimens, inconsistencies exist; however, results reported by Wang showed 1.4-inch-diameter specimens only slightly stronger than 2.8-inch-diameter specimens. Considering all the other factors involved in evaluating liquefaction potential, it is reasonable to assume the slight effect of specimen size which they observed to be negligible.

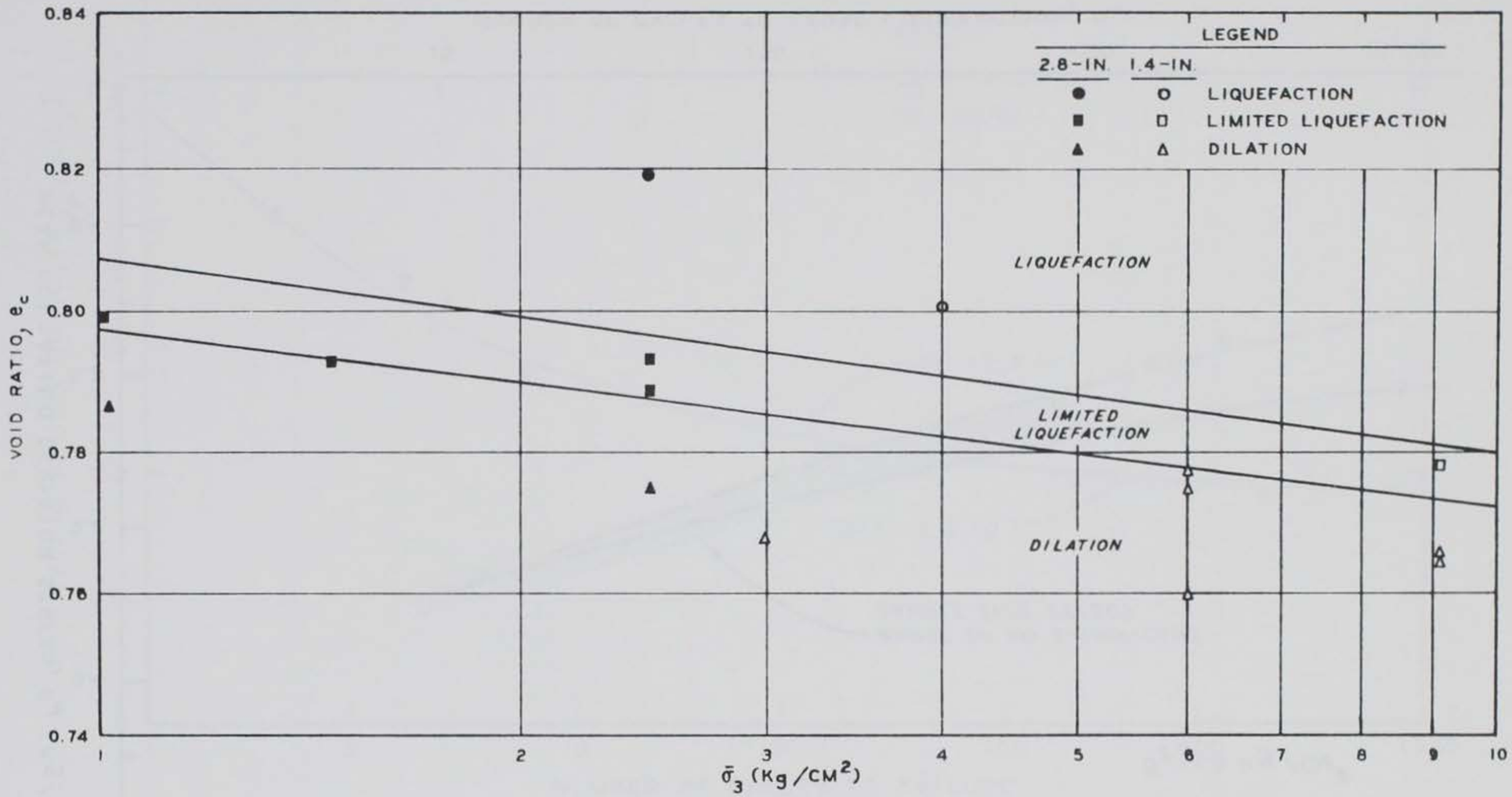

Figure 2. Effect of specimen size on liquefaction response under monotonic load (after Durham and Townsend 1973)

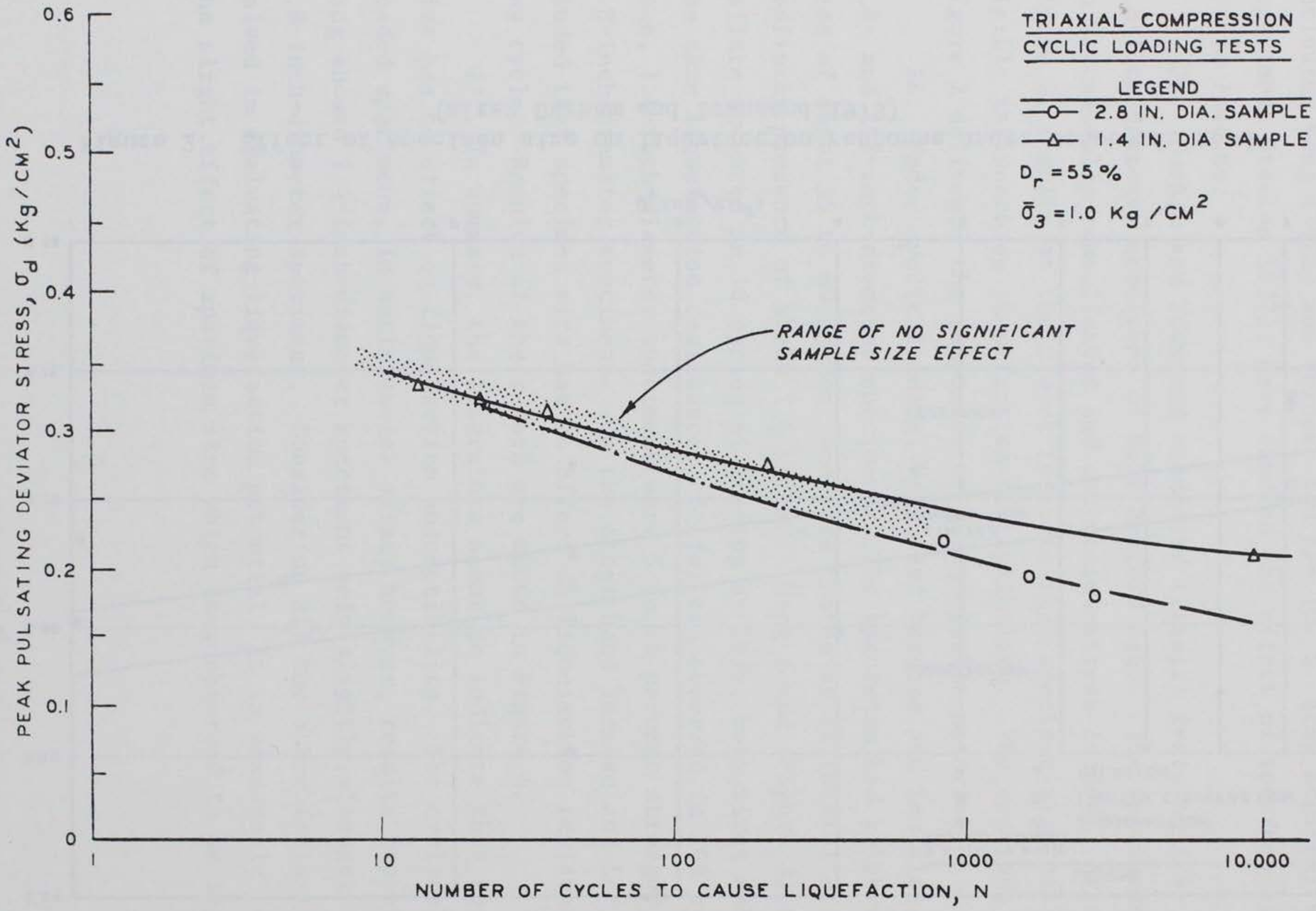

Figure 3. Comparison of cyclic liquefaction response on 1.4- and 2.8-inch-diameter specimens (after Wang 1972)

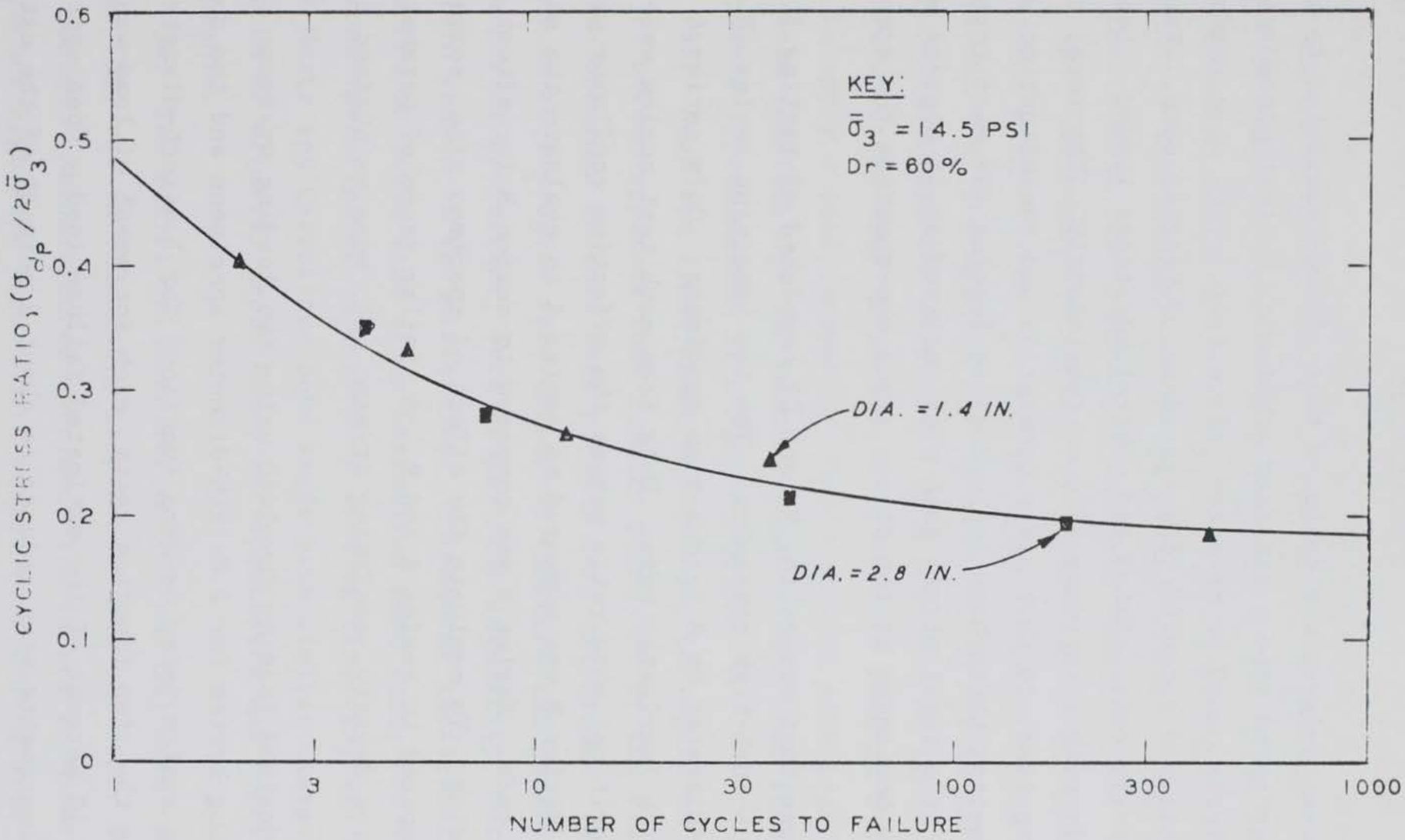

Figure 4. Comparison of cyclic liquefaction response of 1.4- and 2.8-inch-diameter specimens (after U. S. Army Engineer Waterways Experiment Station 1977)

PART III: TEST PROGRAM AND PROCEDURE

Test Program

28. A test program was designed that allowed variables to be individually incorporated into a standard monotonic $\bar{R}$ test procedure so that their effects could be measured. Five test series were conducted. Each series utilized reconstituted specimens of Banding sand. Specimens were isotropically consolidated and controlled-stress loaded. Load was applied axially either incrementally or continuously. The total confining pressure equal to that after saturation and consolidation was maintained constant throughout the undrained loading for each test. This resulted in a total stress path plot inclined at 45 degrees with a positive slope beginning at the stress state representing the consolidation phase.

29. Three test series (A, B, and D) consisted of testing 1.4-inch-diameter by 3.5-inch-high specimens. The two remaining series (H and I) used 2.8-inch-diameter by 6.5-inch-high specimens. Only series A and I were tested with lubricated ends. Data from each test series were used to produce a critical void ratio versus the effective confining pressure curves. Series B was compared to series A to evaluate the effect of lubricated ends. Series D was compared to series B for effect of method of loading. To evaluate the effect of specimen size, series H and I were compared to series A and B. A similar range of parameters such as relative density, confining stress, etc. were maintained for all series.

30. Undrained loading involved using two loading systems: the peumatic loading system for 2.8-inch-diameter specimens and the dead-weight loading system (step or ramp function) for 1.4-inch-diameter specimens. In the step function tests, each increment of load was approximately 10 percent of the estimated failure load. Upon approaching failure, increments were reduced to about 2 percent of the estimated failure load. Spacing of increments was usually at 1-minute intervals.

31. Continuous applied load was used to achieve a ramp rate.

Water was used as the loading medium. The ramp loading rates were approximately equivalent to the corresponding incrementally loaded series. Rates ranged from 0.075 lb/sec (0.0012 ft^3/sec) to 0.031 lb/sec (0.0005 ft^3/sec). One loading rate per specimen was used. Load reduction upon approaching failure was not made. It was decided that the procedure of neglecting small incremental loads in trying to match times to failure was an adequate approximation since, even combined, the small loads were less than one large incremental load. A typical step and ramp load versus time graphic is shown in Figure 5.

32. The pneumatic system, is considered to be an incremental loading system but, in fact, is a quasi-ramp function. Upon examination, it is evident that the load is not applied over a finite time (as with incremental loading) but is applied over a period of time. The degree of influence of the ramp is unknown. It usually took an average of 5 seconds to apply a load increment. However since each load increment was then held constant for the next 55 seconds, the load increment is a reasonable approximation of a step function.

33. Near the final phase of testing, in regard to method of loading, it became apparent that results presented by the literature and results obtained in this test program were different. The testing techniques in this program were throughly examined and judged sound. Inherent material properties, such as particle angularity, were considered as possible causes of the difference. Subsequent additional testing was conducted on Montz sand since Carrollton Bend sand, the sand used by the previous investigator of method of loading (Torrey), was not available. Since Montz and Carrollton Bend sands have similar characteristics and are both of alluvial deposition, the substitute was considered acceptable.

34. Two additional test series (MD and MB) were conducted. One series (MB) was incrementally step loaded and the other series (MD) was ramp loaded. Reconstituted specimens 1.4 inches in diameter by 3.5 inches high were used. Both series were tested with nonlubricated ends. The specimens were undrained, isotropically consolidated, and

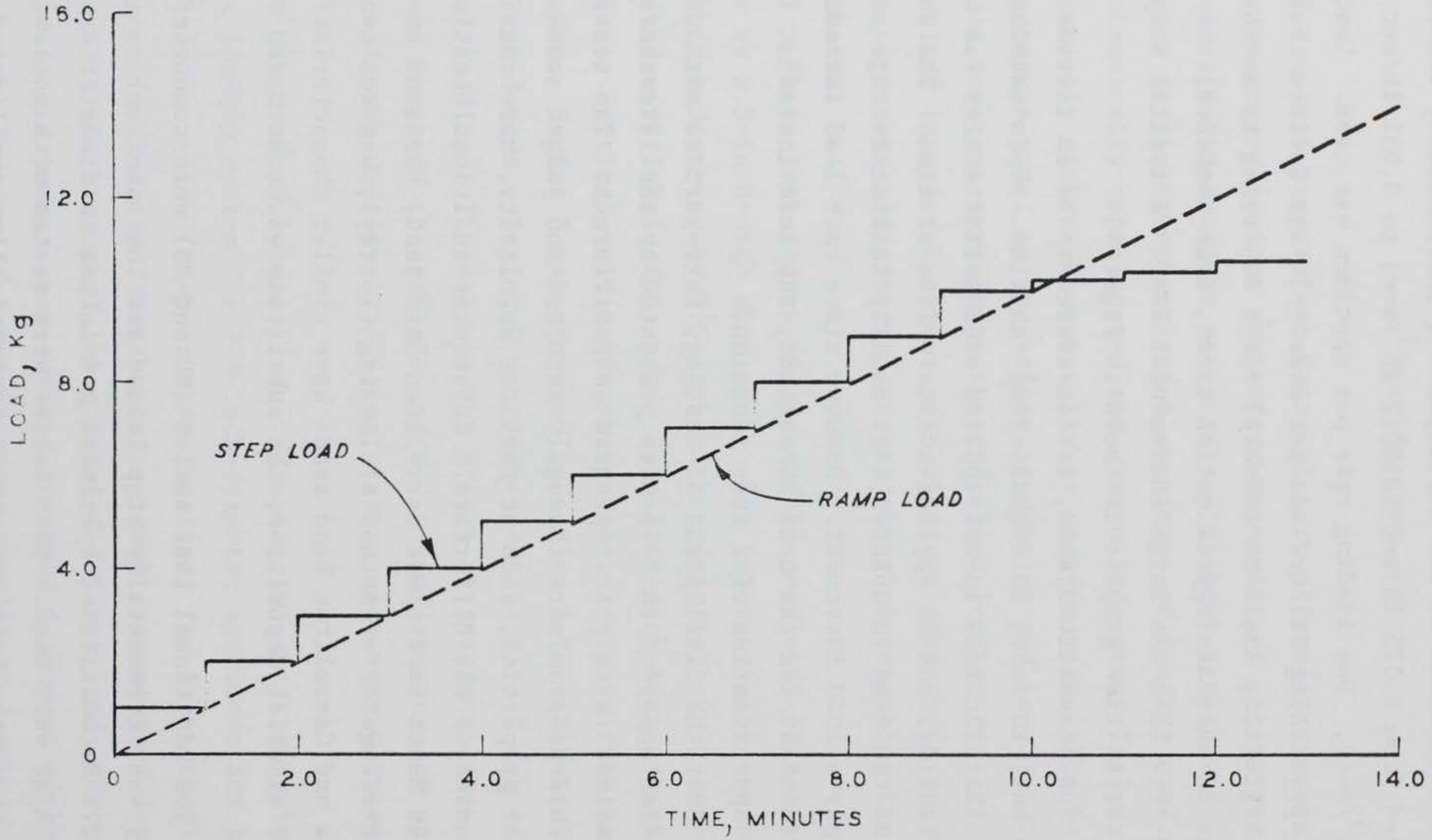

Figure 5. Illustration of step and ramp loading functions for 1.4-inch-diameter specimen

controlled-stress loaded. The overall test program including series MD and MB is shown in Table 1.

Materials

35. Banding Sand, an Ottawa sand, is a fine white uniform quartz sand manufactured from the St. Peter sandstone in Ottawa, Ill. The material has subrounded to subangular grains and its specific gravity is 2.65. The microphotographs in Figure 6 indicate that the degree of angularity increases somewhat with decreasing particle size.

36. For the Banding Sand used in this test program the D_{10} size is 0.12 mm. The coefficients of uniformity and curvature are 1.58 and 1.08, respectively. A gradation curve of the sand is shown in Figure 7. The maximum and minimum void ratios as determined by Castro (1969) are 0.84 and 0.50, respectively. It is noted that these values of maximum and minimum void ratios do not necessarily represent the maximum and minimum void ratios at which the material can exist in nature, but instead reflect the laboratory procedure used; therefore, Castro's values are acceptable.

37. Microphotographs of the Montz sand are shown in Figure 8. The material, although more angular than Banding Sand, also has a specific gravity of 2.65. The coefficients of uniformity and curvature are 1.73 and 1.36, respectively. The D_{10} size is 0.09 mm. A gradation curve is shown in Figure 9. The maximum and minimum void ratios were determined by a procedure outlined in a Waterways Experiment Station Potamology Investigation (U. S. Army Engineer Waterways Experiment Station 1952). The determined void ratios were 0.95 and 0.61, respectively. Table 2 lists the index properties for both sands.

Test Procedure

Specimen preparation

38. Because loose sands are most susceptible to the phenomenon of liquefaction, all specimens were built in a loose state. Specimen

Table 1

Summary Matrix of Test Program

Test Series	Material	Specimen Size, in. Diam	Specimen Size, in. Height	Method of Loading	Loading System	End Platens
A	Banding Sand	1.4	3.5	Step	Deadweight	Lubricated (L)
B	Banding Sand	1.4	3.5	Step	Deadweight	Nonlubricated (NL)
D	Banding Sand	1.4	3.5	Ramp	Deadweight	Nonlubricated (NL)
H	Banding Sand	2.8	6.5	Step	Pneumatic	Nonlubricated (NL)
I	Banding Sand	2.8	6.5	Step	Pneumatic	Lubricated (L)
MB	Montz Sand	1.4	3.5	Step	Deadweight	Nonlubricated (NL)
MD	Montz Sand	1.4	3.5	Ramp	Deadweight	Nonlubricated (NL)

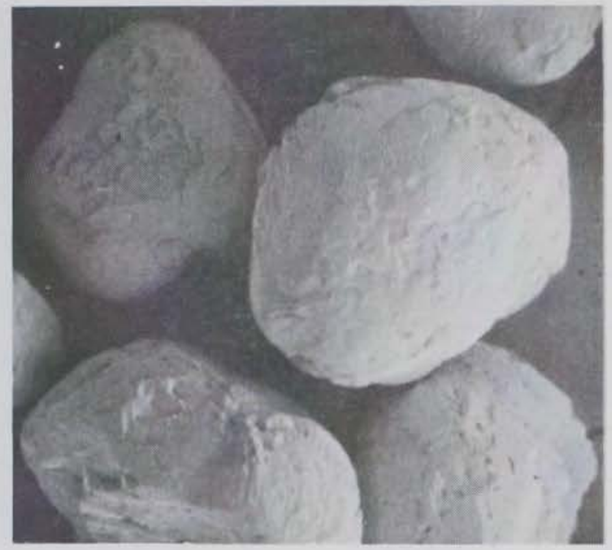

SIEVE SIZE 40-50
(40X)

SIEVE SIZE 50-70
(40X)

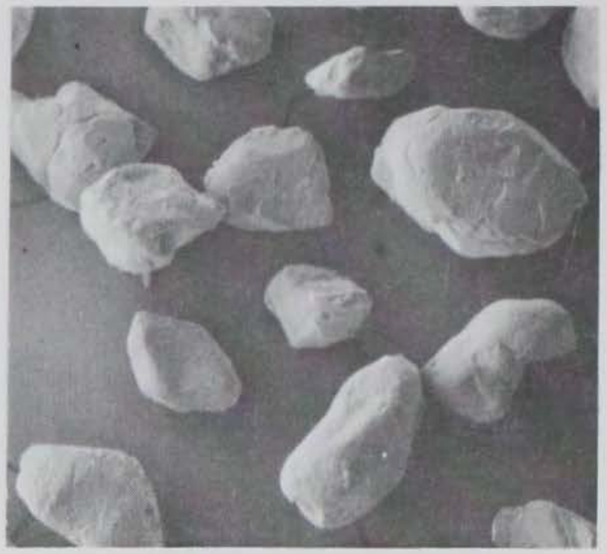

SIEVE SIZE 70-100
(40X)

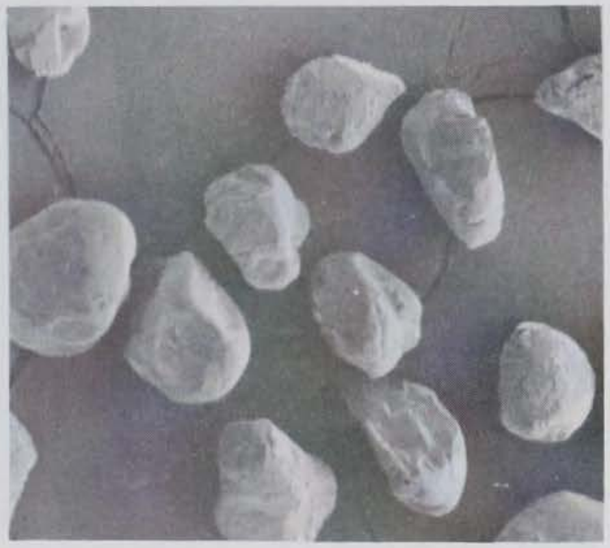

SIEVE SIZE 100-140
(40X)

SIEVE SIZE 140-200
(40X)

SIEVE SIZE, PAN
(40X)

Figure 6. Microphotographs, Banding Sand

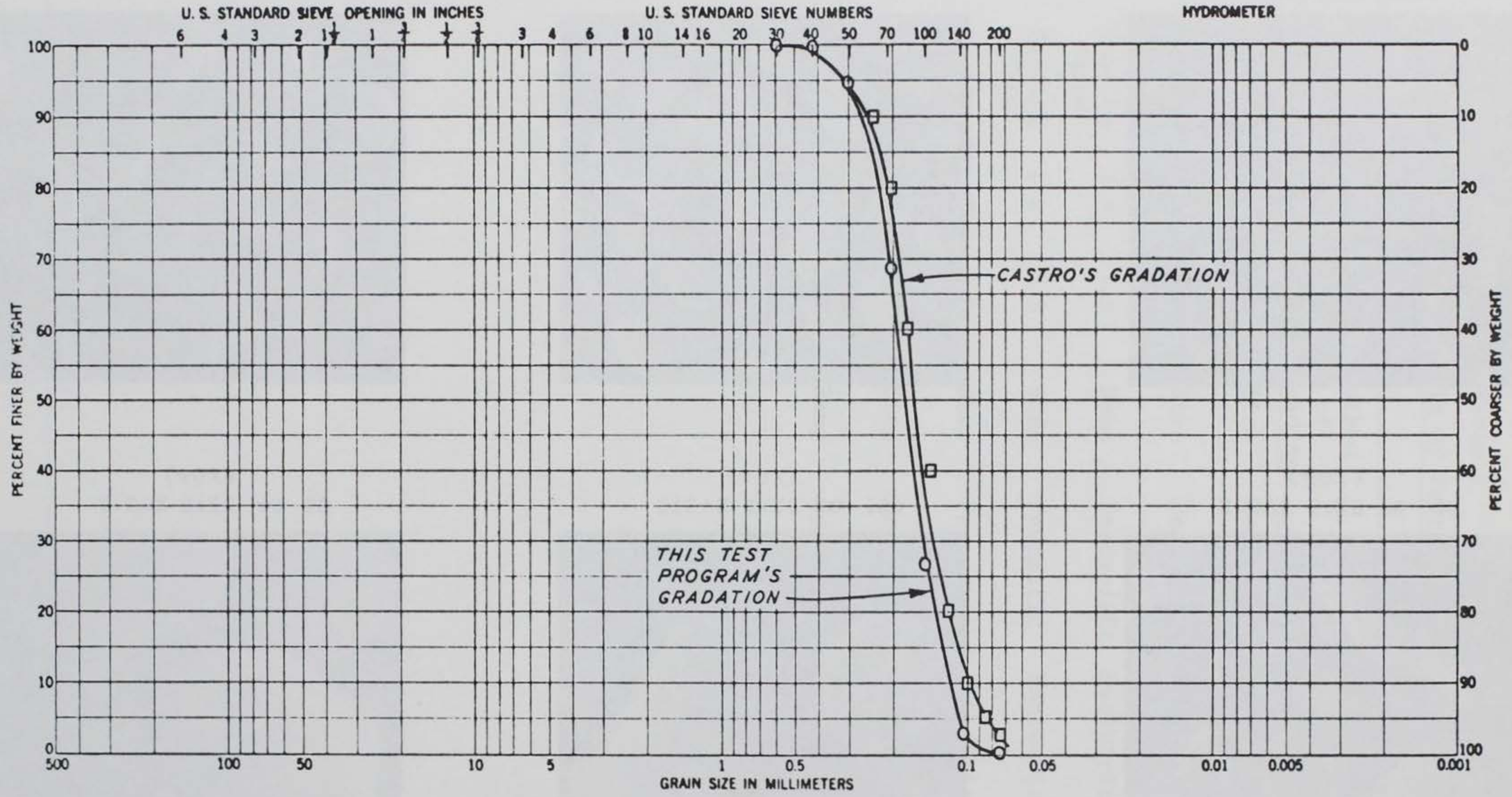

Figure 7. Comparison of gradation curves, Banding Sand, as used by G. Castro and by this investigator

SIEVE SIZE 50
(40X)

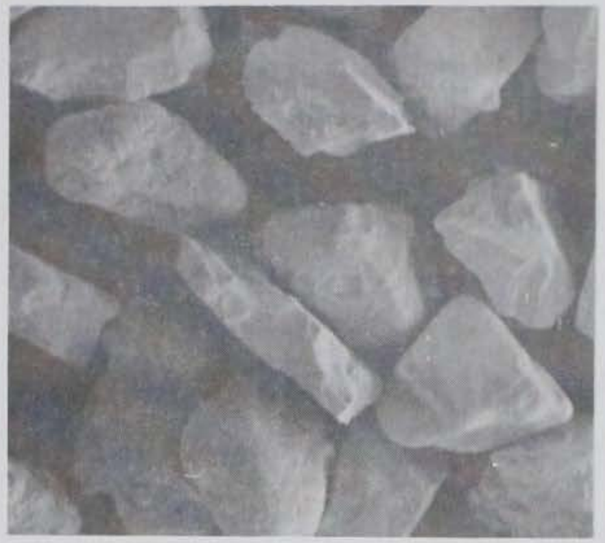

SIEVE SIZE 70
(40X)

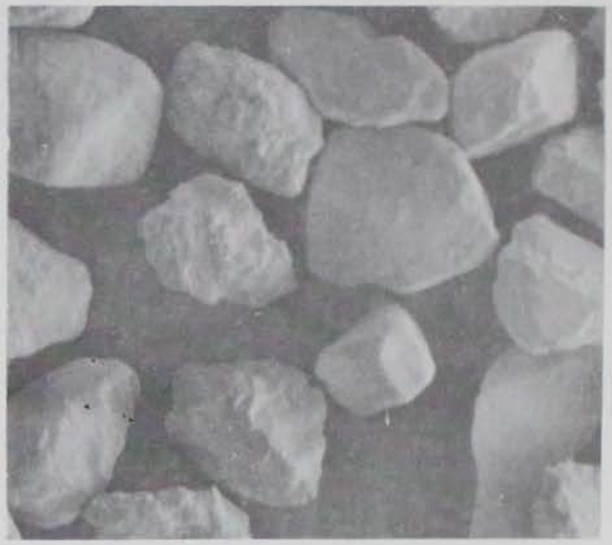

SIEVE SIZE 100
(40X)

SIEVE SIZE 140
(40X)

SIEVE SIZE 200
(40X)

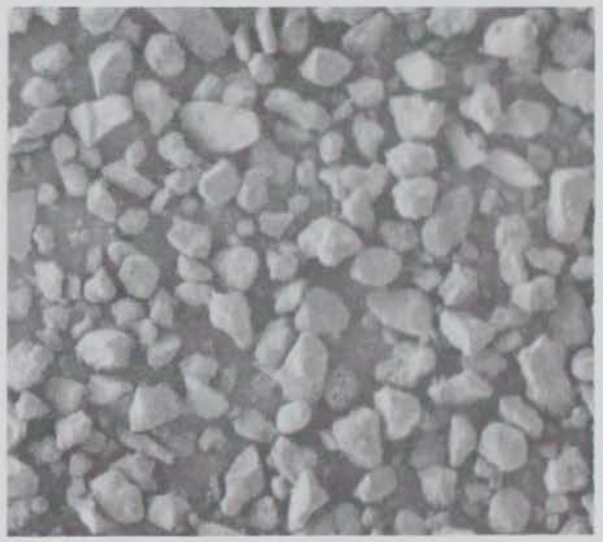

SIEVE SIZE, PAN
(40X)

Figure 8. Microphotographs, Montz sand

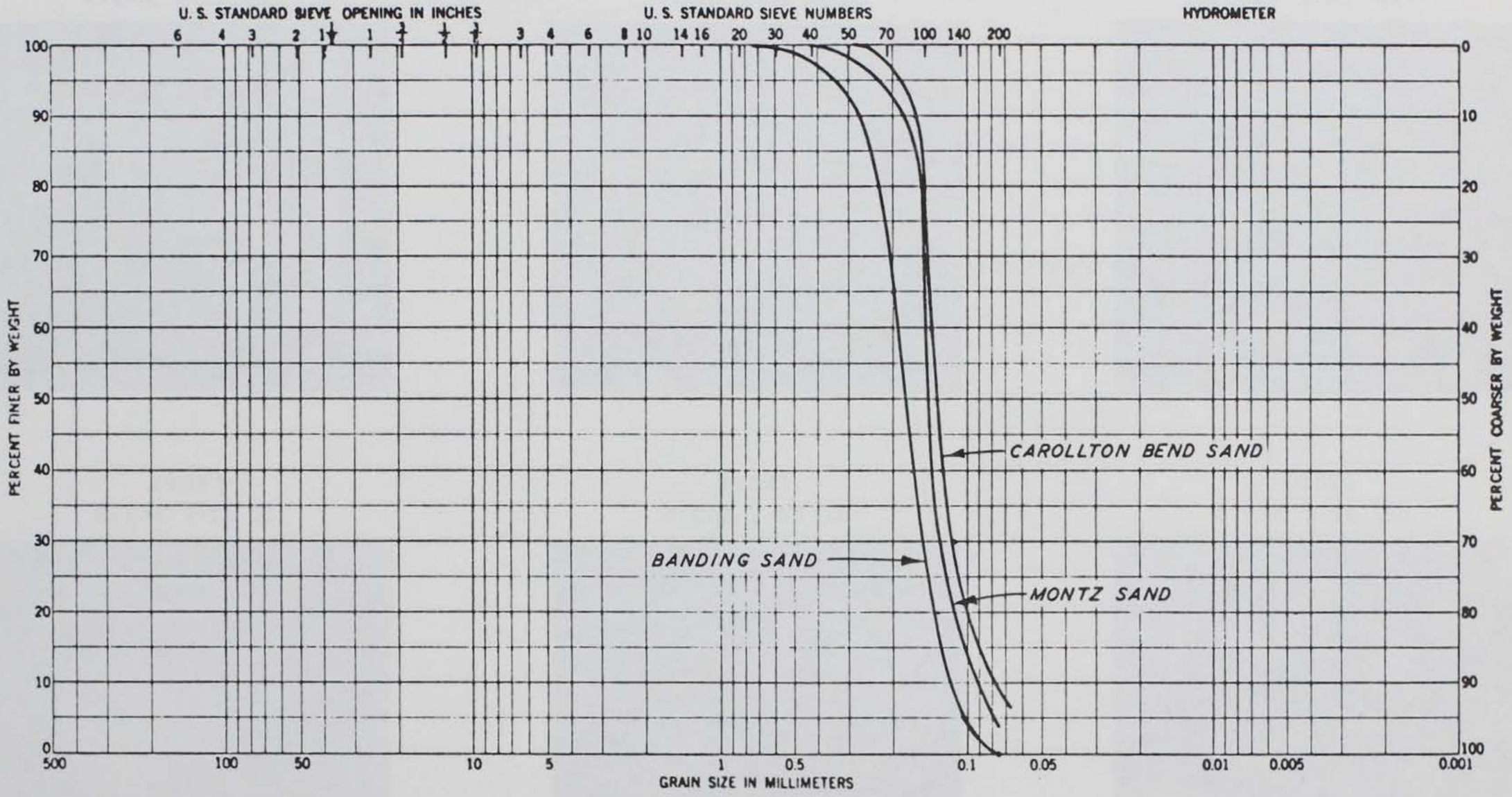

Figure 9. Gradation curve of Banding Sand, Montz sand, and Carrollton Bend sand depicting their relationship

Table 2

Index Properties of Materials

Properties	Banding Sand	Montz sand
Specific Gravity, G_s	2.65	2.65
Coefficient of Uniformity, C_u	1.58	1.73
Curvature Coefficient, C_c	1.08	1.36
D_{10}	0.12 mm	0.09 mm
e_{max}	0.84	0.95
e_{min}	0.50	0.61

target relative density ranged from 7 percent to 30 percent. In order to build specimens at the extremely loose state, small amounts of water were added to ovendried sand. The water added to the sand caused a bulking effect (i.e., apparent cohesion among the sand grains). Initially, 5 percent water was added, but this was later changed to 7 percent. The two percent increase in water content resulted in a marked increase in the ease of specimen handling. Ten percent water by weight was also tried but it was found that the additional water resulted in difficulty in de-airing the specimen. An initial molding water content of 7 percent was selected for the test program.

39. The molds used to reconstitute the test specimens are shown in Figures 10 and 11. The small specimen mold dimensions are approximately 3.5 inches high by 1.4 inches in inside diameter. Dimensions for the larger mold are 6.5 inches high by 2.8 inches in inside diameter. The inside diameter measurements of both molds take into account the thickness of a porous nonwoven fiberglass liner and the specimen membrane. The liner, which is the same height as the molds, is placed between the mold and specimen membrane to assure a uniform application of vacuum. Application of vacuum is necessary to snugly draw the membrane against the inside of the mold before reconstituting the specimen. The mold has a side port for connecting to a vacuum source. The weight and the size of the 2.8-inch-diameter mold allowed it to stand upright and in position during the reconstitution process. The 1.4-inch-diameter mold, because of its small size, was supported by a clamping system as shown in Figure 10.

40. A moist-tamping technique, developed by the Waterways Experiment Station and described by Mulilis, Chan, and Seed (1975), was used to make all reconstituted specimens. (Castro's technique differed somewhat; see Appendix A.) Specimens having a 1.4-inch diameter or 2.8-inch diameter were built in 5 and 6 layers, respectively. The reconstitution technique incorporated "under-compaction"; i.e., starting from the bottom layer, each layer was built one percent denser than the previous layer with the top layer at the target density. The rationale for this procedure is based on the assumption that the compactive effort applied

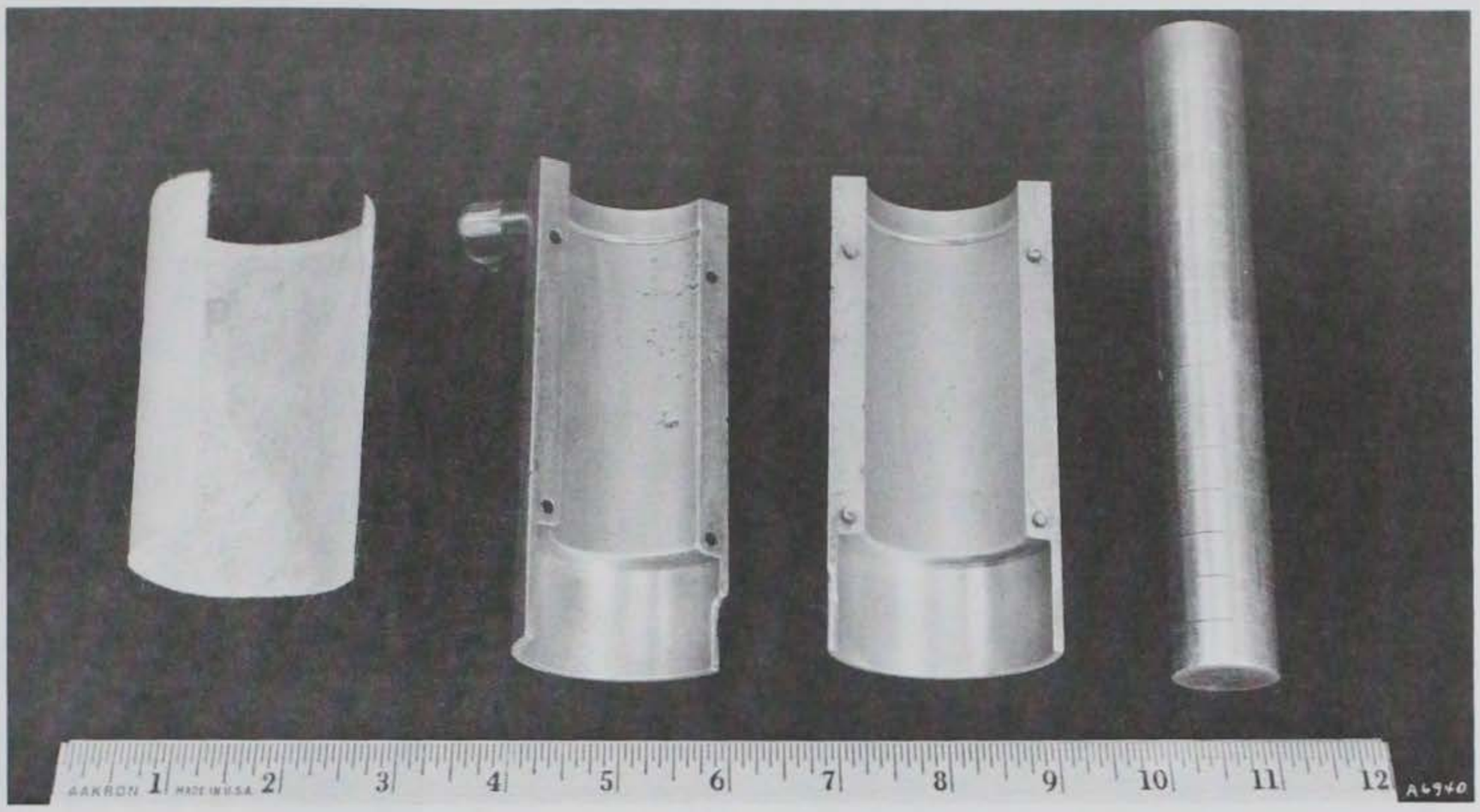

a. Specimen mold

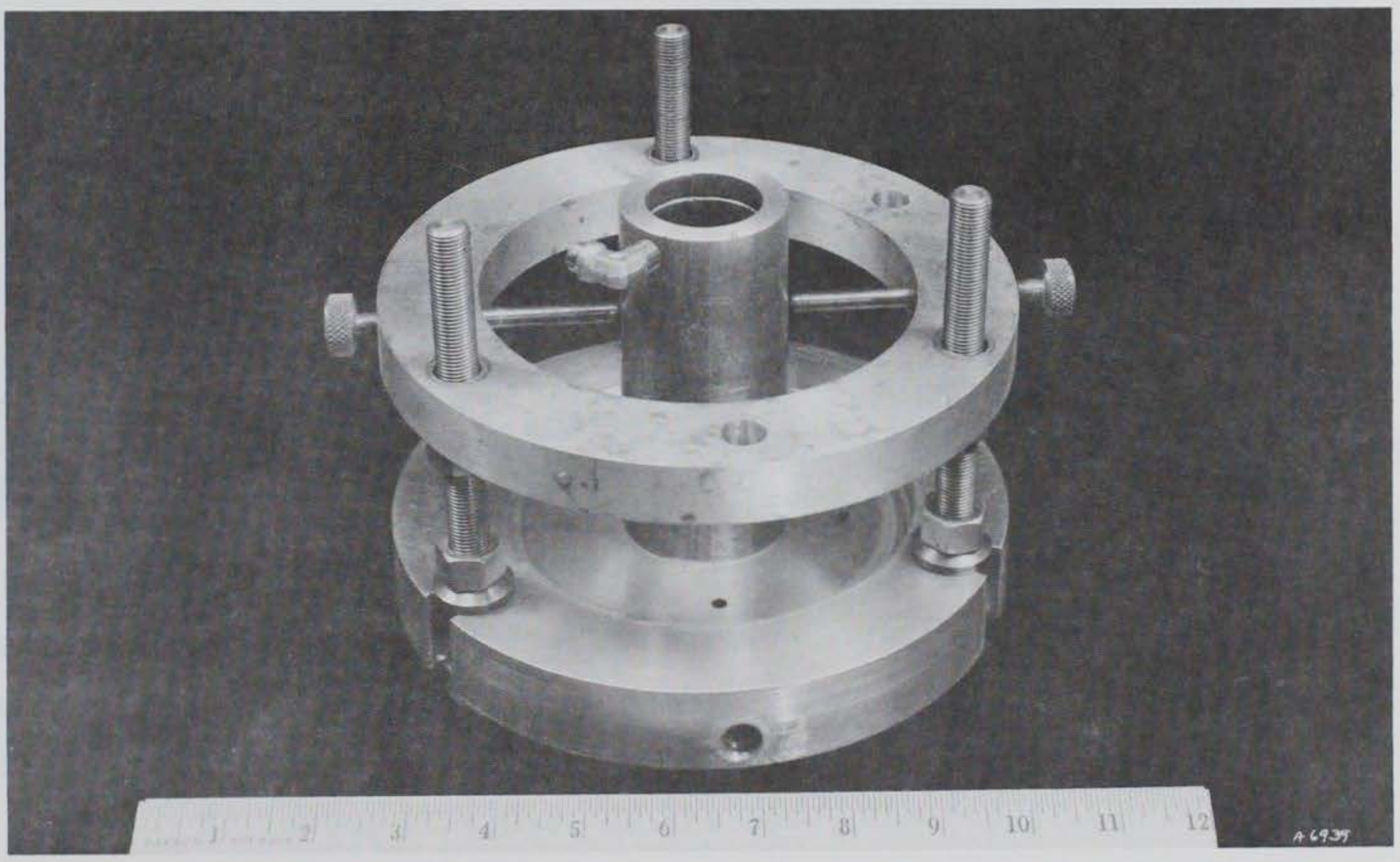

b. Clamping system

Figure 10. 1.4-inch-diameter specimen mold and clamping system

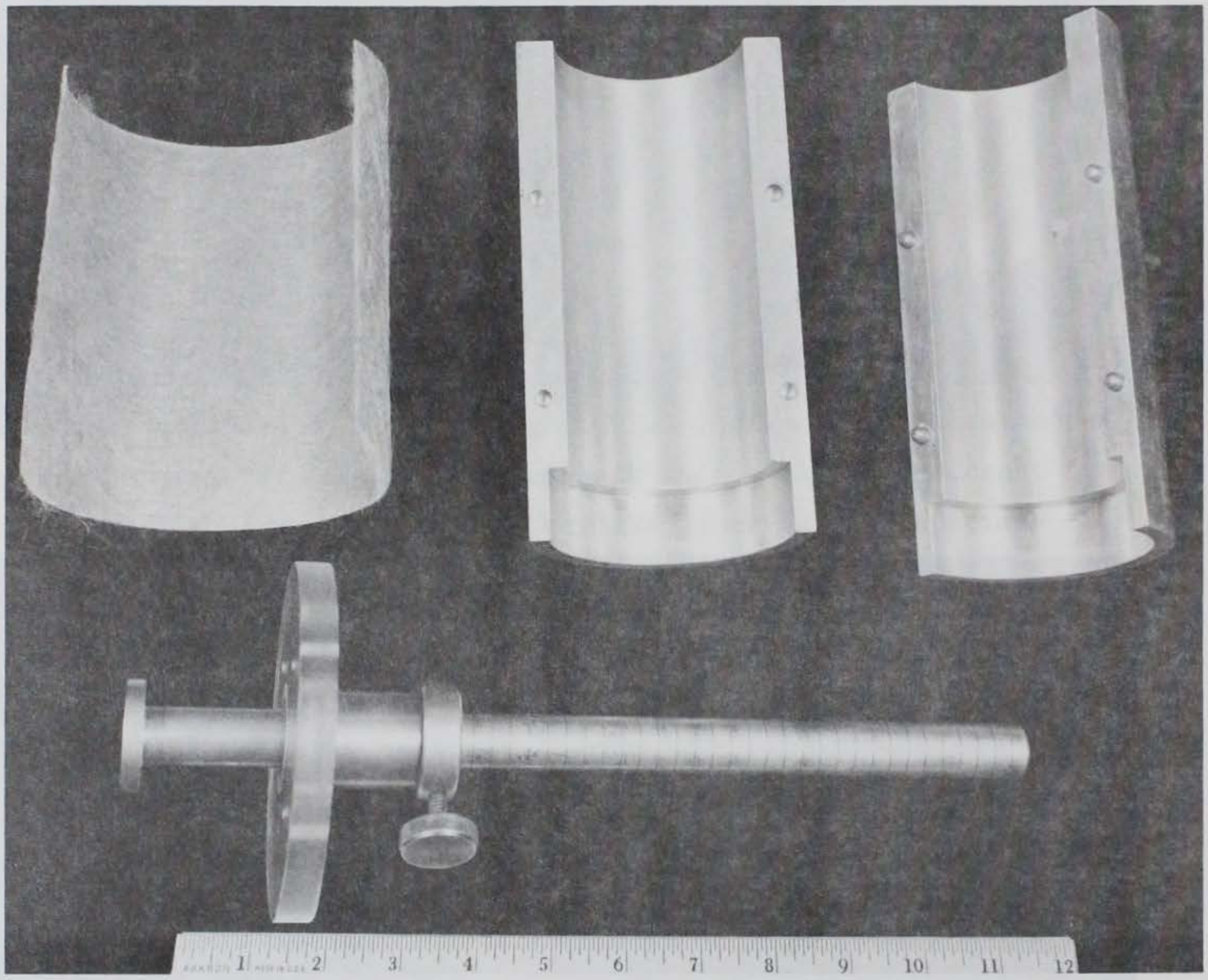

Figure 11. 2.8-inch-diameter specimen mold

to each succeeding layer also densifies the preceding layer. Reasonably uniform density distribution is believed to have been achieved. Good results with this procedure have been reported in the literature (Torrey 1981).

41. In preparing the specimen, the proper amount of sand to achieve the target density of a given layer was weighed to the nearest 0.01 g. Seven percent by weight of water was added. The sand and water was thoroughly mixed and allowed to cure for about 30 minutes in a closed container. Following the curing time, the sand was placed into the specimen mold in layers. Each layer of the 1.4-inch specimen was 0.7 inch high. Each layer of the 2.8-inch specimen was 1.083 inches. For 1.4-inch specimens, the compactive effort was accomplished by using a 6-inch, 1-inch-diameter blunt-ended aluminum rod (see Figure 10) and applying force in a light pressing fashion by hand. The rod was graduated for the 0.7-inch increment. This provided an easy check as to when enough compaction was accomplished and it also provided a check for layer levelness. Each layer was scarified before placement of the next layer to help ensure specimen continuity from layer to layer. Scarification within 1/16 inch of the membrane was avoided to prevent development of voids adjacent to the membrane at the layer contacts.

42. The 2.8-inch specimens were reconstituted in a similar fashion. However, a differently designed compaction apparatus, which ensured exact height placement of each layer, was used. The apparatus is shown in Figure 11. After a predetermined amount of sand was poured into the mold, the compaction hammer (adjusted to the right height) was placed into position over the mold. The hammer was gently raised and lowered firmly, thus providing compactive effort to the sand. The compactive effects could be observed through the clear plexiglass shoulder of the apparatus.

43. Following placement of the sand, the top platen was put in place and the membrane was pulled up and securely fastened with an O-ring. A 10-psi vacuum was applied to each specimen to provide an effective confining pressure and the mold was removed. Three diameter measurements were taken at the top, middle, and bottom portions of the

specimen using a thin steel circumferential tape (Pi tape). The measurements, made to the nearest 0.001 inch, were then averaged to obtain the specimen diameter.

44. The heights of the 2.8-inch-diameter specimens were measured by a cathetometer graduated in hundredths of a centimetre. The heights of the 1.4-inch-diameter specimens were measured to the nearest 0.001 inch by using a system of several pieces of equipment: a plexiglass cylinder, a dial gage graduated to 0.001 inch, a 3.5-inch-tall steel billet (dummy specimen), and a 6-inch-long steel bar (see Figure 12). The cylinder was placed over the reconstituted specimen. With the steel bar placed over the center of the specimen and across the cylinder, a steady reference position was found on the bar with the dial gage and the distance to the specimen top cap was measured. Four measurements were taken 90 degrees apart. Initial readings were made using the steel billet with specimen top platen in place. Final measurements were made with the soil specimen between the platens. The initial readings were averaged and the final readings were averaged. The difference in the two averaged readings was used to calculate the initial specimen height. Successive readings using this method were repeatable within 0.002 inch.

45. Before the next phase of testing was done, the specimen was checked for leaks. Membranes of thickness of about 0.012 inch were used to separate the specimen from the chamber fluid. Smaller thickness membranes (prophylactics--thickness of about 0.006 inch) were tried but proved ineffective in providing leakage protection. Even with the thicker membranes some specimens developed leaks. When leaks occurred, a rubber latex compound was spread over suspected areas: specimen/platen interface, folded seams of the membrane, etc. Another successful practice in preventing leaks has been to smear a small coating of silicone grease around the outside edge of the end caps before placing the rubber membrane in place. This provides a seal as well as filling in small scratches on the end caps.

Saturation

46. The process of saturation consisted of two phases: seepage saturation and back-pressure saturation. After the initial specimen

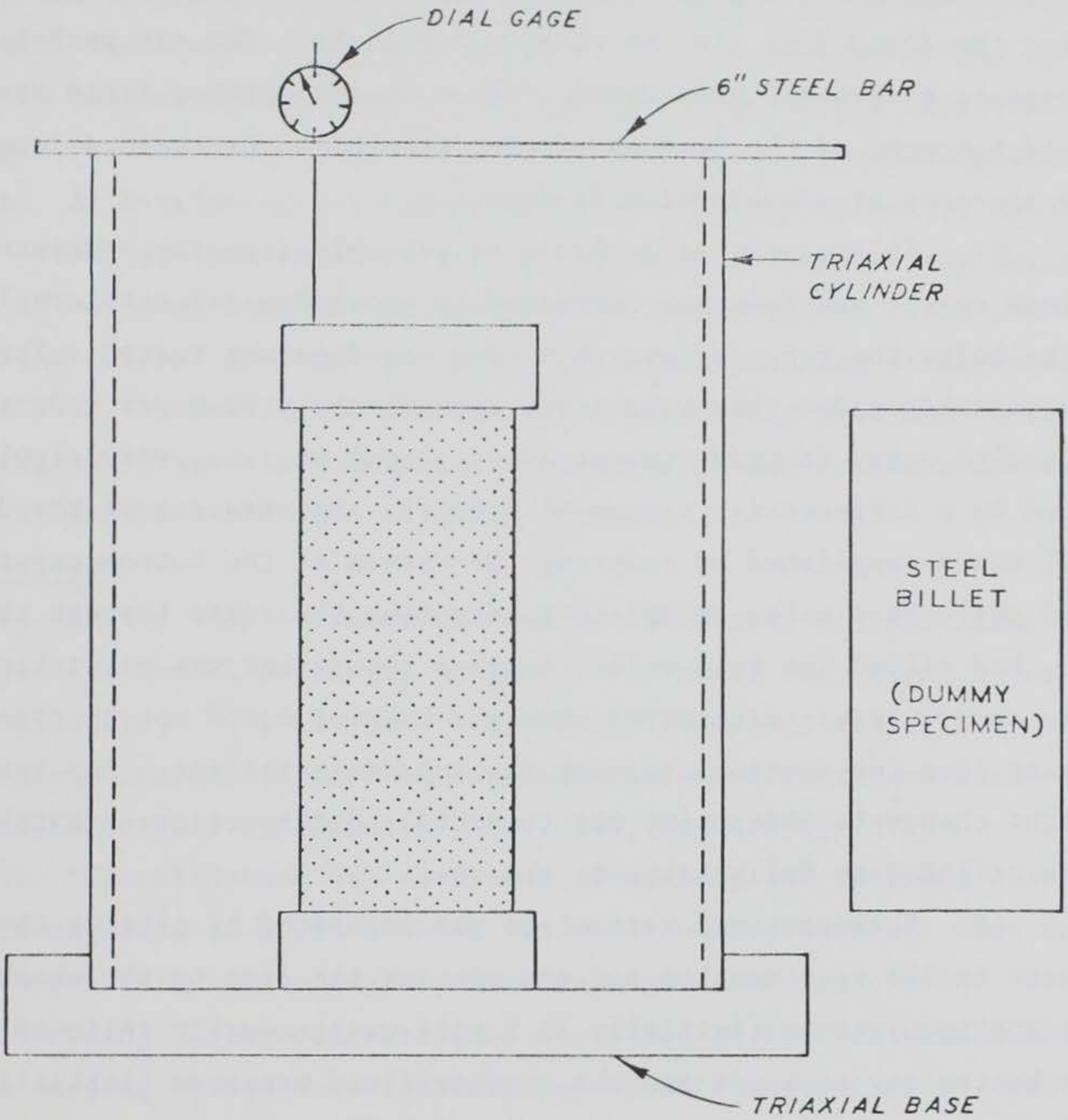

NOTE: DRAWING NOT TO SCALE

Figure 12. Apparatus used to measure initial height of 1.4-inch-diameter specimens

dimensions were determined, the triaxial chamber was assembled and fluid (water) was added to the chamber and brought to a level about 2-1/2 inches above the specimen top cap. This left an air pocket between the fluid line and the chamber top plate. The air pocket was necessary to prevent pressure variation in the chamber fluid due to the rapid movement of the loading piston, brought on by rapid deformation of the specimen at liquefaction failure.

47. To evacuate as much air as possible from the specimen, the vacuum on the specimen was increased to a maximum value tolerable--a value below the range of overstressing any specimen tested. The specimen was left under this vacuum for approximately 20 hours. De-aired distilled water (oxygen content about 1 ppm) was then very slowly introduced by a differential vacuum of 0.5 psi. Maintenance of the differential was accomplished by reducing the vacuum at the bottom cap to 13.0 psi. When water, displacing air along its route through the specimen, had filled the soil voids, seepage saturation was discontinued. This condition was determined when air bubbles could not be observed coming from the specimen through the top drainage line. Any specimen height change to this point was recorded. Back-pressure saturation was then utilized to fully saturate the soil.

48. Back-pressure saturation was initiated by closing the vacuum source to the specimen top cap and opening the line to the chamber fluid. The specimen vacuum (initially 13.5 psi) was gradually relieved through the bottom cap to 5 psi and the chamber fluid pressure (initially about 0 psi) was gradually increased to 5 psi. The specimen vacuum was then relieved to 0 psi and the chamber pressure was subsequently raised to, usually, 10 psi.

49. Back pressuring was usually performed in increments of 10 psi, depending on the desired effective confining pressure after consolidation. The pore fluid pressure and the chamber pressure were simultaneously increased. A 3- to 5-minute period was allowed for equalization of pressure throughout the specimen, followed by an additional simultaneous incremental increase in the chamber and pore pressures.

50. Complete saturation was achieved when an incremental increase

in the chamber pressure produced an identical change in magnitude of the pore pressure within the isolated specimen. This was accomplished by closing the specimen drainage valve and increasing the chamber pressure by 5 psi. The observed increase in pore pressure divided by the increase in chamber pressure gives Skempton's B parameter (Headquarters, Department of the Army, in press). A B-value of 1.0 means complete saturation. A B-value of 0.98 means the specimen is very nearly saturated and R tests at this value give good results. As reported by Mulilis et al. (U. S. Army Engineer Waterways Experiment Station 1976b), no significant effect on results can be distinguished using B-values from 0.91 to 0.98. A B-value of about 0.98 was generally obtained in this test program. Typically, complete saturation of the specimen was obtained with a back pressure of 60 to 100 psi.

Consolidation

51. After completion of the saturation phase, all specimens were isotropically consolidated ($K_c = \bar{\sigma}_3/\bar{\sigma}_1 = 1$), under the effective confining pressure, $\bar{\sigma}_3$, at which they would be tested. Effective confining pressures (difference in applied chamber pressure and back pressure) used were approximately 1.0, 2.0, and 4.0 kg/cm^2.

52. Consolidation was performed by opening the specimen drainage valve to a graduated burette which was under back pressure. Once the specimen was fully consolidated, the drainage valve was closed. Volume change occuring during consolidation was taken as the difference between burette reading before consolidation and burette reading after consolidation. The volume change result and the void ratio after saturation were then used to calculate the void ratio after consolidation.

53. The chamber pressure developed during back-pressure saturation and subsequently increased to affect the desired effective confining pressure, resulting in piston uplift. The amount of uplift, P_u, was determined by the equation

$$P_u = \sigma_3 \times A_{ROD} - (\text{weight of piston + any attachments})$$

where A_{ROD} is the cross-sectional area of the loading piston. To

counteract the uplift force, an equal amount of axial load (plus usually an additional pound to counteract friction) was applied which resulted in good piston/specimen contact. At this point the amount of specimen axial deformation due to saturation was recorded, as measured by a Linear Variable Differential Transformer (LVDT) and as referenced to the specimen height before saturation. Over the range of testing variables, axial deformation varied from negative 0.006 inch to positive 0.023 inch and averaged 0.010 inch. It is to be noted that any change in specimen height as measured by the LVDT was used to calculate void ratio changes within the specimen.

Axial loading

54. After the consolidation stage of the test was completed, the valves were closed and the axial load was applied.

PART IV: EQUIPMENT AND INSTRUMENTATION

Equipment

55. All specimens were controlled-stress loaded. Two loading systems were used. A pneumatic system was used for the 2.8-inch specimen (see Figure 13). The 1.4-inch specimens were loaded by a deadweight system either as an incremental step function or as a continuous ramp function (Figure 14).

56. The triaxial compression chamber consisted primarily of a headplate and a baseplate separated by a transparent plexiglass cylinder. Any number of references give detailed descriptions of triaxial compression chambers. The cylinder wall was 1/4 inch thick and its inside diammeter was 5-1/4 inches. Metal constriction bands were used around the cylinder to prevent fracture when chamber pressures exceeded 100 psi.

57. The triaxial loading pistons used were ground and polished case-hardened steel rods. Their diameters were 1/2 inch for 1.4-inch specimens and 3/4 inch for the 2.8-inch specimens. Linear ball bushings were used for piston guides because they allowed movement of the piston with a minimum of friction. Leakage around the piston was prevented by O-rings. The 1.4-inch specimen piston end is fitted with a conical tip (shown in Figure 14) designed to fit a recess in the specimen top cap. This was done to limit cap tilt during specimen loading. Piston friction, being a negligible amount (Headquarters, Department of the Army, in press), was not measured and thus was not used in calculations; also, normal error associated with electrical transducers (load cell) would overshadow piston friction.

58. Specimen cap and base for 1.4-inch specimens were constructed of clear plexiglass material and were larger in diameter than the test specimen. The 2.8-inch specimen caps were smooth and of polished steel and also oversized. The oversized end caps were selected to facilitate lubrication of the end platens. The use of oversized ends also proved to be advantageous because it tended to improve continuity of stress

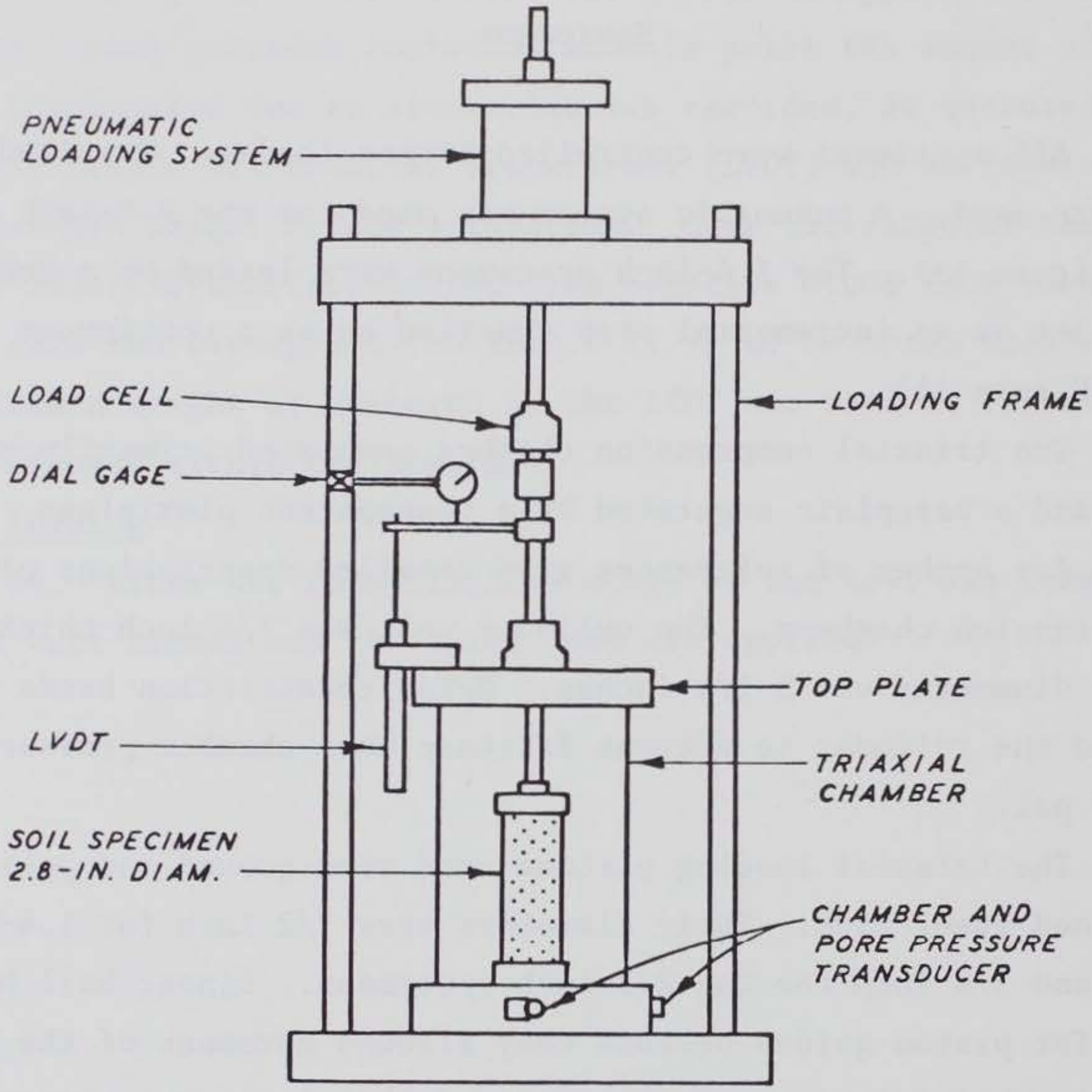

SCHEMATIC OF $\bar{R}$ TRIAXIAL TEST EQUIPMENT

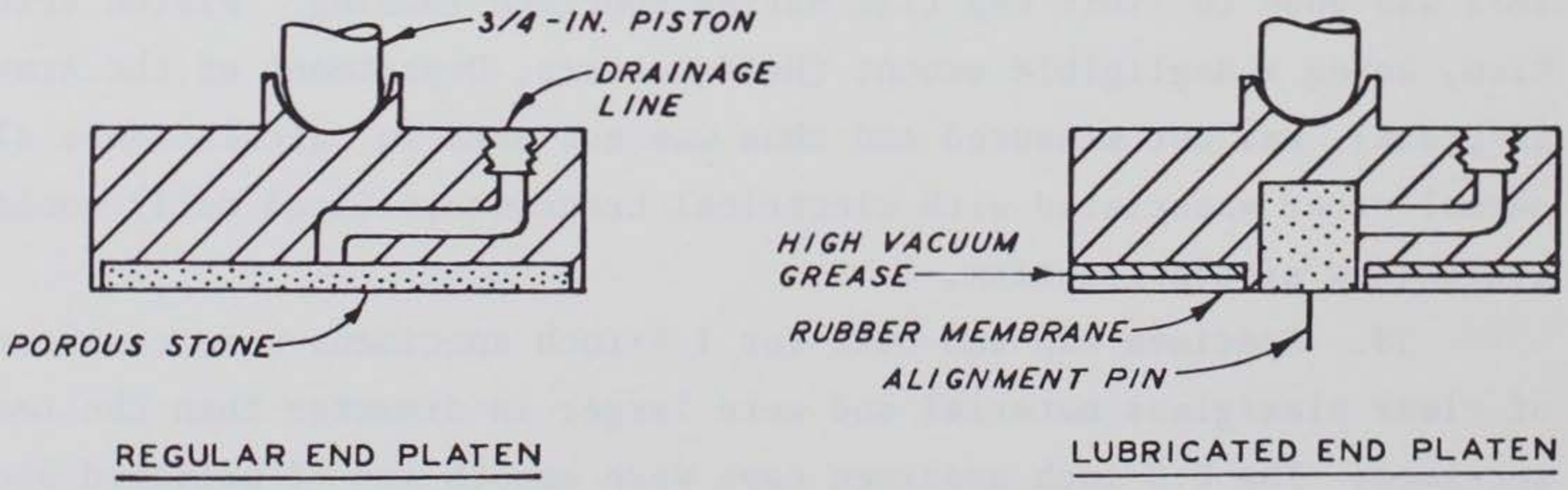

REGULAR END PLATEN

LUBRICATED END PLATEN

Figure 13. Pneumatic loading system with regular and lubricated end platens used for 2.8-inch-diameter specimens

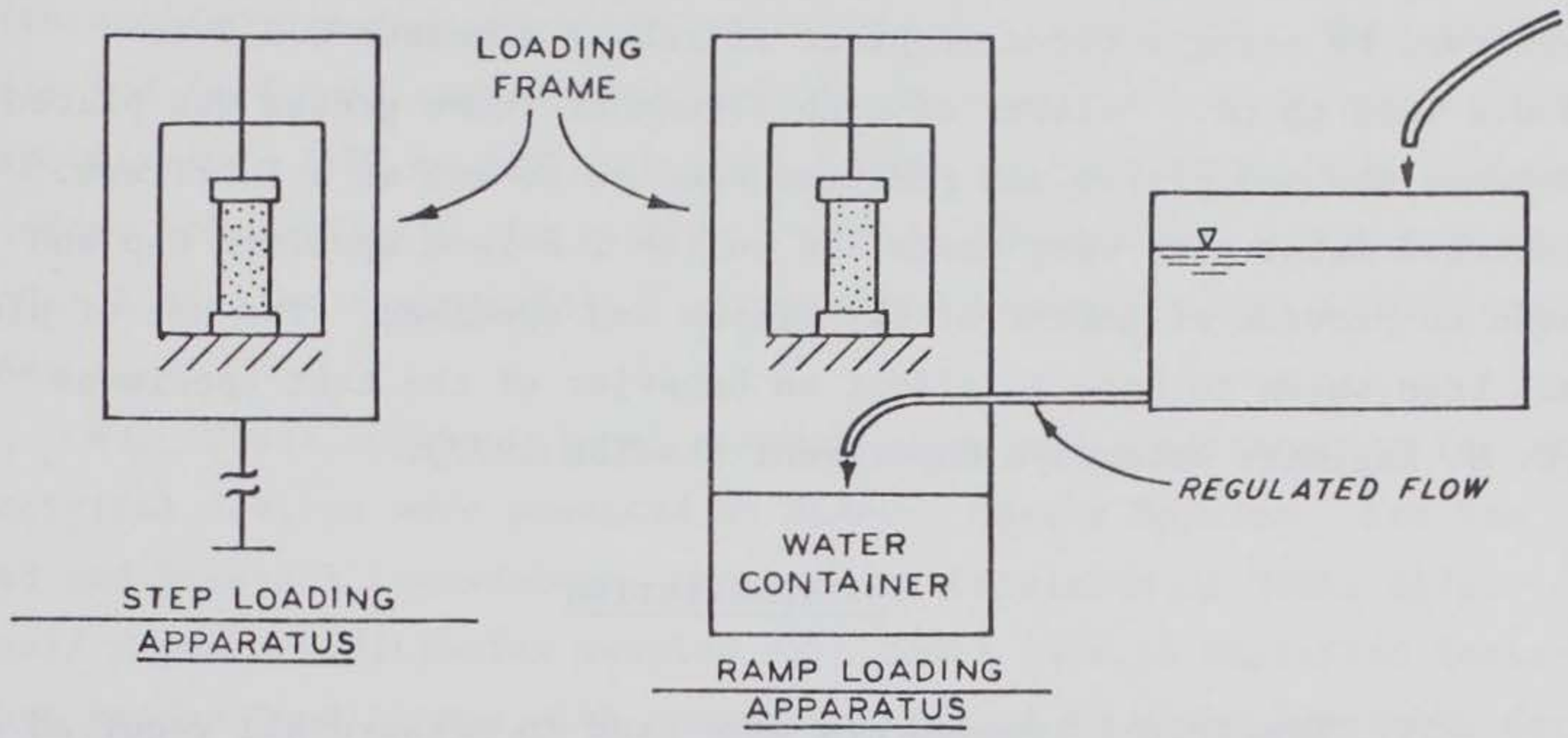

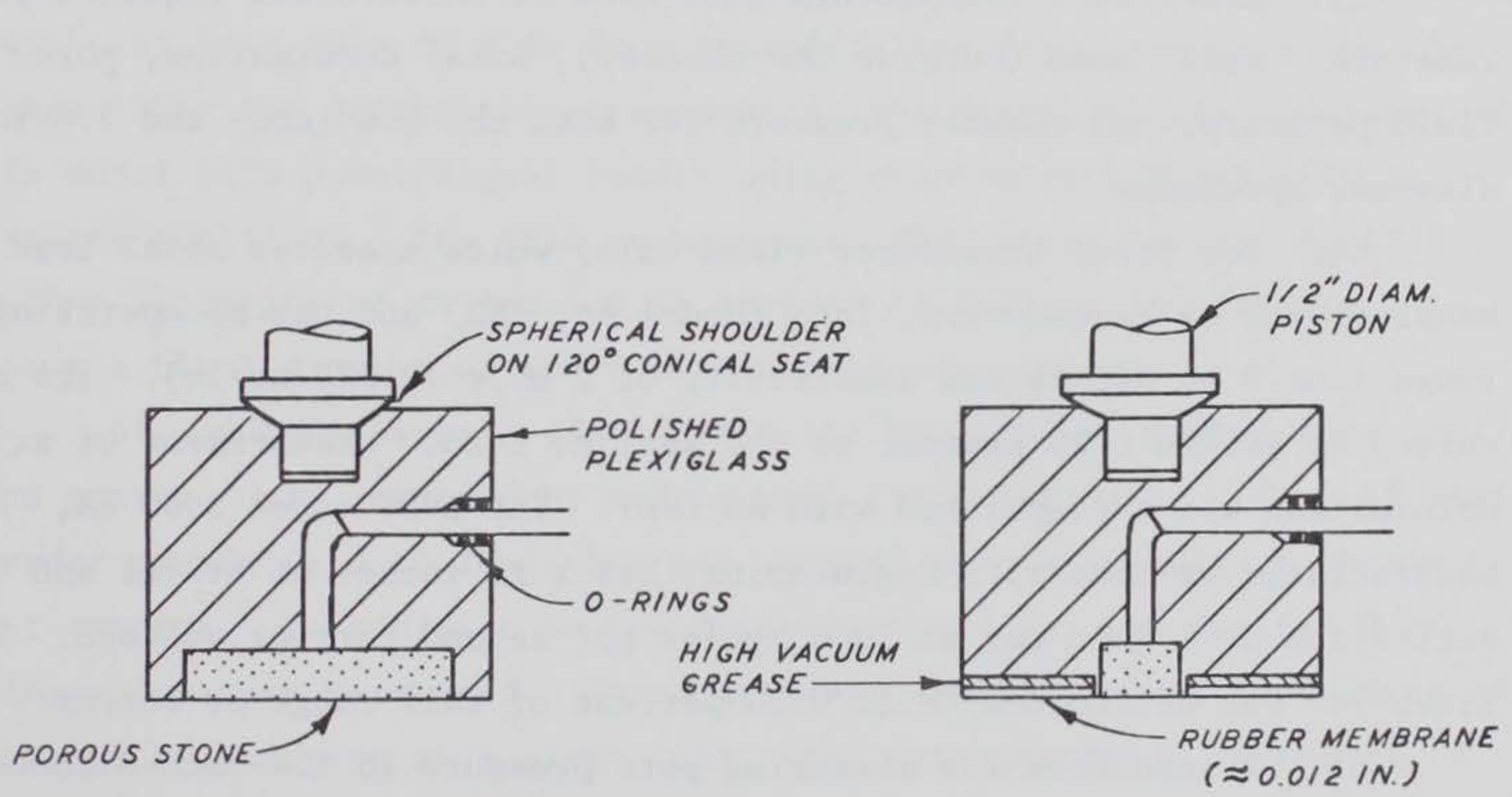

Figure 14. Deadweight loading system used with regular and lubricated end platens in 1.4-inch-diameter specimen testing

distribution across the platen/specimen interface. End platens of the type described by Rowe and Barden (1964) were used. Figures 13 and 14 show schematics of both sizes of end platens. Low frictional ends were achieved by using a circular piece of rubber membrane 0.010 to 0.012 inch thick. A layer of high vacuum silicone grease was placed between the end platen and membrane section to act as a lubricant. Centered metal pins were installed on the 2.8-inch specimen cap and base to provide alignment of the platen and specimen. The use of pins has been shown to have no effect on behavior of the test specimens (U. S. Engineer Waterways Experiment Station 1977).

Instrumentation

59. Electrical transducers were used to measure all required parameters: axial load (outside the chamber), axial deformation, pore fluid pressure, and chamber pressure for both the 2.8-inch- and 1.4-inch-diameter specimens.

60. The force transducer (load cell) which measures axial load is manufactured by Transducers, Inc. (Model No. 182) and has an operating range from 0 to 500 lb and sensitivity of 2 mv/v (0.020 mv/lb). Its accuracy is within 0.25 percent of the applied load. Measurement of axial deformation was accomplished with an LVDT. The LVDT model 2000 HR, manufactured by Schaevitz Engineering, has a ±2 inches of travel and excitation of 1 volt rms at 3000 cycles per second carrier voltage. The linearity was determined to be 0.25 percent of full range or better.

61. Transducers for measuring pore pressure in 1.4-inch-diameter specimens and chamber pressure (pressure cells) were Model No. D-HF, manufactured by the Baldwin-Lima-Hamilton (BLH) Corporation. Their range was ±0 to 200 psi. Accuracy is within 0.25 percent of applied range. Their sensitivity is 3 mv/v (0.075 mv/psi).

62. For 2.8-inch-diameter specimens, similar transducers, with identical ranges and capabilities were used with one exception. The load cell used for the 2.8-inch specimens was a BLH Model No. U3G1 with a working range from 0 to 1000 lb. Its sensitivity is 3 mv/v (0.005 mv/lb).

The accuracy is within 0.25 percent of applied load. Calibration of the LVDT was performed using a vernier caliper readable to 0.0001 inch. Calibration of all other tranducers was accomplished using a system which applied a series of known loads to each transducer. The pressure cells and load cell output were read to the nearest 0.1 psi and 0.1 lb, respectively. LVDT output were read to the nearest 0.001 inch. Figure 13 shows schematically the placement of transducers for a 2.8-inch specimen. A similar arrangement of transducers was used for 1.4-inch specimens.

63. Power supply, signal conditioning, and amplification for all electrical devices were provided by Endevco Master Modules. For the load and pressure transducers, the modules consisted of Model 4470 power/ signal conditioning coupled with Model 4476.2A Amplified Resistance Bridge Conditioner with output voltage of ±5 v and linearity derivation of less than ±2.5 mv from best-fit line from zero over the ±5-v range. For the deformation transducers, the Master Module consisted of the Model 4470 power/signal conditioning coupled with Model 4478.1A Carrier Amplifier. For this arrangement, the output voltage is ±2.5 v with a linearity of at least 0.25 percent of full scale. Figure 15 shows a block diagram of the instrumentation package.

64. Output signals (data) from the transducers were automatically and continuously recorded by a Honeywell 1912 Visicorder. Several Visicorder speeds (1.0 to 16 inches per second) were available to obtain output records. In addition to the printed recording, two digital Doric microvoltmeters were used. These displays allowed visual monitoring of any two transducers at a given time. All data generated in the early portion of the loading were manually recorded from the voltmeters. Since liquefaction failure occurs over a very small time increment (tenths of a second), the Visicorder was used to acquire data near and after peak deviator stress. A dial gage, positioned as shown in Figure 13, was also used to monitor deformation preceding liquefaction for all tests.

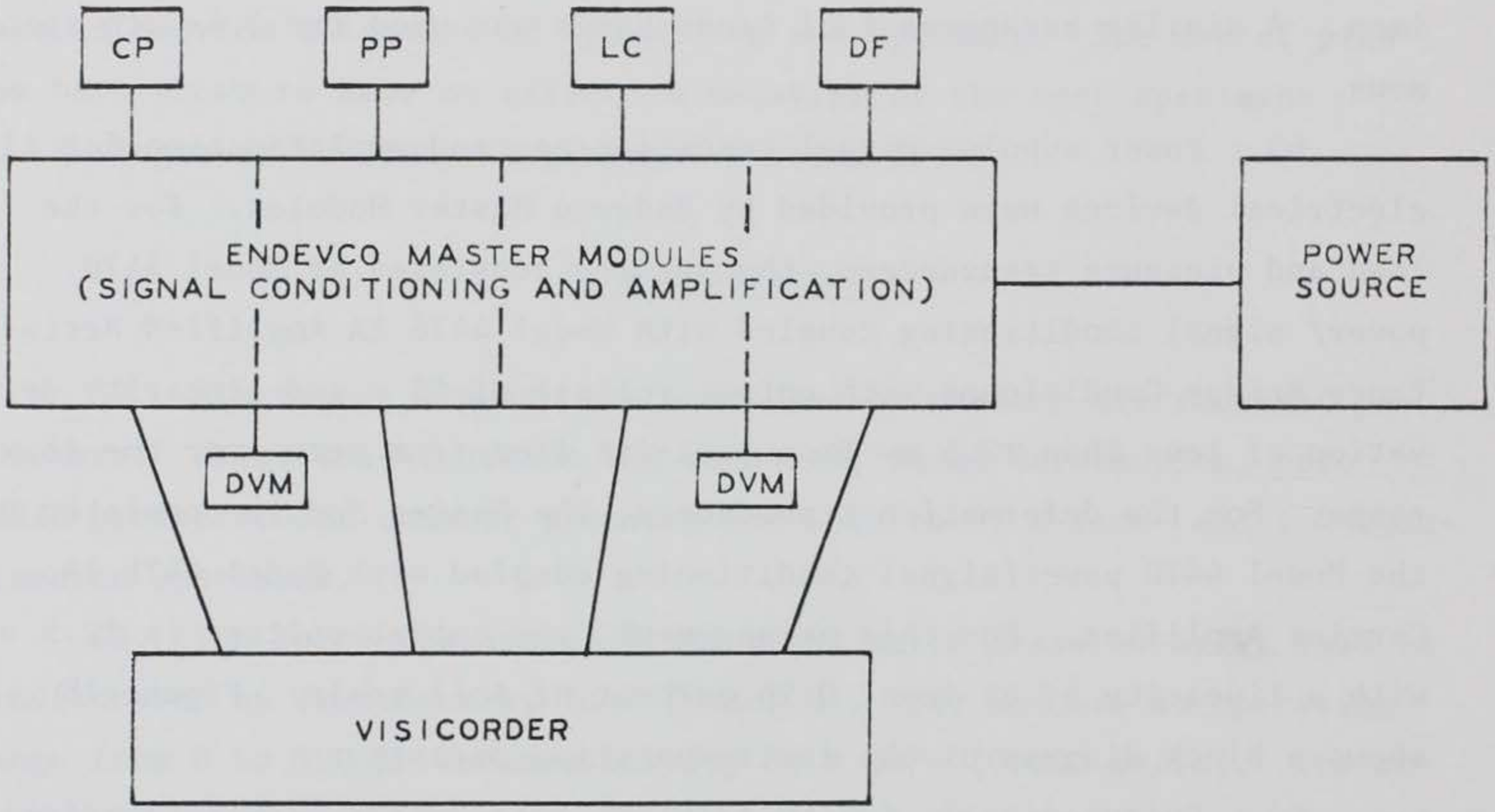

LEGEND

CP	CHAMBER PRESSURE
PP	PORE PRESSURE
LC	LOAD CELL
DF	LINEAR VARIABLE DIFFERENTIAL TRANSFORMER (LVDT)
DVM	DIGITAL VOLTMETER

Figure 15. Block diagram of instrumentation equipment

PART V: COMPUTATIONS AND DATA REDUCTION

Data Extraction from Visicorder Plots

65. During the loading, data prior to peak deviator stress were recorded manually from digital voltmeters. At the point of impending specimen collapse, which was indicated by steadily accelerating deformation and excess pore pressure, the Visicorder was turned on at a rate of 10 inches/second and to obtain specimen behavior during rapid straining. A tracing of a typical visicorder record of load, deformation, pore pressure, and chamber pressure for a specimen which liquefied is shown in Figure 16. It is noted that oscillation of the load curve, after specimen failure, is due to a condition external to the specimen. This condition is reflected in the fact that only 0.0008 inch of movement on the load cell transducer is needed to register the transducer maximum force. The abrupt impact of the loading system on the collapsed (failed) specimen initiates a small dynamic effect which is detected by the load cell transducer and thus oscillation of the load curve.

66. For that portion of each test documented by the Visicorder, the data for each test parameter had to be scaled from the trace on the Visicorder readout. The data so extracted were tabulated for input to the computer codes described below.

Computer Codes

67. All computations demanded for data reduction were accomplished using the computer code GDHERB. The program, written by G. Durham and subsequently modified, is given in Appendix B. Program GDHERB reduces data for isotropic and anisotropically consolidated $\bar{R}$ tests which are axially loaded under constant σ_3. The code provides tabulated listings of input and calculated data. In addition, the program produced plots of stress versus axial strain, excess pore pressure versus axial strain, and effective stress path [$\bar{Q} = (\bar{\sigma}_1 - \bar{\sigma}_3)/2$ vs $\bar{P} = (\bar{\sigma}_1 + \bar{\sigma}_3)/2$]. The computer calculations are described below.

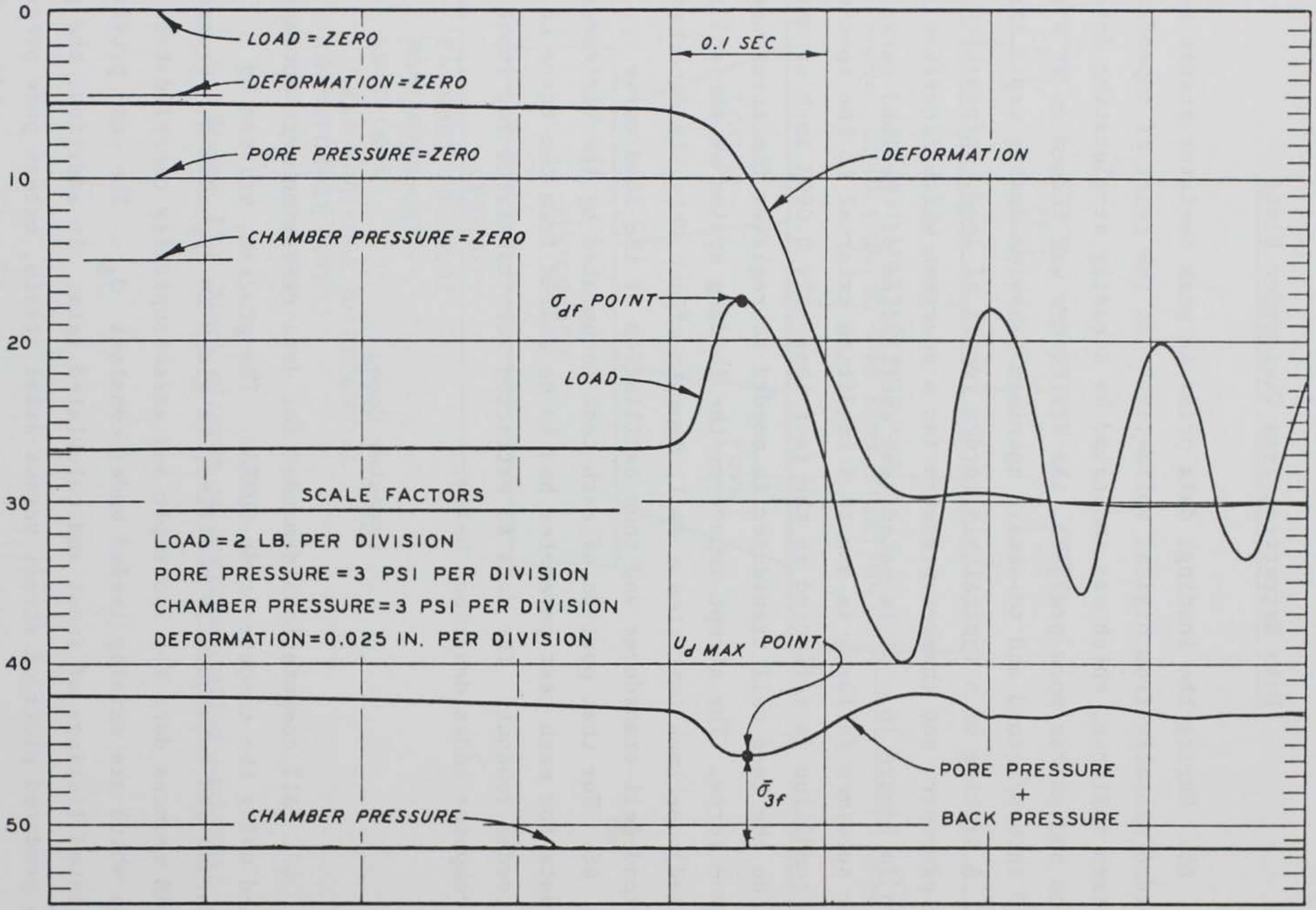

Figure 16. Facsimile of Visicorder readout for a specimen exhibiting liquefaction

Void ratio

68. Initial void ratio was calculated using hand-measured specimen dimensions, the specific gravity of solids, and the dry weight of the ovendried specimen obtained after test as follows:

$$e_i = \frac{G_s \gamma_w}{\gamma_d} - 1.000$$

where

e_i = initial void ratio

G_s = specific gravity of solids

γ_w = unit weight of water, gm/cm^3

γ_d = dry unit weight of the specimen, gm/cm^3

Computations were made for void ratio after saturation, e_{as}, using the relationship given above after correcting the initial dry density for any volume change noted by axial deformation during the back-pressure procedure. That volume change was determined using the change in specimen height to calculate the specimen area after saturation by the formula:

$$AAS = \frac{HINT - 2\ CHAS}{HINT}\ AIS$$

where

AAS = specimen area after saturation

HINT = initial height of the specimen

CHAS = axial change in height during saturation

AIS = initial area of specimen

This relationship was derived by assuming that radial deformations equalled axial deformations during the saturation phase of the test (Headquarters, Department of the Army, in press). To obtain void ratio after consolidation, e_c, the dry density after saturation was corrected directly from the change in volume during consolidation as provided by the change in burette reading.

Axial load

69. The axial load actually borne by the specimen (as previously described) was corrected by the amount of force (uplift) exerted against the loading piston by the chamber pressure. The following uplift equation (Headquarters, Department of the Army, in press) was used:

$$\text{Uplift} = A_{ROD} \times \sigma_3 - (\text{weight of piston + any attachment})$$

where

Uplift = force in pounds generated on the loading piston by σ_3 acting opposite in direction to the applied load

A_{ROD} = cross-sectional area of piston, square inches

σ_3 = chamber pressure, psi

Axial stress

70. The axial stress was calculated after correcting the specimen area after consolidation according to the change in axial strain as follows:

$$A_c = \frac{A_i}{1 - \Delta\varepsilon}$$

where

A_c = corrected specimen area, cm^2

A_i = specimen area after consolidation, cm^2

$\Delta\varepsilon$ = axial strain expressed as a decimal

Taking into account piston uplift, the following computation was made:

$$\sigma_1 = \sigma_3 + \frac{\text{Axial Load Corrected For Uplift}}{A_c}$$

where

σ_1 = axial stress

PART VI: PRESENTATION OF RESULTS AND ANALYSIS

71. Plots of the deviator stress and induced pore pressure versus axial strain and $\bar{Q}$ versus $\bar{P}$ (effective stress path) plots for all test series are given in Appendix C. In general, deviator stress-strain plots showed axial strain developing to about 2 percent before specimen collapse occurs. Examination of pore pressure versus strain plots shows that maximum pore pressure generation lagged behind the development of peak deviator stress. This was expected since the loading system maintained its load on the specimen throughout the deformation phase. The maximum pore pressure generally developed slightly after minimum deviator stress. In addition an evaluation of stress path plots shows reasonable pore pressure response as indicated by the stress path's definition of the effective failure envelope (α angle). The α-angles, determined by projection from the origin to the maximum principal effective stress ratio and the abscissa axis, are shown in Table 3 for individual specimens. With the α-angle and the relationship that $\sin \phi' = \tan \alpha$, the effective angle of internal friction can be determined. Determination of the generally accepted delineation of liquefaction responses (liquefaction, limited liquefaction, dilative) were not differentiated in this test program. The interest was merely whether or not liquefaction developed.

72. The critical void ratio curve, $\bar{e}_f$ curve, is developed by plotting the effective minor principal stress at failure, $\bar{\sigma}_{3f}$ versus the void ratio after consolidation, e_c. A cohesionless soil's critical state, which defines the boundary between contractive and dilative behavior in shear, is a function of the effective minor principal stress at failure. Castro (1969) used this relationship to plot the critical void ratio line.

73. Figure 17 shows the data from the reference series (Series A) plotted as the critical void ratio curve for this test program. Figure 18 compares the established critical void ratio curve for Banding sand, as determined by Castro, to the reference series curve developed here. As can be seen, the curves match very well, which indicates

Table 3

Summary of Test Data

Test No.	Dia. in.	$\bar{\sigma}_c$ kg/cm^2	e_c	D_{rc} %	B Value	σ_{dP} kg/cm^2	ε_p %	σ_{df} kg/cm^2	ε_f %	U_{dmax} kg/cm^2	$\bar{\sigma}_{3f}$ kg/cm^2	α degrees	Press & Stress vs Axial Strain & Stress Path
A1	1.4	1.00	0.751	26	0.97	0.72	1.4	0.37	5.1	0.95	0.05	33.0	Figure B1
A2	1.4	1.00	0.759	24	0.90	0.61	1.3	0.41	3.6	0.98	0.02	42.3	B2
A3	1.4	1.40	0.671	50	1.00	*D	D	D	D	0.30	--	--	B3
A4	1.4	0.90	0.754	25	1.00	0.61	1.0	0.28	5.5	0.87	0.03	37.4	B4
A5	1.4	1.41	0.709	39	0.97	1.85	0.9	0.98	6.5	1.06	0.34	30.6	B5
A6	1.4	1.00	0.733	31	0.97	0.76	1.6	0.52	3.4	0.91	0.09	36.2	B6
A7	1.4	2.10	0.761	23	0.97	1.21	1.0	0.36	9.0	2.04	0.06	36.7	B7
A8	1.4	1.97	0.754	25	0.98	1.15	1.2	0.46	6.2	1.91	0.06	38.4	B8
A9	1.4	2.00	0.748	27	0.98	1.30	1.0	0.44	5.8	1.89	0.11	32.7	B9
A10	1.4	4.00	0.747	27	0.98	1.92	0.7	0.64	6.8	3.87	0.13	33.2	B10
A11	1.4	4.00	0.720	35	0.98	2.35	1.0	0.80	6.1	3.75	0.25	29.5	B11
A12	1.4	4.00	0.714	37	0.96	2.75	1.2	1.75	3.6	3.31	0.69	28.6	B12
B1	1.4	1.10	0.744	28	0.98	0.89	0.6	0.41	7.1	1.04	0.06	36.1	B13
B2	1.4	1.00	0.764	22	0.97	0.70	0.4	0.39	3.0	0.97	0.03	40.9	B14
B3	1.4	2.00	0.783	17	0.96	1.12	0.5	0.32	2.9	1.99	0.01	41.6	B15
B4	1.4	1.94	0.740	29	0.98	1.07	0.3	0.33	3.4	1.83	0.11	28.9	B16
B5	1.4	2.01	0.739	30	0.98	1.27	0.2	0.38	5.4	1.83	0.18	27.2	B17
B6	1.4	4.07	0.753	26	0.98	2.03	0.7	0.55	6.0	3.96	0.11	35.3	B18
B7	1.4	4.00	0.725	34	0.98	2.38	0.5	0.97	3.8	3.72	0.28	30.5	B19
B8	1.4	4.00	0.719	36	0.94	2.29	0.9	0.67	7.9	3.74	0.26	28.9	B20
D1	1.4	1.00	0.751	26	1.00	0.88	0.7	0.42	5.9	0.93	0.07	34.9	B21
D2	1.4	2.01	0.760	24	0.98	1.40	0.5	0.39	4.0	1.95	0.06	36.2	B22
D3	1.4	2.00	0.735	31	0.98	1.46	0.3	0.51	3.1	1.87	0.13	32.6	B23
D4	1.4	2.03	0.732	32	0.98	1.57	0.3	0.69	3.2	1.78	0.25	32.0	B24
D5	1.4	4.03	0.767	22	0.98	2.33	0.7	0.36	5.2	3.99	0.04	39.8	B25
D6	1.4	4.00	0.724	34	0.96	2.69	0.9	1.20	5.2	3.53	0.47	28.5	B26
H1	2.8	2.00	0.717	36	0.98	1.57	0.8	1.00	3.7	1.61	0.39	30.0	B27
H2	2.8	4.00	0.699	42	0.98	3.76	0.9	1.92	8.6	3.15	0.85	27.9	B28
I1	2.8	2.00	0.750	27	0.98	1.27	0.3	0.36	8.6	1.96	0.04	39.8	B29
I2	2.8	2.00	0.726	34	0.98	1.54	0.8	0.79	6.5	1.68	0.32	28.2	B30
I3	2.8	3.80	0.735	31	0.98	2.67	0.7	0.90	--	3.65	0.15	28.6	B31
MB1	1.4	2.00	0.890	17	0.98	1.25	1.1	0.48	9.3	1.89	0.11	33.0	B32
MB2	1.4	4.00	0.851	29	0.98	2.73	2.2	2.05	5.8	3.18	0.82	29.0	B33
MD1	1.4	1.00	0.895	16	0.97	0.78	1.0	0.26	--	0.96	0.04	35.9	B34
MD2	1.4	2.00	0.886	19	0.98	1.25	1.0	0.39	6.0	1.93	0.06	36.8	B35
MD3	1.4	3.00	0.845	31	0.98	2.25	2.5	1.98	7.9	2.22	0.78	28.8	B36

*D - Dilative specimen.

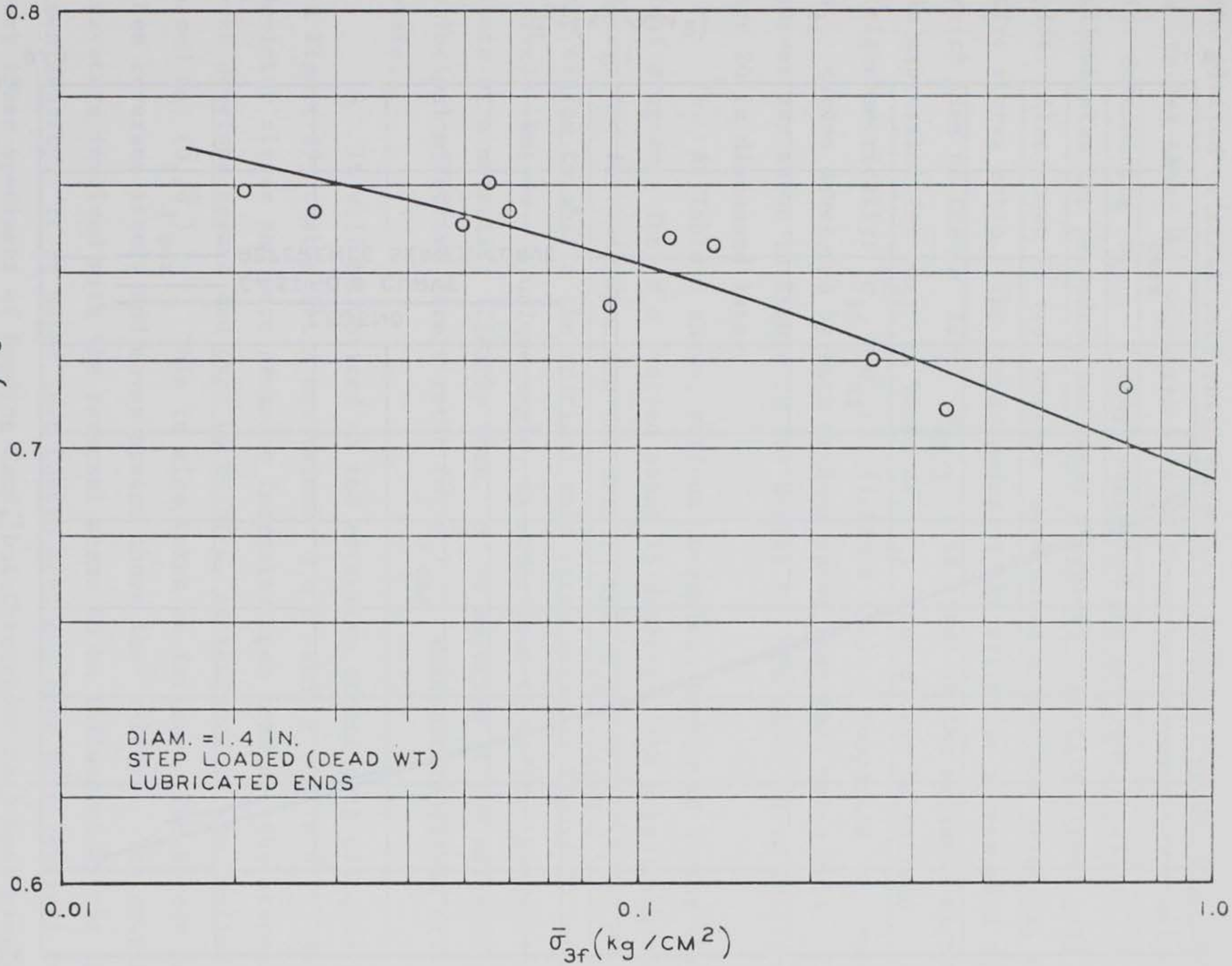

Figure 17. Critical void ratio curve, A-series (reference series), Banding Sand

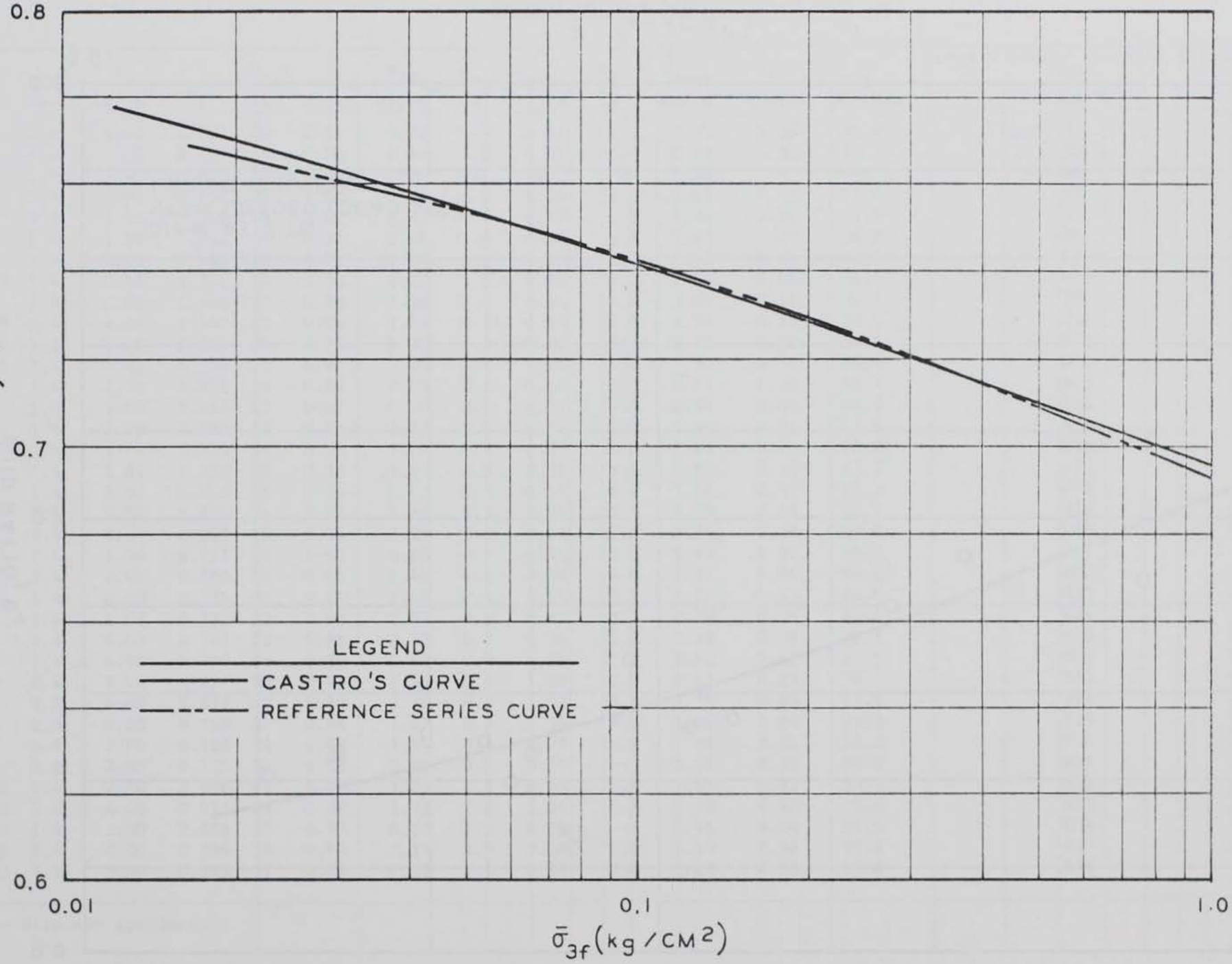

Figure 18. Comparison of reference series critical void ratio curve with the critical void ratio curve developed by Castro

consistency in testing technique and a very high probability that this is the actual curve for Banding Sand. Another check on the validity of the plotted critical void ratio curve is a method based on σ_{df} and α rather than $\bar{U}_{dmax}$, which is read from the Visicorder, and was used for determining $\bar{\sigma}_{3f}$. Torrey* suggested the procedure. Figure 19 illustrates the procedure and shows a typical effective stress path plot. Also shown is its α-angle determined at maximum principal effective stress ratio. The lowest point of the effective stress path plot which lies on the α line, $\sigma_{df/2}$, is taken in the ordinate direction. An expression for $\bar{\sigma}_{3f}$ in terms of σ_{df} and α can be derived trigonometrically: $\bar{\sigma}_{3f} = \sigma_{df}/2 \ (1/\tan \alpha - 1)$. Comparing e_c versus $\bar{\sigma}_{3f}$ curves developed by both methods shows that they match well. The curves are shown in Figure 20 for Series A. The upper curve in Figure 20 is discussed later.

74. As Table 3 shows, various α-angles developed during the test program. The α's varied about 15 degrees. The actual angle determined for each specimen was used in the $\bar{\sigma}_{3f} = \sigma_{df/2} \ (1/\tan \alpha - 1)$ expression to obtain the critical void ratio curve in Figure 20 (upper curve). But α, a unique angle, is understood to define the critical state of a material. Clearly then, α as selected at the maximum principal effective stress ratio $(\bar{\sigma}_1/\bar{\sigma}_3)_{max}$ does not represent critical state.

75. It will be noticed on the effective stress path plot, as shown in Figure 19, that point A has values $Q = 0$ and $P = \bar{\sigma}_3 = \bar{\sigma}_c$. As the deviator stress and pore pressure increases upon loading, the stress path develops upward and over to point C, at tangency to the α-line based on $(\bar{\sigma}_1/\bar{\sigma}_3)_{max}$. This is also taken as failure. The stress path then reverses itself and moves upward above the α-line. The amount of curvature involved with the reversal seems to be influenced by the specimen density. It is noted that Castro does not show this reversal for very loose specimens of Banding Sand, but throughout this test program

---

* Personal communication, Victor Torrey III, Geotechnical Laboratory, U. S. Army Engineer Waterways Experiment Station, Vicksburg, Miss.

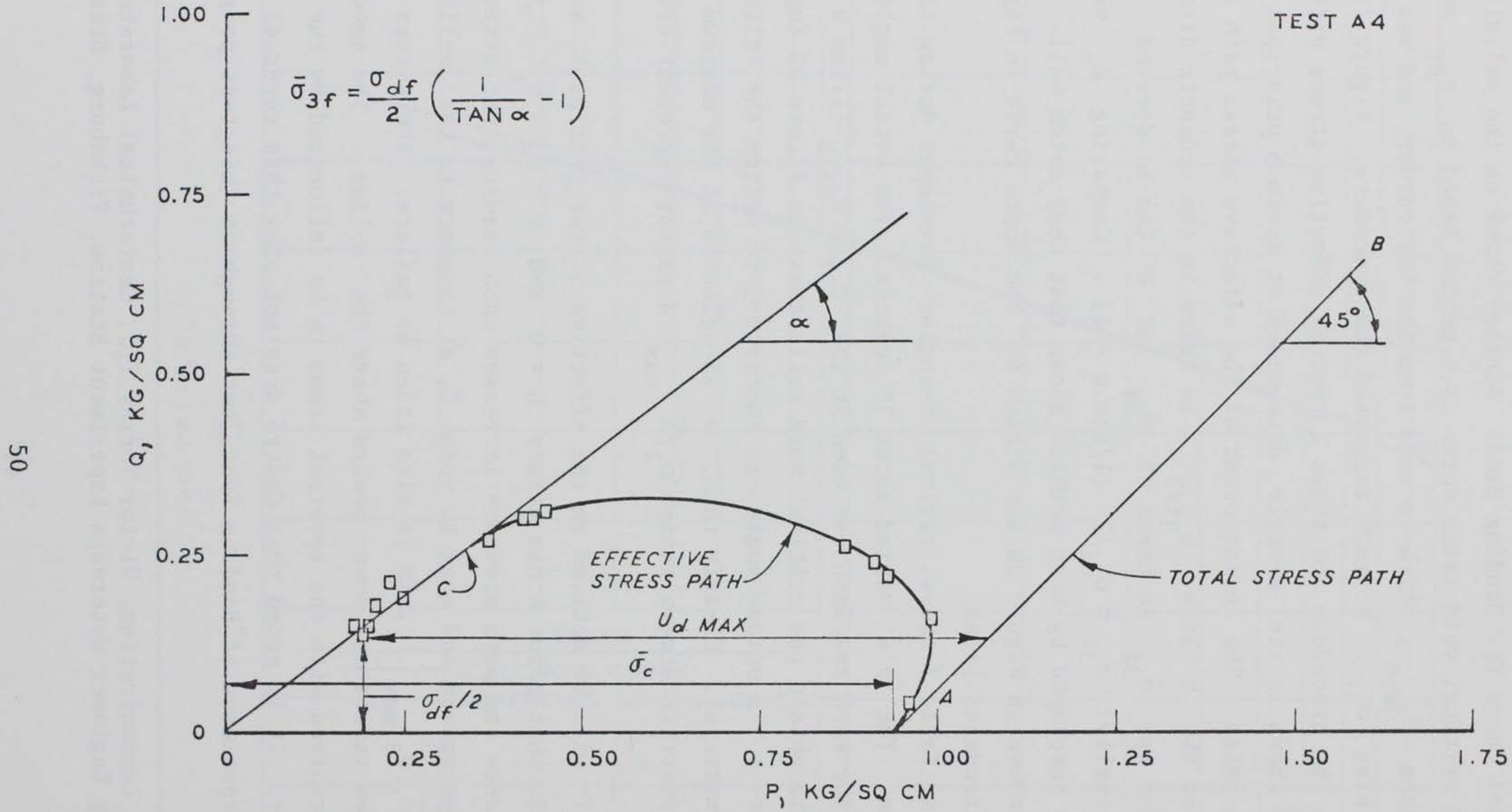

Figure 19. Typical effective stress path plot used to illustrate alternate procedure for determining $\bar{\sigma}_{3f}$, minor effective principal stress at failure

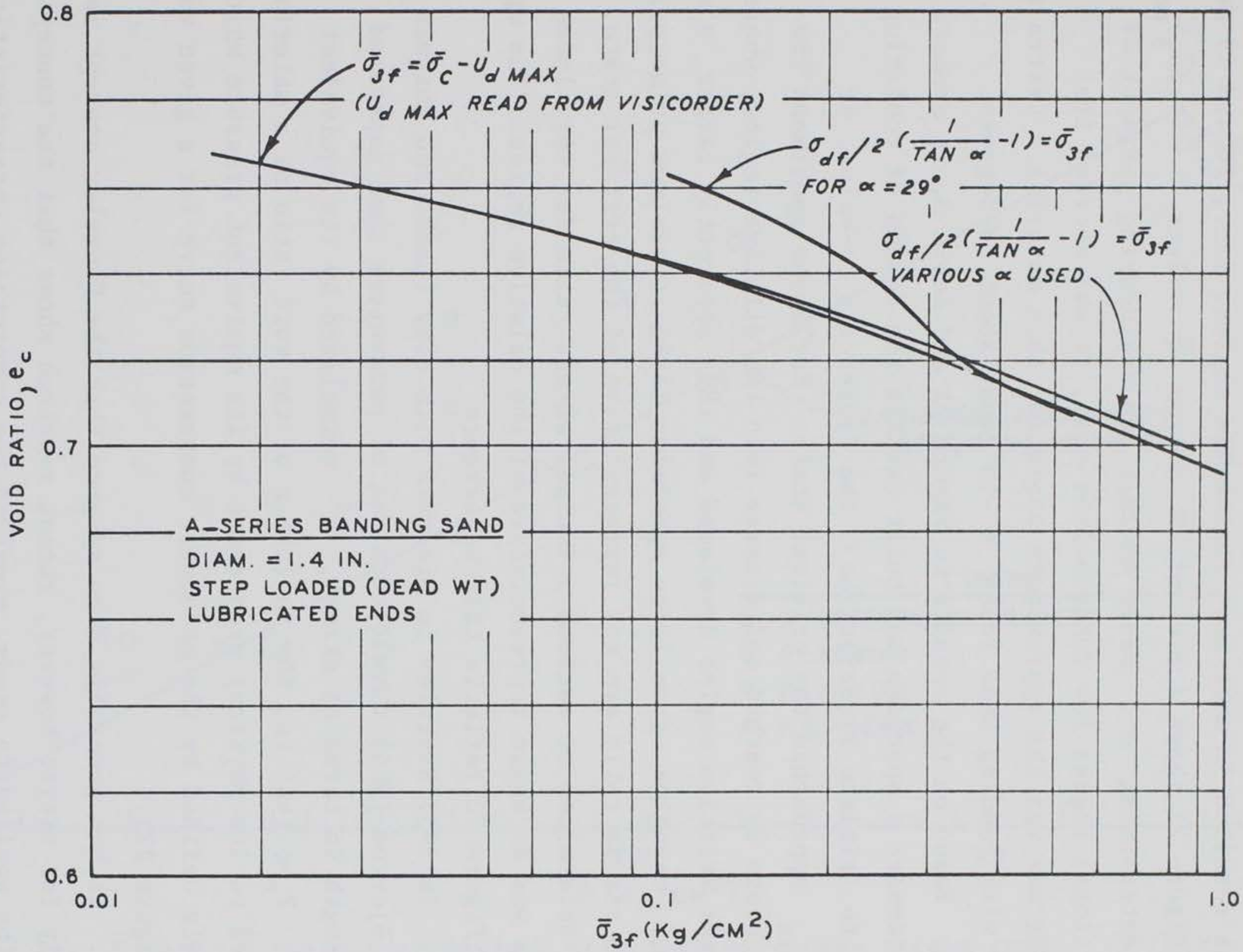

Figure 20. Comparison of $\bar{e}_f$ curves as determined by: 1) $\bar{\sigma}_{3f}$ from Visicorder, 2) $\sigma_{df}/2(1/\tan\alpha - 1) = \bar{\sigma}_{3f}$ at various α's, and 3) $\sigma_{df}/2(1/\tan\alpha - 1) = \bar{\sigma}_{3f}$ using α = 29 degrees

the stress path reversed itself consistently after developing maximum pore pressure. Furthermore, by looking at Table 3 it can be seen that larger α-angles generally developed for looser specimens. Denser specimens resulted in much more reasonable angles, i.e., 28 and 29 degrees. Figure 21 shows a plot of $\bar{P}$ versus $\bar{Q}$ values at $(\bar{\sigma}_1/\bar{\sigma}_3)_{max}$ used in determining α. Based on this and engineering judgment of the frictional angles for cohesionless soil, it was decided that α = 29 degrees was the approximate angle for this material. Castro in his work with Banding sand found α to equal about 28 degrees.

76. Based on the results in Figure 21 and Table 3, it appears that the denser a specimen was built (within the domain of confining pressure to initiate liquefaction), the closer its α-value at $(\bar{\sigma}_1/\bar{\sigma}_3)_{max}$ approached the critical state. For loose specimens the critical state is reached and crosses into the dilative region, whereupon larger friction angles developed and thus apparently larger α's. Therefore, α-angles from loose specimens taken at maximum principal effective stress ratio are not representative of the critical state. What was determined at maximum principal stress ratio for very loose specimens was an angle representative of the dilative region. The upper curve in Figure 20 reflects this occurrence.

77. In 1937 Hvorslev in his work with clay (Lambe and Whitman 1979 and Bjerrum 1954) developed a set of parameters that expressed soil strength in terms of stress, P, normalized by its equivalent pressure, P_e; that is, the influence of the void ratio of a material is related to its physical properties by its equivalent pressure which is uniquely defined by the oedometer compression curve for a given void ratio (Figure 22).

78. It has generally been assumed that the Hvorslev concept is valid only for clays; however, recent research shows that the concept also can be applied to sands, provided the compression characteristics are properly defined.* A particular finding was that by

---

* Personal communication, John Peters and Victor Torrey III, Geotechnical Laboratory, U. S. Army Engineer Waterways Experiment Station, Vicksburg, Miss.

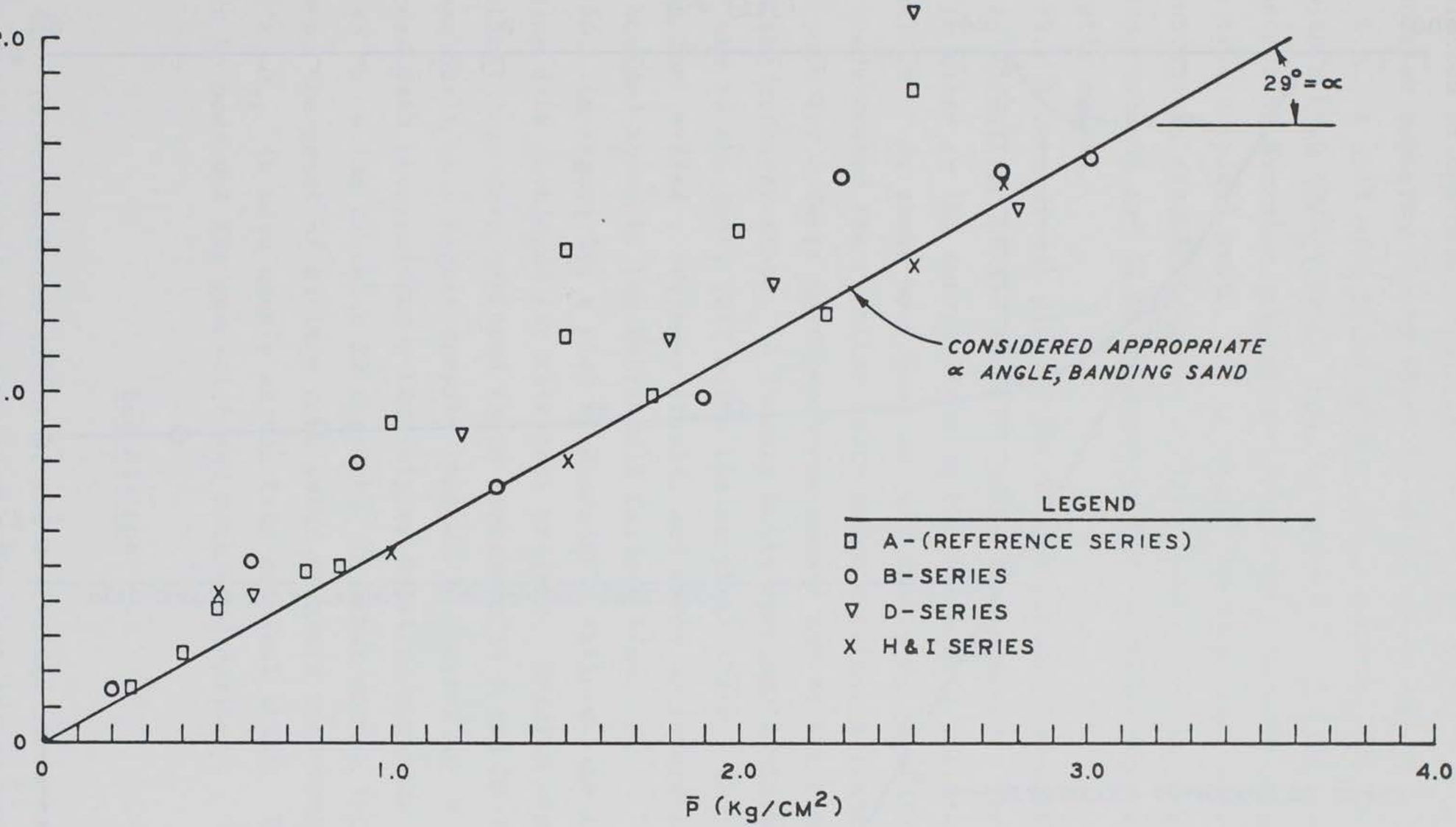

Figure 21. $\overline{P}$ and $\overline{Q}$ values at maximum principal effective stress ratio $(\overline{\sigma}_1/\overline{\sigma}_3)_{max}$ as used in determining the α-angle of Banding Sand

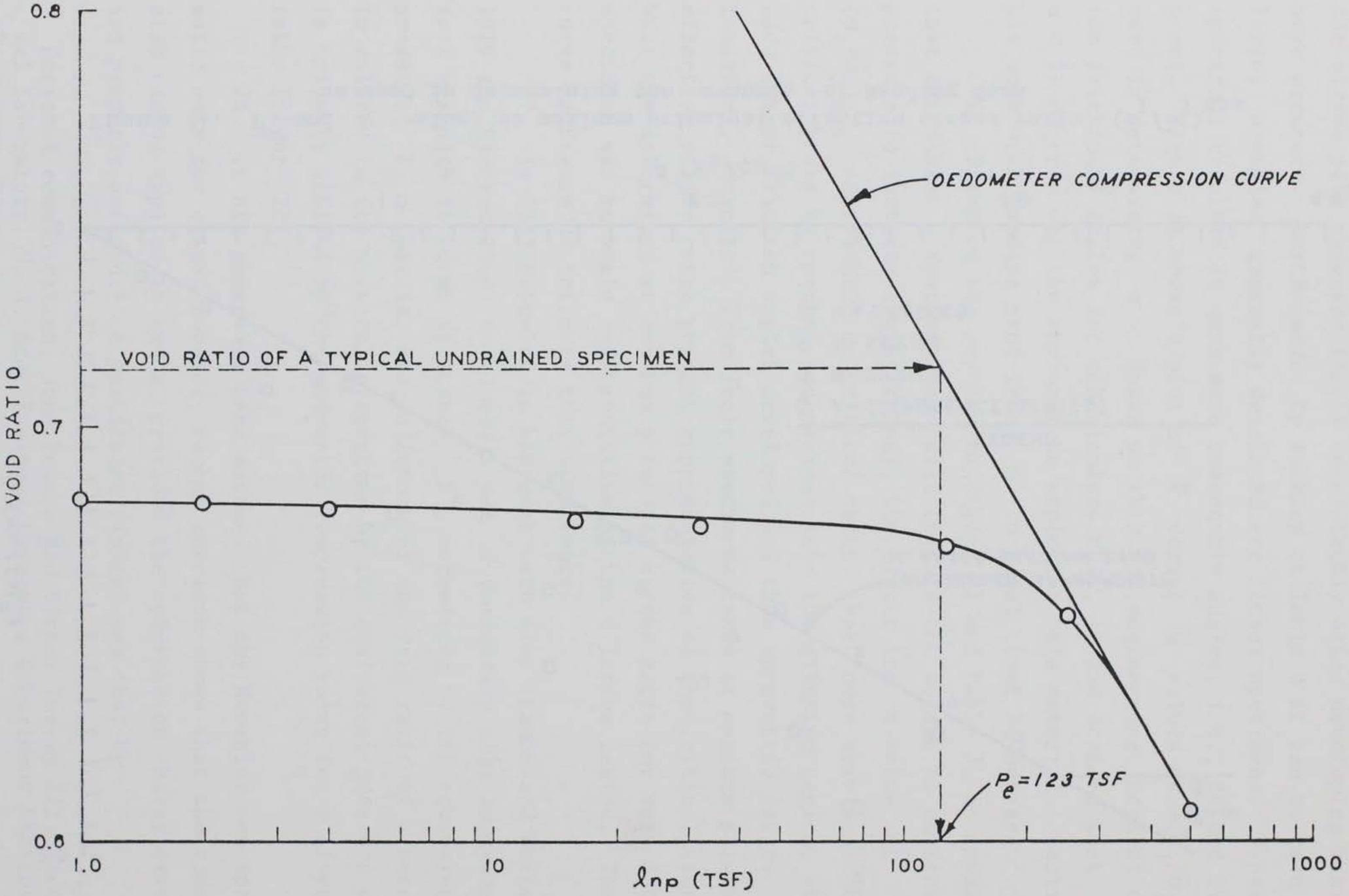

Figure 22. Compression curve of Banding Sand as used in determining Hvorslev's equivalent pressure

manipulation of the basic equations of critical state soil mechanics, the Hvorslev cohesion can be shown to be the dilatancy strength component; i.e., a soil with a low (P/P_e) ratio tends to dilate; whereas, soil with a high (P/P_e) ratio tends to contract. Taking this further, the concept of Hvorslev parameters can probably be used to determine a soil's true critical state. It is noted, however, that utilization of this concept in establishing the critical state is still a matter that requires research and is by no means proven; nevertheless, the potential apparently exists.

79. A theoretical plot of Hvorslev's failure law with stress paths in normalized stress space is shown in Figure 23. The critical state is taken as the intersection of the Hvorslev's failure line and the α-line . As shown by Figure 23, any specimen, regardless of density, tends toward the critical state under continuous loading. The stress path for a dense specimen moves upward and to the right, heading toward the critical state. A loosely built specimen's stress path moves upward and to the left, just below the critical state. The path then crosses the α-line , reverses itself, and moves on toward the critical state bounded above by the Hvorslev's failure line.

80. In Figure 24, a plot of Hvorslev's failure line is presented, utilizing data developed for this test program. Results similar to the theoretical case were achieved (note specimens A4-4 and D2-3). Specimen A4-4 was built at a higher density than D2-3. Measuring α at the point of stress path reversal shows that higher density specimens tend to develop an α value of about 29 degrees. In other words, for the denser specimen, the point of maximum pore water pressure corresponding to Castro's $\bar{\sigma}_{3f}$ is more nearly at the true critical state. Thus, this appears to bear out the general trend mentioned earlier.

End Platens

81. To evaluate the effect of end restraint, specimens with lubricated and nonlubricated ends were used. Two test series were conducted on 1.4-inch-diameter specimens using deadweight and incremental loading.

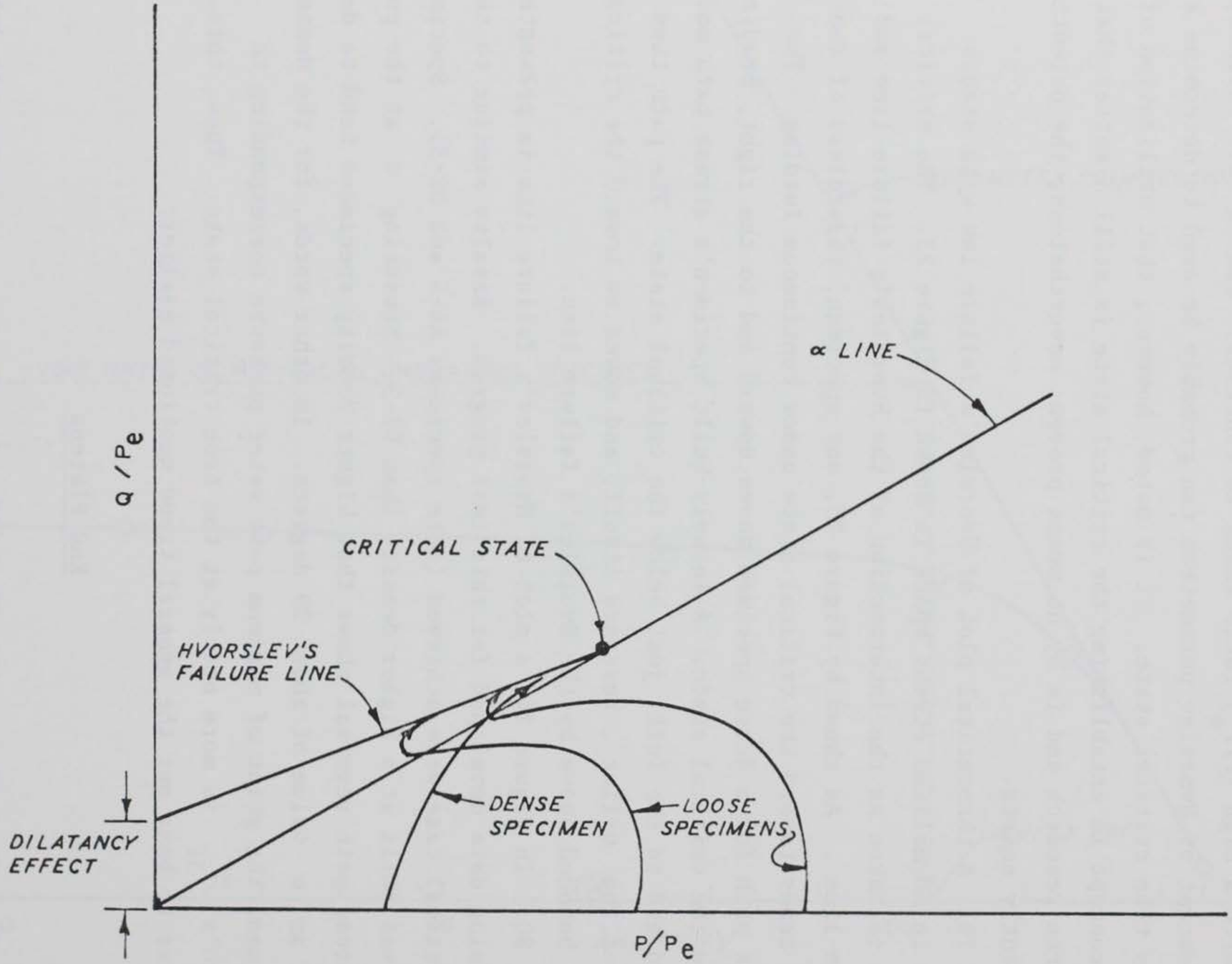

Figure 23. Hvorslev's theoretical failure line

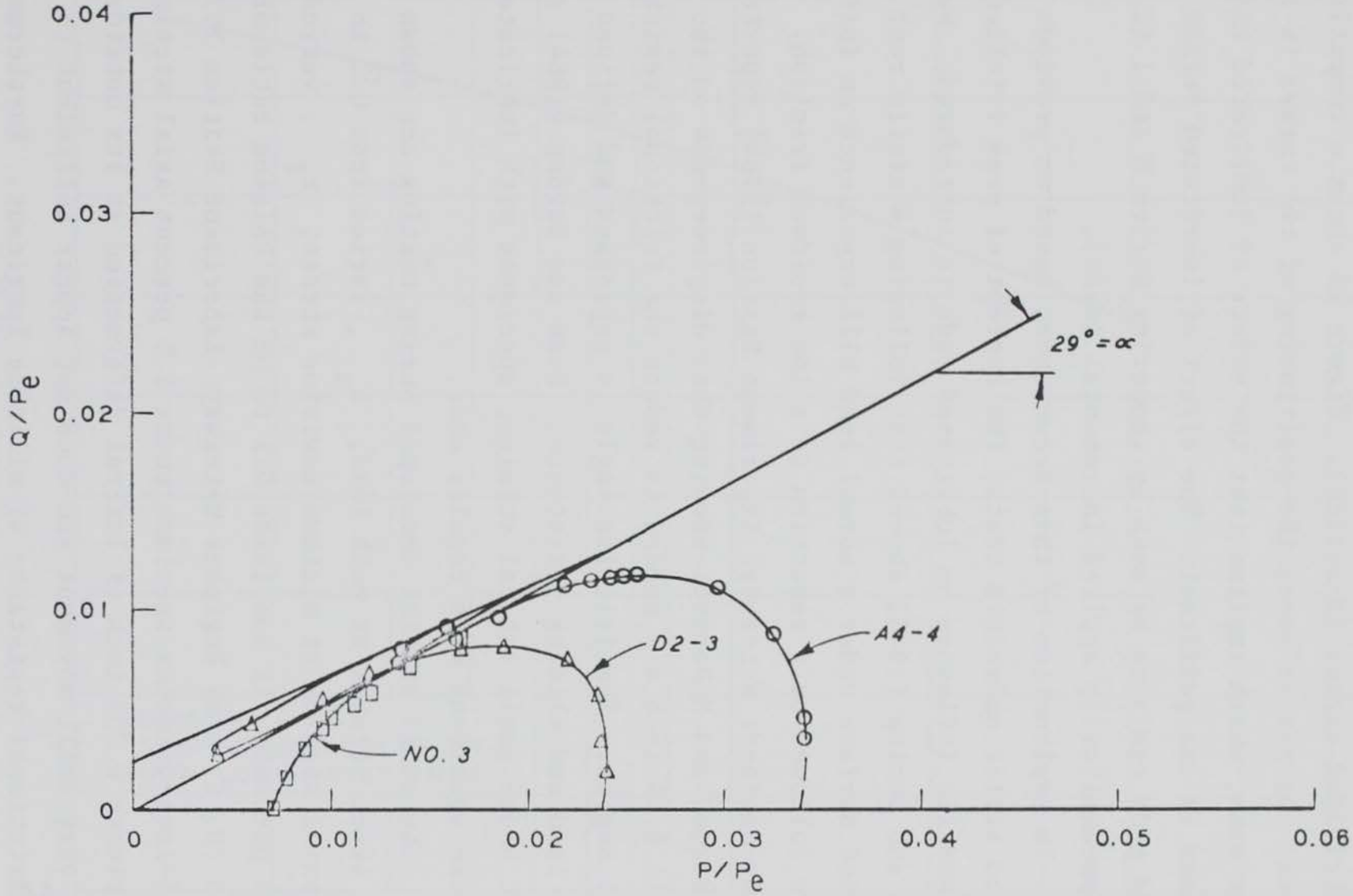

Figure 24. Illustration of Hvorslev's failure using actual test data

One series was with lubricated ends and the other series without. The lubricated series also served as the previously discussed calibration series (A-series). Figure 25 shows the critical void ratio curve for the nonlubricated series (B-series). Figure 26 shows a comparison of both series. As can be seen, the positioning of the curves is relatively the same, which implies that the effect of lubricated ends on Banding Sand is insignificant. The effect of lubricated versus non-lubricated ends can also be seen by comparing Series H and I (2.8-inch-diameter pneumatically applied incremental loads).

82. In explanation of this occurrence, based on previous results obtained on static undrained tests, the concept of peak frictional resistance and its influence on lubricated ends is introduced. Work done by Duncan and Dunlop (1968) showed that following a static rest period, a lubricated surface under a normal load will experience an initial high resistance followed by a reduction to a low residual friction. Lee (U. S. Army Engineer Waterways Experiment Station 1976a) reported results of Barden and McDermott showing that displacements on the order of 0.025 to 0.05 inch are needed to reduce the frictional resistance angle to 1 degree. The friction angle is expressed and defined in terms of normal load and sliding resistance. Rowe and Barden (1964) also state that under small lateral strains, specimens with lubricated ends behaved like specimens with regular ends.

83. The axial strains developed during testing are shown in Table 3. Axial strains at peak load, ε_p, varied from 0.2 to 2.5 percent and axial strains at minimum deviator stress, ε_f, varied from 2.9 to 9.3 percent. If one takes 0.5 to be the Poisson ratio of saturated sand (U. S. Army Engineer Waterways Experiment Station 1976a), then a 1.4-inch-diameter specimen under 2.5 percent axial strain would only experience 0.009 inch of lateral deformation at its outside edge. This is a very small movement and does not appear sufficient to overcome the peak frictional resistance of silicone lubricant. Furthermore, an axial strain at minimum deviator stress of 9.3 percent would only cause 0.033 inch of movement. Therefore, it seems unlikely that the use of

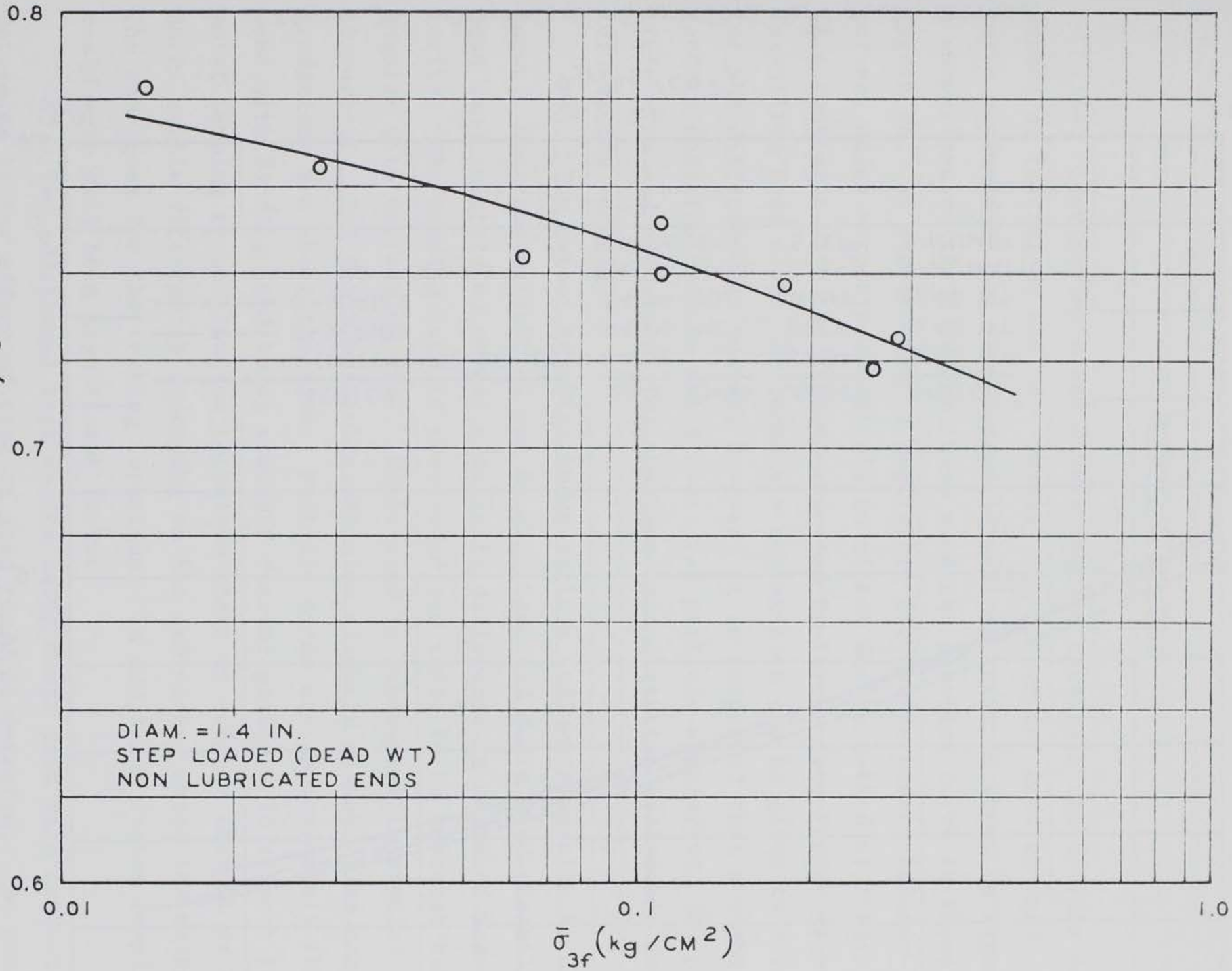

Figure 25. Critical void ratio curve, B-series, Banding Sand

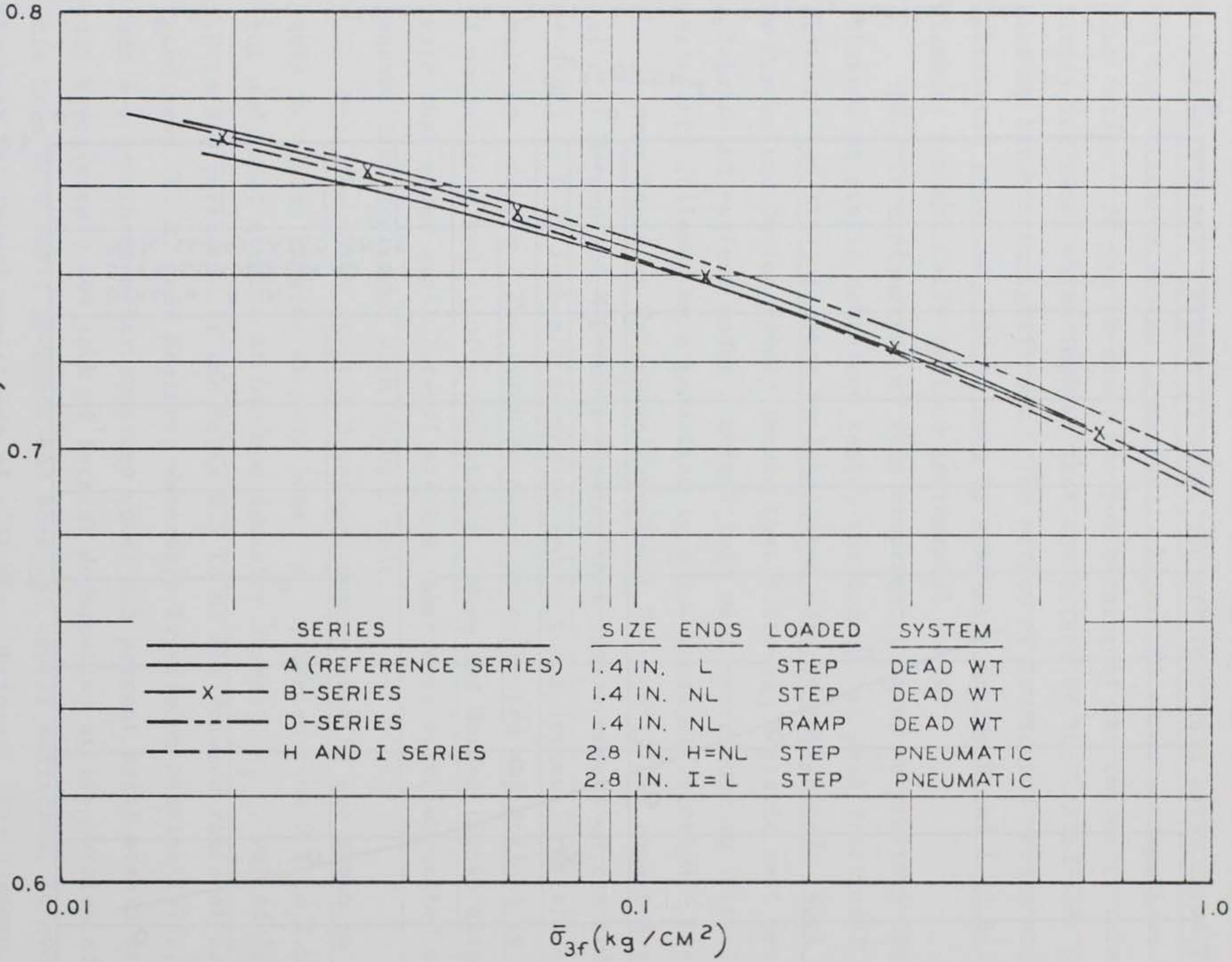

Figure 26. Comparison of critical void ratio curves, all test series, Banding sand

lubricated ends will contribute to a better program for monotonic liquefaction testing.

Method of Loading

84. Test series A and D were used to ascertain the effects of the method of loading on the e_c versus $\bar{\sigma}_{3f}$ curve for Banding Sand. The curve produced by the ramp-loaded (D-series) tests is shown in Figure 27. A comparison of the D-series curve with the A-series curve is shown in Figure 26. As can be seen, a negligible difference exists between the curves, which suggests relatively no effect due to method of loading. This contrasts with the finding reported by Torrey (see Figure 1) using Carrollton Bend sand. No immediate explanation can be given to account for the difference in curves; however, it is suspected that a number of factors contribute among which are: (a) particle angularity, (b) particle size and gradation, (c) specimen reconstitution procedure, and (d) testing technique.

85. The extent to which these factors influence results is unknown. Microphotographs of the Banding Sand and Montz sand (Carrollton Bend sand substitute) reveal a definite difference in terms of angularity. The Banding Sand is subrounded and tends to be somewhat subangular with decreasing size. Montz sand is subangular to angular throughout. The Montz particles are also slightly platey. The sand gradations are about the same. Particle sizes are approximately the same with Banding Sand being somewhat coarser graded. In respect to the moist tamping reconstitution technique there is concern that it produces subtle differences depending on the individual using the method. The same goes for the testing technique. In addition, system compliance could very well be a significant factor.

86. Two additional test series using Montz sand were conducted to determine if any effect of type of load could be detected. The results of the two test series are shown in Figure 28. From the results, absolute certainty of influence could not be determined. However, it could probably be stated that the incrementally loaded specimens tended to

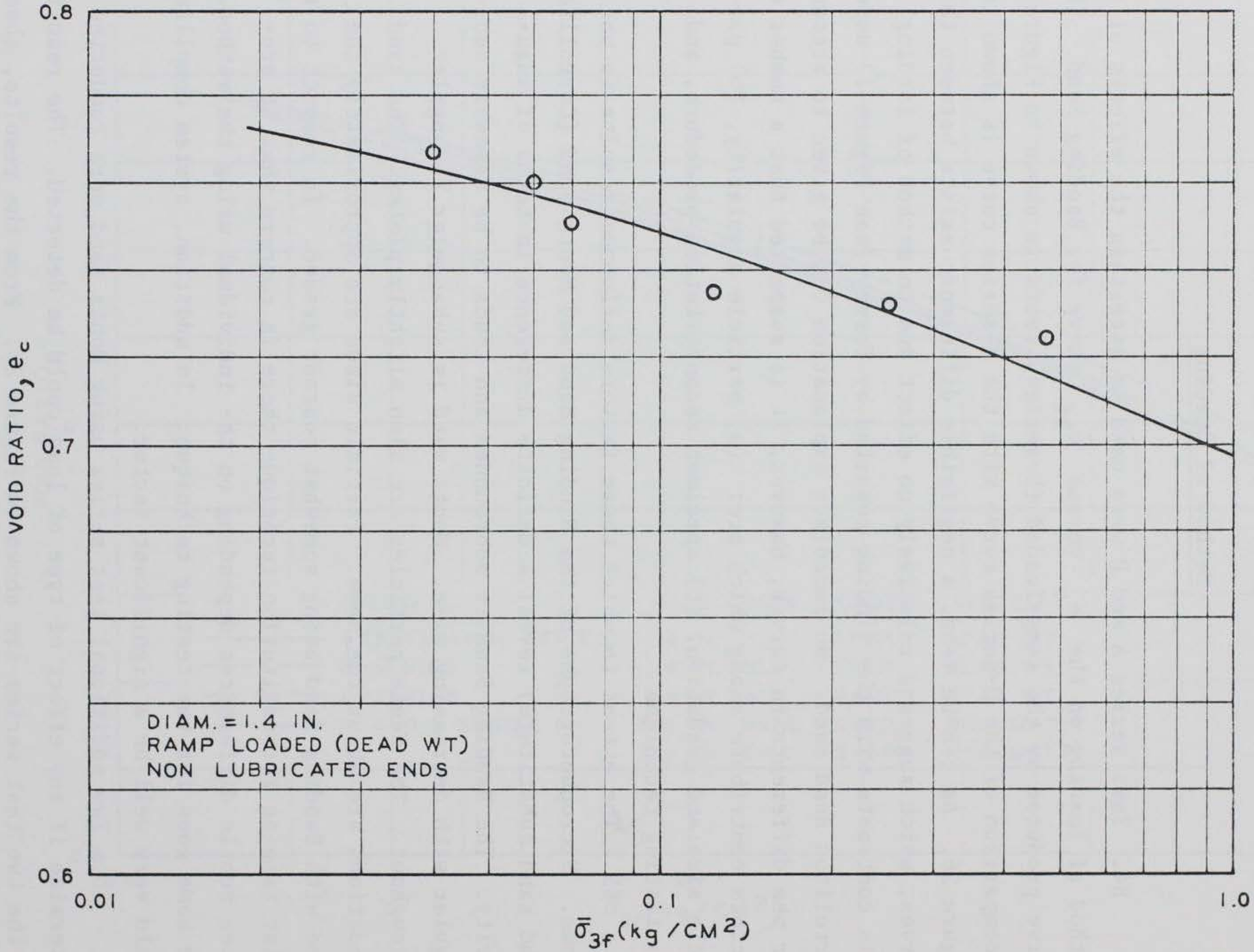

Figure 27. Critical void ratio curve, D-series, Banding Sand

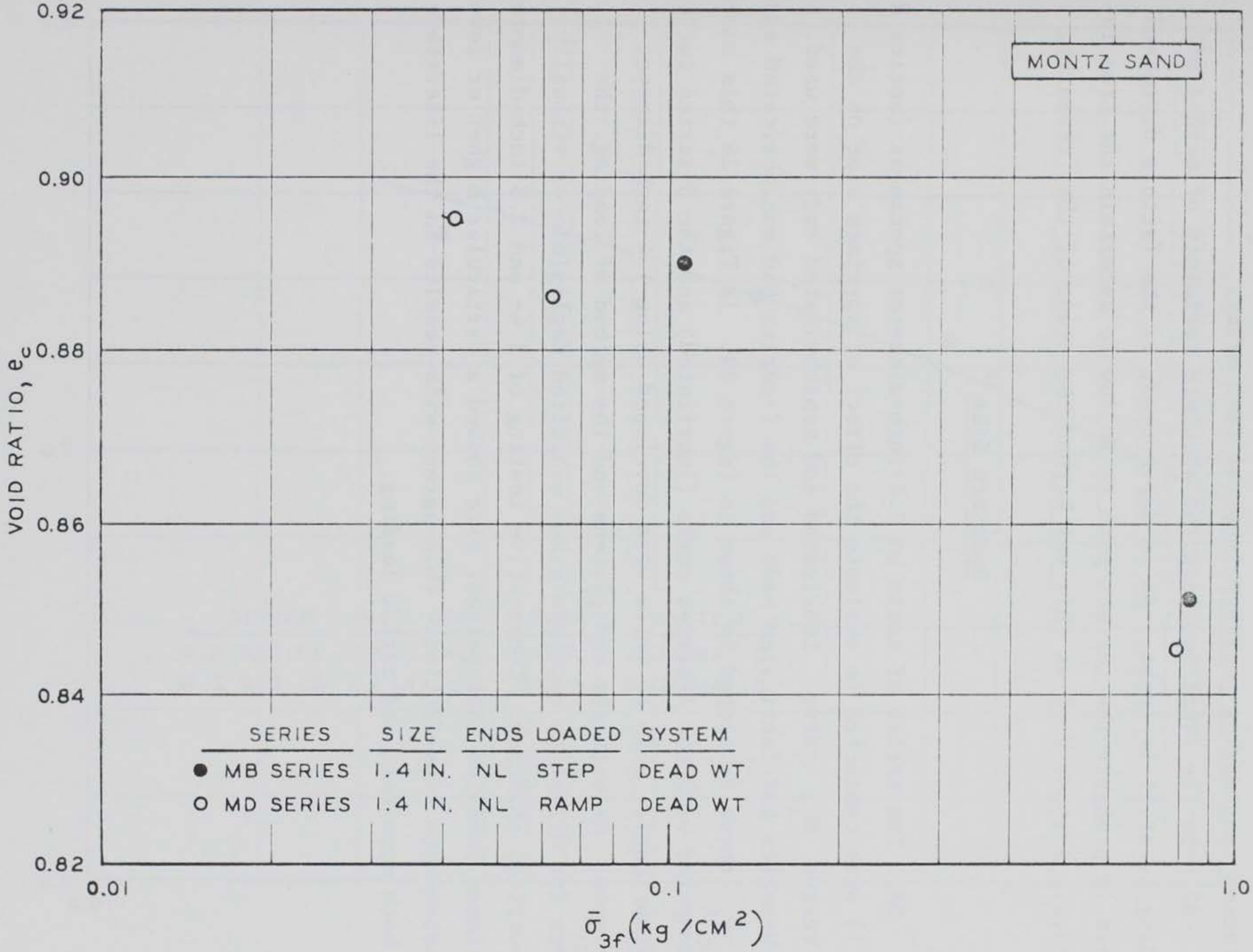

Figure 28. Critical void ratio curve, Montz sand, generated using step and ramp loading

produce a higher critical void ratio curve than the continuous load case. But in view of the limited testing, this would be a very liberal interpretation considering possible inherent test error.

87. In the final analysis the absolute certainty of method of loading is still in doubt. An in-depth study of the factors discussed herein is probably the correct path to follow to ascertain the true influence. A study such as this was beyond the scope of this research.

Specimen Size

88. Two series of tests on 2.8-inch-diameter specimens (series H and I) were conducted to evaluate the effect of specimen size on the e_c versus $\bar{\sigma}_{3f}$ curve. Lubricated and nonlubricated ends were used. The H-series had lubricated ends and the I-series had nonlubricated ends. The $\bar{e}_f$ curve developed is shown in Figure 29. In Figure 26 this curve is compared with the A-series curve (lubricated) and the B-series curve (nonlubricated) both of which were developed using 1.4-inch-diameter specimens. As with the end platens and the method of loading, the curves for different specimen sizes exhibited negligible or virtually no position shifting. Comparative testing of 1.4- and 2.8-inch-diameter specimens revealed that neither size showed a particular higher or lower resistance to liquefaction. This agrees with results in the literature for both monotonic and cyclic loading.

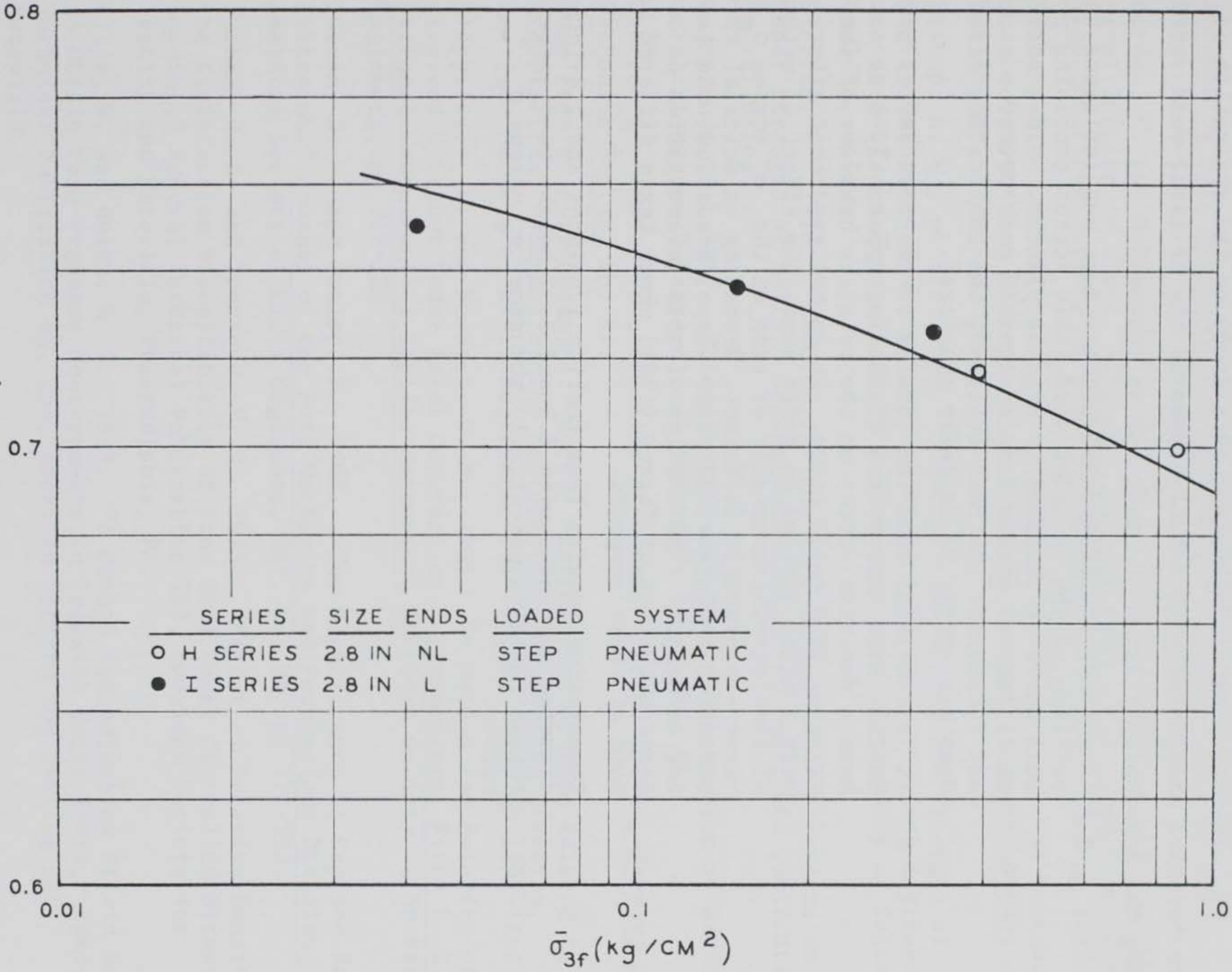

Figure 29. Critical void ratio curve, H and I series, Banding sand

PART VII: CONCLUSIONS

89. The conclusions drawn from this study on the evaluation of uncertainties associated with establishment of the critical void ratio using the monotonic triaxial $\bar{R}$ test are as follows:

a. The use of lubricated end platens does not influence the position of the critical void ratio versus confining pressure curve as compared to regular platens. Since only small lateral strain develops before peak deviator stress and subsequent specimen collapse, the lubricating effect does not appear to be fully mobilized.

b. It is concluded from the results of two test series using Banding Sand that method of loading apparently does not have a decisive effect on the relative behavior of the critical void ratio curve. It is believed that after very limited testing on Montz sand, the effect of method of loading--incrementally or ramp on the e_c versus $\bar{\sigma}_{ef}$ curve--is probably different, depending on material reconstitution technique, particle shape, gradation, and testing technique. The results of this investigation do not agree with that of Torrey (1981) whose tests differed in some of these respects.

c. Comparative results from testing 1.4-inch- and 2.8-inch-diameter specimens with 2.5 and 2.32 height-to-diameter ratios revealed essentially the same e_c versus $\bar{\sigma}_{ef}$ curves.

REFERENCES

Balla, A. 1960. "Stress Conditions in Triaxial Compression," Journal of Soil Mechanics and Foundation Division, Proceedings, American Society of Civil Engineers, Vol 86, SM5, p 57.

Barden, L. and McDermott, J. W. 1965. "The Use of Free Ends in Triaxial Testing in Clays," Journal, Soil Mechanics and Foundations Division, American Society of Civil Engineers, Vol 91, No. SM6, pp 1-23.

Bishop, A. W. and Green, G. E. 1965. "The Influence of End Restraint on the Compression Strength of a Cohesionless Soil," Geotechnique, Vol 15, No. 3, pp 243-265.

Bishop, A. W., et al. 1960. "Factors Controlling the Strength of Partly Saturated Cohesive Soils," American Society of Civil Engineers Research Conf. on Shear Strength of Cohesive Soil, University of Colorado, Boulder, Colo.,

Bjerrum, L. 1954. "Theoretical and Experimental Investigations on the Shear Strength of Soils," Norwegian Geotechnical Institute Publication No. 5, Oslo.

Casagrande, A. 1979. "Liquefaction and Cyclic Deformation of Sands, A Critical Review," Harvard Soil Mechanics Series No. 88.

Castro, G. 1969. "Liquefaction of Sands," Ph. D. thesis, Harvard Soil Mechanics Series, No. 81.

Committee on Soil Dynamics. 1978. "Definitions of Term Related to Liquefaction," Journal of the Geotechnical Engineering Division, American Society of Civil Engineers, Vol 104, No. GT9, pp 1197-1200.

D'Appolonia, E. and Newmark, N. M. 1951. "A Method for Solution of Restrained Cylinder Under Axial Compression," Proceedings, First U. S. National Conference of Applied Mechanics, American Society of Mechanical Engineers, pp 217-226.

Duncan, J. M. and Dunlop, P. 1968. "The Significance of Cap and Base Restraint," Journal of the Soil Mechanics and Foundations Division, American Society of Civil Engineers, SMI, Vol 94, pp 271-290.

Durham, G. N. and Townsend, F. C. 1973. "Effect of Relative Density on the Liquefaction Susceptibility of Fine Sand Under Controlled Stress Loading," Special Technical Publication 523, American Society for Testing and Materials, Philadelphia, Pa.

Ellis, W. and Holtz, W. G. 1959. "A Method for Adjusting Strain Rates to Obtain Pore Pressure Measurements in Triaxial Shear Tests," Special Technical Publication No. 254, American Society for Testing and Materials.

Filon, L. N. G. 1902. "The Elastic Equilibrium of Circular Cylinders under Certain Practical Systems of Load," Philosophical Transactions of the Royal Society, London, Series A, Vol 198, pp 147-233.

Headquarters, Department of the Army. In press. "Laboratory Soils Testing," Engineer Manual EM 1110-2-1906, Office of the Chief of Engineers, Washington, D. C.

Kirkpatrick, W. M., Seals, R. K., and Newman, F. B. 1974. "Stress Distributions in Triaxial Compression Samples," Journal, Geotechnical Engineering Division, American Society of Civil Engineers, Vol 100, No. GT2, pp 190-196.

Lambe, T. W. and Whitman, R. V. 1979. "Series in Soil Mechanics," John Wiley and Sons, New York.

Lee, K. L. and Seed, H. B. 1964. Discussion on "Importance of Free Ends in Triaxial Testing," Journal of the Soil Mechanics and Foundations Division, American Society of Civil Engineers, SM6, Vol 90, pp 173-174.

Mulilis, J. P., Chan, C. K., and Seed, H. B. 1975. "The Effects of Method of Sample Preparation on the Cyclic Stress-Strain Behavior of Sands," Report No. EERC-75-18, University of California, Berkeley.

Olson, R. E. and Campbell, L. M. 1964. Discussion on "Importance of Free Ends in Triaxial Testing," Journal of the Soil Mechanics and Foundations Division, American Society of Civil Engineers, SM6, Vol 90, pp 167-173.

Pickett, G. 1944. "Application of Fourier Method of Solution of Certain Boundary Problems in the Theory of Elasticity," Journal of Applied Mechanics, American Society of Mechanical Engineers, Mech. Eng. 11, A-17.

Raju, V. S., Sadasivan, S. K., and Venkataraman, M. 1972. "Use of Lubricated and Conventional End Platens in Triaxial Test on Sands," Soil and Foundations, Japanese Society of Soil Mechanics and Foundation Engineering, Vol 12, No. 4, pp 35-43.

Rowe, W. D. and Barden, L. 1964. "Importance of Free Ends in Triaxial Testing," Journal of Soil Mechanics and Foundations Division, American Society of Civil Engineers, SMI, Vol 90, pp 1-27.

Roy, M. and Lo, K. Y. 1971. "Effect of End Restraint on High Pressure Tests of Granular Materials," Revue Canadienne de Geotechnique, Vol 8, No. 4, pp 579-588.

Shockley, W. G. and Ahlvin, R. G. 1960. "Nonuniform Condition in Triaxial Compression Test Specimens," Proceedings, Soil Conference on Shear Strength of Cohesive Soils, American Society of Civil Engineers, Boulder, Colo., pp 341-357.

Taylor, D. W. 1941. "Cylindrical Compression Research Program on Stress Deformation and Strength Characteristics of Soils," Seventh Progress Report to U. S. Corps of Engineers, Massachusetts Institute of Technology, Cambridge, Mass.

Torrey, V. H. 1981. "Some Effects of Rate of Loading, Method of Loading, and Applied Total Stress Path on the Critical Void Ratio of Fine Uniform Sand," Ph. D. dissertation, Texas A&M University, College Station, Tex.

U. S. Army Engineer Waterways Experiment Station, CE. 1952. "Potamology Investigation--Summary Report of Soil Stuides," Report No. 12-2, Vicksburg, Miss.

U. S. Army Engineer Waterways Experiment Station, CE. 1970. "The Influence of End Restraint and Method of Consolidation on the Drained Triaxial Compressive Strength of Crushed Napa Basalt," Miscellaneous Paper No. S-70-18, Vicksburg, Miss.

U. S. Army Engineer Waterways Experiment Station, CE. 1976a. "Influence of End Restraint in Cyclic Triaxial Tests," Report No. S-76-1, Vicksburg, Miss.

U. S. Army Engineer Waterways Experiment Station, CE. 1976b. "The Effects of Cyclic Triaxial Testing Techniques on the Liquefaction Behavior of Monterey No. 0 Sand," Miscellaneous Paper No. S-76-6, Vicksburg, Miss.

U. S. Army Engineer Waterways Experiment Station, CE. 1977. "Effect of Frictionless Caps and Bases in Cyclic Triaxial Tests," Contract Report No. S-77-1, Vicksburg, Miss.

Wang, M. S. 1972. "Liquefaction of Triaxial Sand Samples Under Different Frequencies of Cyclic Loading," M.S. thesis, University of Western Ontario, London, Canada.

APPENDIX A: SYNOPSIS OF TEST PROCEDURE, TRIAXIAL EQUIPMENT, AND MATERIAL USED BY CASTRO

Description and Property of the Sand

1. The sand used was a sand sold by the Ottawa Silica Co., Ottawa, Ill., under the trade name of Banding Sand. It is manufactured from the St. Peter Sandstone by screening and washing. It is a uniform, clean, fine quartz sand with subrounded to subangular grains. The specific gravity of the grains is 2.65. The sand's D_{10} size is 0.097 mm and its coefficient of uniformity 1.8.

2. The maximum void ratio was determined by pouring ovendried sand through a funnel to which was attached 0.5 cm below its tip a horizontal piece of cardboard from which the sand spilled into a 7.3-cm-diameter and 10.1-cm-high mold. The cardboard was kept at a distance of not more than 3 mm over the surface of the sand in the mold, and a spiral motion was described with the funnel in order to keep the surface of the sand approximately level at all times. An average of three such determinations gave a maximum void ratio of 0.84.

3. The minimum void ratio was determined on ovendried sand using the same mold as above by hammering forcefully the sides of the mold and also over a plate on top of every one of three layers. An average of three such determinations gave a minimum void ratio of 0.50.

Triaxial Equipment

4. The equipment consists essentially of an instrumented triaxial cell and a loading device. One of the triaxial cells in existence in the Harvard Soil Mechanics Laboratory was modified to install a force transducer to measure the axial load and also to use lubricated ends. The triaxial cell is designed to test specimens 1.4 inches in diameter and 3.5 inches high. The axial load is applied by a 3/8-inch-diameter piston, which is guided by two ball bushings and has a grease seal to control leakage. A piston of 1/4-inch diameter with a similar arrangement was also used during this investigation.

5. The loading device consists of a loading yoke with a hanger for the weights with which the load is applied. Counterweights to

balance the deadweight of the yoke and hanger are applied through a pulley arrangement consisting of a flexible steel cable passing over a 24-inch bicycle wheel. The total weight of the loading system (chiefly loading yoke and counterweight) is about 30 kg.

6. The lubricated ends used are of the type developed by Rowe in England. A high vacuum silicone grease made by Dow Corning Corp., Mich., was used for lubrication. (A stopcock silicone grease was first used, but its viscosity was not high enough and the grease flowed from under the rubber disc and into the porous element.)

Instrumentation

7. In those specimens which developed liquefaction, the rate of deformation was very fast after the failure had been induced, which made it necessary to use electrical transducers to measure axial load, pore pressure, and axial deformation when the rate of deformation was fast. Three force transducers, for different load ranges, manufactured by Dynisco, Cambridge, Mass., were used that had the following characteristics:

Model	FT1-50	FT2-1C	FT2SP-2C
Force range, lb	0 to 50	0 to 100	0 to 100
Natural frequency cycles/second	12,000	10,000	10,000
Repeatability, percentage of full scale	0.1	0.1	0.1
Excitation voltage, vDC	6	6	6
Output, mv/kg	0.958	0.615	0.253

8. Two pressure transducers were used to measure the pore pressure. One of them is the model GT-20 manufactured by General Transducer Co., Santa Clara, Calif., which has a pressure range of 0- to 250-psi absolute pressure. Its natural frequency is 50,000 cycles/second and its repeatability is 0.1 percent of full scale. It works with an excitation voltage of 10 vDC and it has an output of 1.752 mv/kg/cm^2. The other pore pressure transducer used is the model PM 131TC, manufactured

by Statham Instruments, Inc., Los Angeles, Calif. It measures the difference between the pressure applied to a diaphragm (the pore pressure) and that applied through a reference pressure port (the chamber pressure) and it is referred to as a differential pressure transducer. It has a range for the pressure difference of 15 psi, and a maximum pressure of 65 psi, the limit of which applies to the larger pressure. It has a natural frequency of 8,500 cycles/second and a maximum combined hysteresis and linearity of 0.75 percent of full scale. It works with an excitation voltage of 5 vDC and it has an output of 18.25 mv/kg/cm^2.

9. A displacement transducer was used to measure the axial deformation during the stages of the tests in which the rate of deformation was too fast to read a conventional dial extensometer. The model selected for this investigation was the model 7DCDT-500 manufactured by Sanborn Co., Waltham, Mass. It has a total range of displacement of 1 inch. It works with an excitation voltage of 6 vDC and it has an output of 6.8 v/inch. It has a maximum nonlinearity of 0.5 percent of full scale and a ripple of 1.2 percent of full scale. It was mounted in the same location as a conventional dial extensometer. It has a moving core loosely fitted into the bore of the core assembly such that, when used in a vertical position, the core is free to follow downward vertical movements up to accelerations of practically 1 g. A conventional dial extensometer was also mounted and because of its greater accuracy it was used whenever the deformations occurred slowly enough to make its reading possible.

10. Two power supplies, model 2005, manufactured by Power Designs, Inc., were used to provide a stable excitation voltage to the transducers. The output voltage provided by these power supplies may be selected from 0 to 20 v, and it would change a maximum of 100 microvolts for a change in load of 100 percent. Its calibration is better than 0.1 percent of the selected voltage + 1 mv.

Test Procedure

Sample preparation

11. The sand was compacted inside a thin rubber membrane supported by a 1.4-inch-diameter by 3.5-inch-high split mold. The sand was mixed with 5 percent distilled water before compaction. Compaction was performed by applying the static weight of a 0.5-inch-diameter aluminum tamper 12 times on the surface of each of 10 layers. The weight of the tamper was varied between 0.3 and 2.7 kg, to achieve the desired relative density between zero and 65 percent. The water content of 5 percent produces bulking of the sand, which has the advantage of reducing substantially the sensitivity to vibrations of the sand in the loose condition.

12. After compaction the top cap was installed and the membrane rolled around it. Vacuum was applied to the interior of the specimen and the mold was removed. One or two additional membranes (depending on the confining pressure to be used) were placed around the specimen and secured to the top and bottom caps by means of O-rings. At this stage the specimen was subject to an effective confining pressure of 0.95 kg/cm^2 applied by the vacuum. The diameter of the specimen was measured in six locations with a dial gage caliper reading to 0.001 in. After the triaxial cell was assembled, the height of the specimen was determined by measuring the distance from the top of the piston to the top of the cell using a dial caliper reading to 0.01 cm.

13. From these measurements the volume of the specimen at this stage of the test was computed. The dry unit weight, the void ratio, and the relative density were computed from the known dry weight of sand used in the specimen. These quantities were used as basic references for determination of all subsequent changes in void ratio and relative density.

Saturation and consolidation

14. The triaxial cell was centered on the loading platform. An initial cell pressure of 1 kg/cm^2 was applied while keeping the drainage valves closed, except in those tests in which $\bar{\sigma}_c$ was less than

1 kg/cm^2. De-aired water was then allowed to flow into the specimen through the bottom cap until the vacuum was reduced to zero. Using a small gradient (about 10 cm of water head), 3 to 5 cm^3 of de-aired water was forced through the specimen in an upward direction until no more air bubbles were observed coming from the top of the specimen. Then a back-pressure of 4 kg/cm^2 was applied to ensure saturation and, finally, for $\bar{\sigma}_c$ larger than 1 kg/cm^2, the effective confining pressure was increased to either 4 or 10 kg/cm^2. The volume decrease caused by the increase in effective confining pressure above 1 kg/cm^2 was measured directly by means of a burette connected to the interior of the fully saturated specimen.

Axial loading

15. After the consolidation stage of the test was completed, the valves were closed and the axial load was applied in increments, usually in 1-minute intervals. The magnitude of the load increments varied according to the expected behavior of the specimen. In those cases in which an abrupt failure was anticipated, the magnitude of the load increments was decreased as failure was approached, from about 10 percent to about 2 percent of the failure load.

APPENDIX B: LISTING OF COMPUTER PROGRAM GDHERB

```
*#RUN GDHERB=(FORM)#02;23
C       08.02.09 07/1681 GDHERB PRG.    USERID: ROSELIQ
C
C       DATA REDUCTION FOR ANISOTROPIC CONSOLIDATED R TEST
C
C
C      GGG      DDDD       H    H   EEEEEE   RRRRR     BBBBB
C     G         D   D      H    H   E        R    R    B    B
C     G  GGG    D    D     HHHHHH   EEEE     RRRRR     BBBBB
C     G   G     D    D     H    H   E        R  R      B    B
C      GGG      DDDD       H    H   EEEEEE   R   R     BBBBB
C
C       PROGRAMMED BY G. DURHAM, MODIFIED BY VIC TORREY
C       CONVERTED TO THE 600-SERIES 07/16/74 BY ARDEN PARK
C       CALCMP PLOTTING 'OPTION' ADDED JULY 1975, BY ARDEN PARK
C       MODIFIED FOR USE BY HERBIE! 04/03/81
C       SUPPORTING FILES FOR THIS PROGRAM INCLUDE:
C           (1) GDATA - - INPUT DATA FILE
C           (2) XYPLT - - PLOTTING SUBROUTINES
C           (3) PCARD - - CARDIN SYSTEM DRIVER FILE
C
C     ---AC           AREA OF SPECIMEN AFTER CONSOLIDATION
C     ---CT`          CHAMBER PRESSURE
C     ---HAC          HEIGHT AFTER CONSOLIDATION
C     ---XLD(I)       LOAD
C     ---DEFL(I)      VERTICAL DEFLECTIONS
C     ---PP(I)        PORE PRESSURES
C     ---ESIG3        INITIAL EFFECTIVE CONFINING PRESSURE
      CHARACTER AN2*36, CRD*80,  TST*12, FNA*4(4)/'/', '*', '*', ';'/
      DIMENSION XLD(32), DEF(32), PP(32), STRAIN(32)
C   - DATA FILE ATTACHMENT -
  100 CONTINUE
          PRINT, 'NAME OF DATA FILE'
          READ 104, FNA(2), FNA(3)
  104     FORMAT (2A4 )
          CALL ATTACH(01, FNA, 3, 0, K1, )
          K2 = FLD(6, 6, K1)
      IF(K2.EQ.0 .OR. K2.EQ.31) GO TO 108
          PRINT, 'ERROR IN ATTACHING DATA FILE'
          PRINT, 'TRY AGAIN...'
          PRINT:
      GO TO 100
  108 CONTINUE
C
  112 READ (01, 116, END=168) AN2
  116     FORMAT (3X, A36)
      READ (01, 118, END=168) CRD
  118 FORMAT(A80)
```

```
      ULF = 0.196
      DECODE(CRD, 120) LNE, TST, CP, N, ULF
  120    FORMAT( V )
      WRITE(23, 124) AN2, TST
  124    FORMAT ('1',  //// , 'TEST: ', A36 // 'SPECIMEN NUMBER: ',
     &       A12 /// 5X, 'TABLE 1 -', 2X, 'INITIAL TEST CONDITIONS' / )
      WRITE(02, 120) 'TEST: ', TST, N
      CALL GDFOR(AC, HAC)
      DO 128 I = 1, N
         READ (01, 120, END=168) LNE, XLD(I), DEF(I), PP(I)
  128 CONTINUE
      ESIG3 = (CP - PP(1)) * 0.0703
      WRITE(23, 132) ESIG3
      WRITE(02,134) ESIG3
  134 FORMAT('EFF CONFINING PRESS: 'F3.0)
  132    FORMAT ( / , 'THE EFFECTIVE CONFINING PRESSURE =',
     &       F5.2, 2X, 'KG/CM2',  / )
      WRITE(23, 136)
  136    FORMAT ( // 5X, 'AREA', 9X, 'HEIGHT', 11X,
     &       'BACK', 10X, 'LOAD',  / , 5X, 'AFTER', 8X,
     &       'AFTER', 10X, 'PRESSURE', 9X, 'ON',  / , 5X,
     &       'CONS', 10X, 'CONS', 26X, 'SPEC', 10X, 'CP',
     &        / , 5X, 'SQ IN', 10X, 'IN', 13X, 'PSI',
     &       11X, 'LBS', 10X, 'PSI',  / )
      WRITE(23, 140) AC, HAC, PP(1), XLD(1), CP
  140    FORMAT (5X, F5.3, 8X, F5.3, 10X, F6.2, 8X, F6.2, 8X, F6.2)
      WRITE(23, 144)
  144    FORMAT ( // , 5X, 'TABLE 2 - TEST DATA',  /
     &       , 5X, 'PISTON', 8X, 'VERTICAL', 11X, 'PORE',
     &        / , 6X, 'LOAD', 11X, 'DEFL', 11X, 'PRESSURE',
     &        / , 5X, '(LBS)', 11X, '(IN)', 12X, '(PSI)',  / )
      WRITE(23, 148) (XLD(I), DEF(I), PP(I), I = 1, N)
  148    FORMAT (5X, F6.2, 9X, F6.4, 10X, F6.2)
      WRITE(23, 152)
  152    FORMAT ('1',  //// 5X, 'TABLE 3 - TEST RESULTS'
     &      / 10X, 'IND PORE', 3X, 'DEVIAT', 5X, 'EFF',
     &       5X, 'EFF', 5X, 'RATIO', 3X, 'NORMAL', 4X,
     &       'SHEAR' / 'STRAIN', 3X, 'PRESSURE', 3X,
     &       'STRESS', 3X, 'SIGMA 1', 1X, 'SIGMA 3', 2X,
     &       'SIGMA 1', 2X, 'STRESS', 4X, 'STRESS',  / ,
     &       4X, '%', 6X, 'KG/CM2', 4X, 'KG/CM2', 3X,
     &       'KG/CM2', 2X, 'KG/CM2', 3X, 'SIGMA 3', 2X,
     &       'KG/CM2', 4X, 'KG/CM2',  / ).
C
C     BEGIN CALCULATING STRAIN,DEVIATOR STRESS (DEVS),EFFECTIVE
C     CONFINING PRESSURE = SIGMA 3 BAR (EFFCP), SIGMA 1 BAR
C     (EMAXPS), RATIO OF SIGMA 1 TO SIGMA 3 (RATIO). NORMAL
C     STRESS AND SHEAR STRESS CALCULATED ON BASIS EFFECTIVE
C     FRICTION ANGLE = 30 DEGREES.
```

```
      DO 164 I = 1, N
         STRAIN(I) = (DEF(I) - DEF(1)) / HAC
         STR = STRAIN(I) * 100.
         ACORR = AC / (1. - STRAIN(I))
         UF2 = 2.167
         IF(ULF .GT. 0.2) UF2 = 2.00
         UPLIFT = ULF*CP - UF2
         DEVS = ((XLD(I) - UPLIFT) * 0.0703) / ACORR
         CPP = PP(I) - PP(1)
         DPP = CPP * 0.0703
         EFFCP = (ESIG3) - DPP
         EMAXPS = (DEVS + EFFCP)
         RATIO = EMAXPS / EFFCP
         XNS = EFFCP + (DEVS / 4.)
         SS = DEVS * 0.433
         WRITE(23, 156) STR, DPP, DEVS, EMAXPS, EFFCP, RATIO, XNS, SS
  156       FORMAT (F6.2, 2F10.2, F9.2, F8.2, 2F9.2, F10.2)
C
C    -    STORE PLOTTING DATA -
            XV2 = (EMAXPS+EFFCP) / 2.0
            YV2 = (EMAXPS-EFFCP) / 2.0
            WRITE(02, 160) STR, DPP, DEVS, XV2, YV2
  160       FORMAT( 5F8.2 )
  164 CONTINUE
C
      GO TO 112
  168 CONTINUE
         PRINT, '    DATA OUTPUT FILE: '23''
         PRINT, '    PLOT FILE: '02''
      STOP
      END
C      08.02.10 04/23/81 GDFOR SBR    USERID: ROSELIQ
      SUBROUTINE GDFOR(AC, HAC)
C
      READ(01,1004) LNE, AIS, HINT, DW, CHAS, VC, HC
C        WHERE:
C          AIS = INITIAL AREA OF SPECIMEN (SQ CM)
C          HINT = INITIAL HEIGHT OF SPECIMEN (CM)
C          DWT = DRY WEIGHT OF SOLIDS (GMS)
C          CHAS = CHANGE IN HEIGHT DURING DEAIRING
C          VC = CHANGE IN VOLUME DURING CONSOLIDATION (CC)
C          HC = CHANGE IN HEIGHT DURING CONSOLIDATION (IN)
C
C    - IDATA CONSTANTS --
C
C      SPECIFIC GRAVITY
         GSP = 2.65
C      MAXIMUM VOID RATIO
      EMX = 0.84
```

```
C      MINIMUM VOID RATIO
          EMN = 0.34
C
C    - INITIAL CONDITIONS -
C
C      INITIAL VOLUME
          VINT = AIS * HINT
C      INITIAL DRY DENSITY
          DDINT = DW / VINT
C      INITIAL VOID RATIO
          EINT = (GSP /DDINT) - 1.0
C      INITIAL RELATIVE DENSITY
          RDINT = ((EMX-EINT)/EMN) * 100.0
C
C    - CONDITIONS AFTER DEAIRING AND SATURATION -
C
C      HEIGHT AFTER SATURATION
          HAS = HINT - 2.54*CHAS
C      AREA AFTER SATURATION
          AAS = AIS * (HINT - 5.08*CHAS) / HINT
C      VOLUME AFTER SATURATION
          VAS = AAS * HAS
C      DRY DENSITY AFTER SATURATION
          DDAS = DW / VAS
C      VOID RATIO AFTER SATURATION
          EAS = (GSP/DDAS) - 1.0
C      RELATIVE DENSITY AFTER SATURATION
          RDAS = ((EMX-EAS)/EMN) * 100.0
C
C    - CONDITIONS AFTER CONSOLIDATION -
C
C      AREA AFTER CONSOLIDATION
          AC = (VAS-VC) / (HAS - 2.54*HC)
C      HEIGHT AFTER CONSOLIDATION
          HAC = (HAS - 2.54*HC) / 2.54
C      VOLUME AFTER CONSOLIDATION
          VAC = VAS - VC
C      DRY DENSITY AFTER CONSOLIDATION
          DDC = DW / VAC
C      VOID RATIO AFTER CONSOLIDATION
          EC = (GSP/DDC) - 1.0
C      RELATIVE DENSITY AFTER CONSOLIDATION
          RDC = ((EMX-EC) / EMN) * 100.0
C
          WRITE(23, 1008) AIS, DDINT, EINT, RDINT, AAS, DDAS, EAS, RDAS,
     &    AC, DDC, EC, RDC
          WRITE(02, 1012) RDINT, RDC, EINT, EC
C
          AC = AC / 6.452
```

```
C
      RETURN
 1004 FORMAT( V )
 1008 FORMAT(//16X, 'SPECIMEN', 5X, 'DRY', 14X, 'RELATIVE'/ 18X,
     &   'AREA', 5X, 'DENSITY', 4X, 'VOID', 5X, 'DENSITY'/
     &   'CONDITIONS', 7X, 'SQ CM', 5X, 'GM/CC', 5X, 'RATIO', 4X,
     &   'PERCENT'// '  INITIAL', 3X, 2F10.2, F11.3, F9.1/
     &   '  AFTER SAT.', 2F10.2, F11.3, F9.1/ '  AFTER CONS.', F9.2,
     &   F10.2, F11.3, F9.1)
 1012 FORMAT(2F10.2, 2F10.4)
      END
```

*

APPENDIX C: TEST DATA

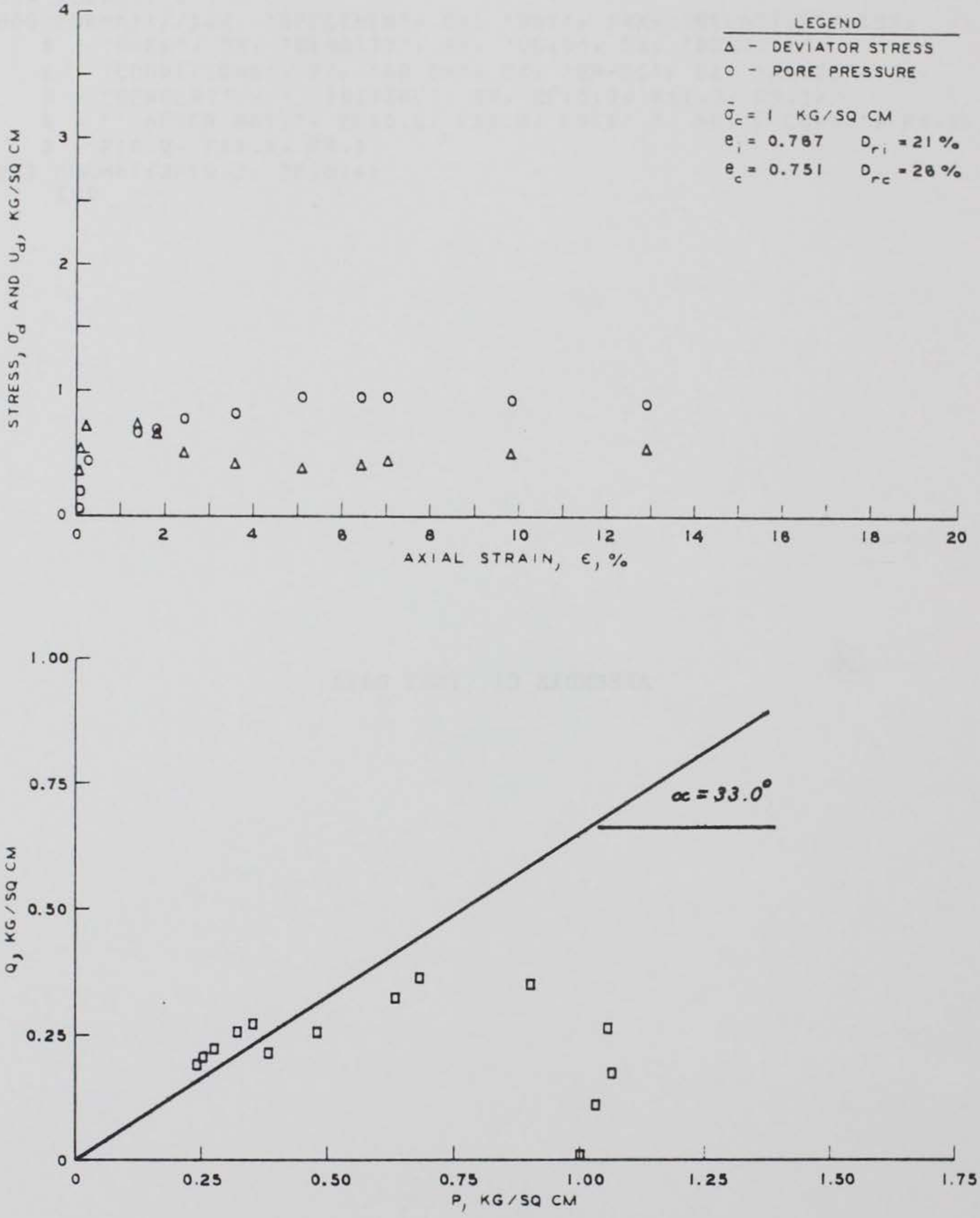

Figure C1. Results of $\bar{R}$ Test A1

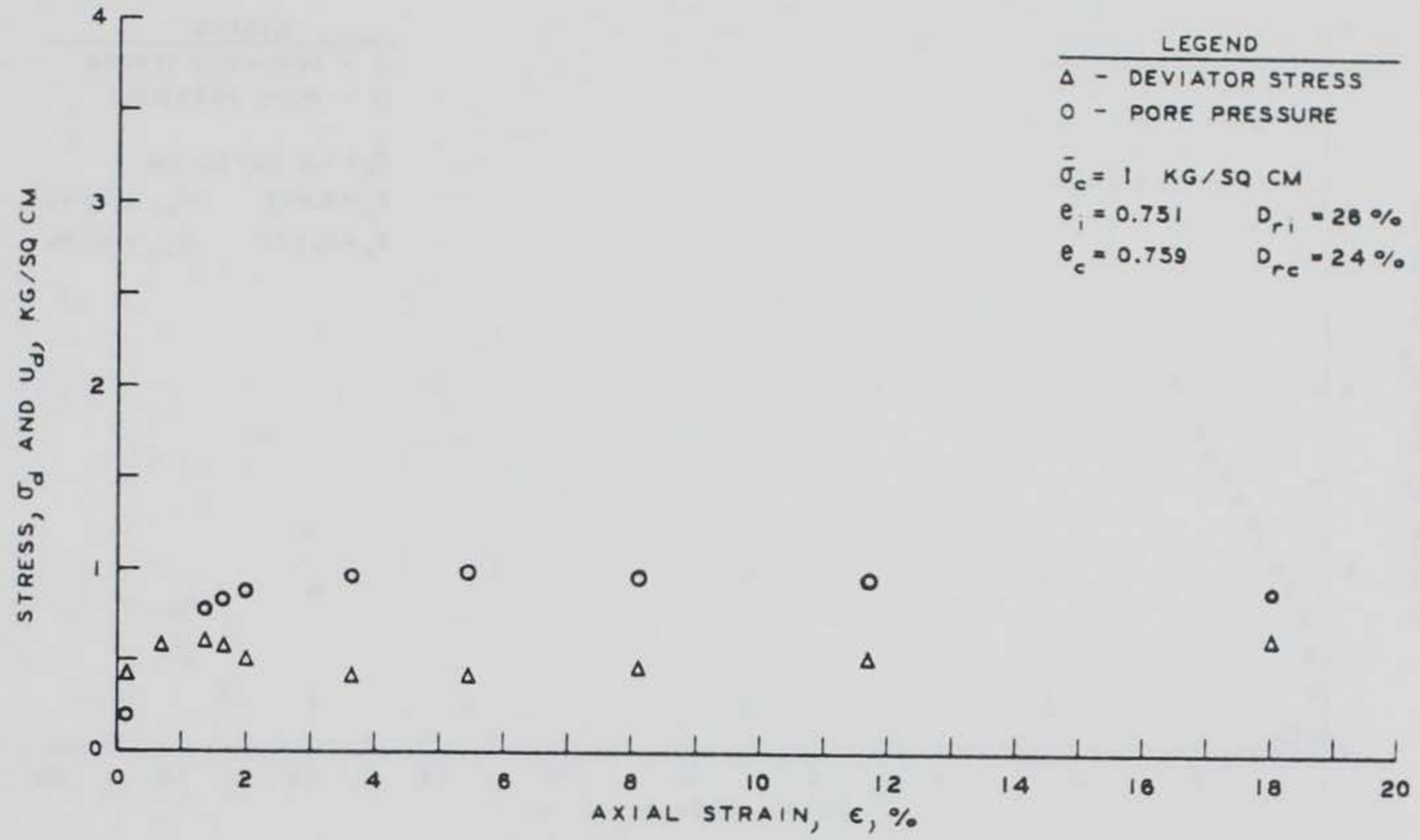

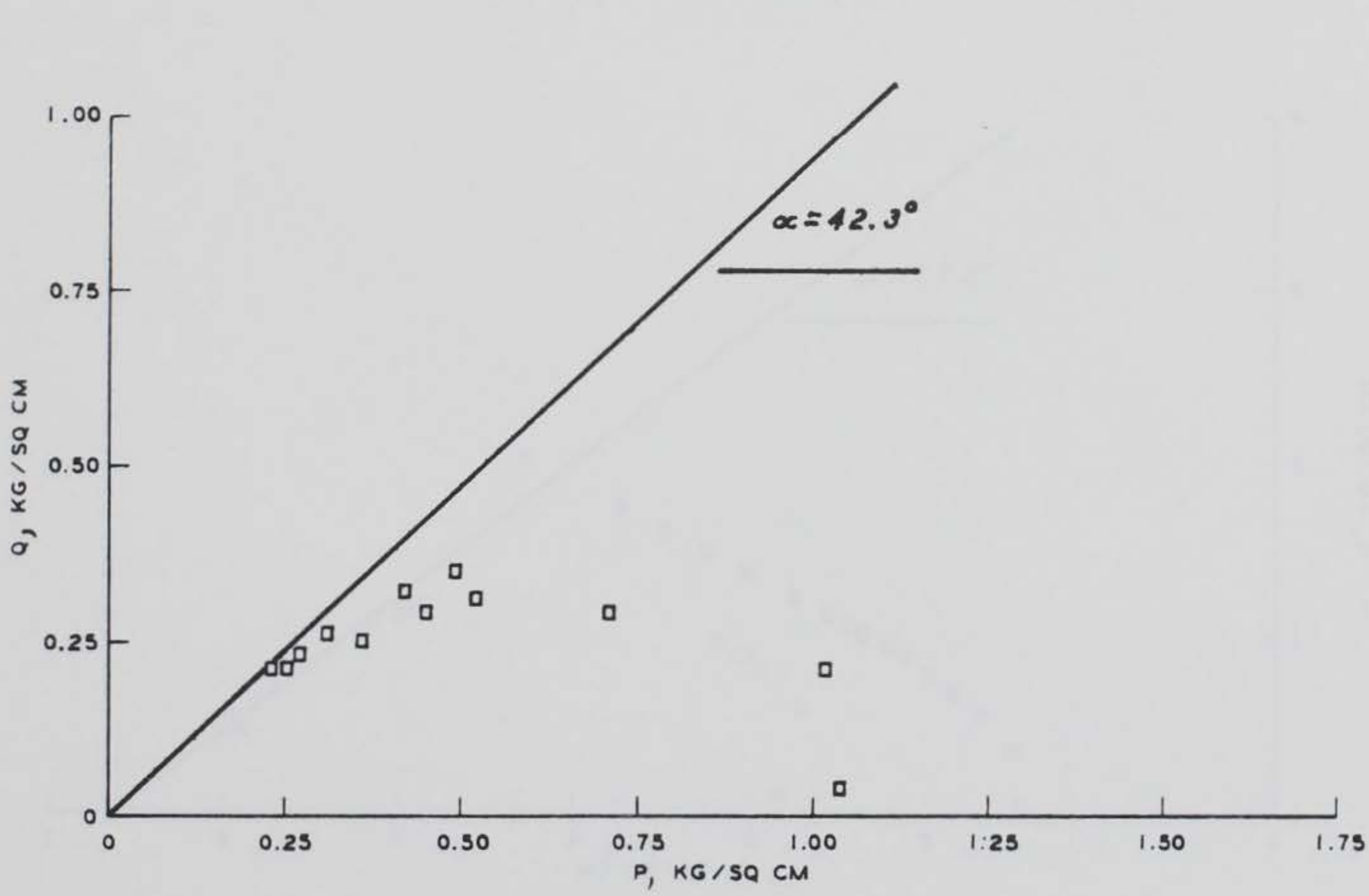

Figure C2. Results of $\bar{R}$ Test A2

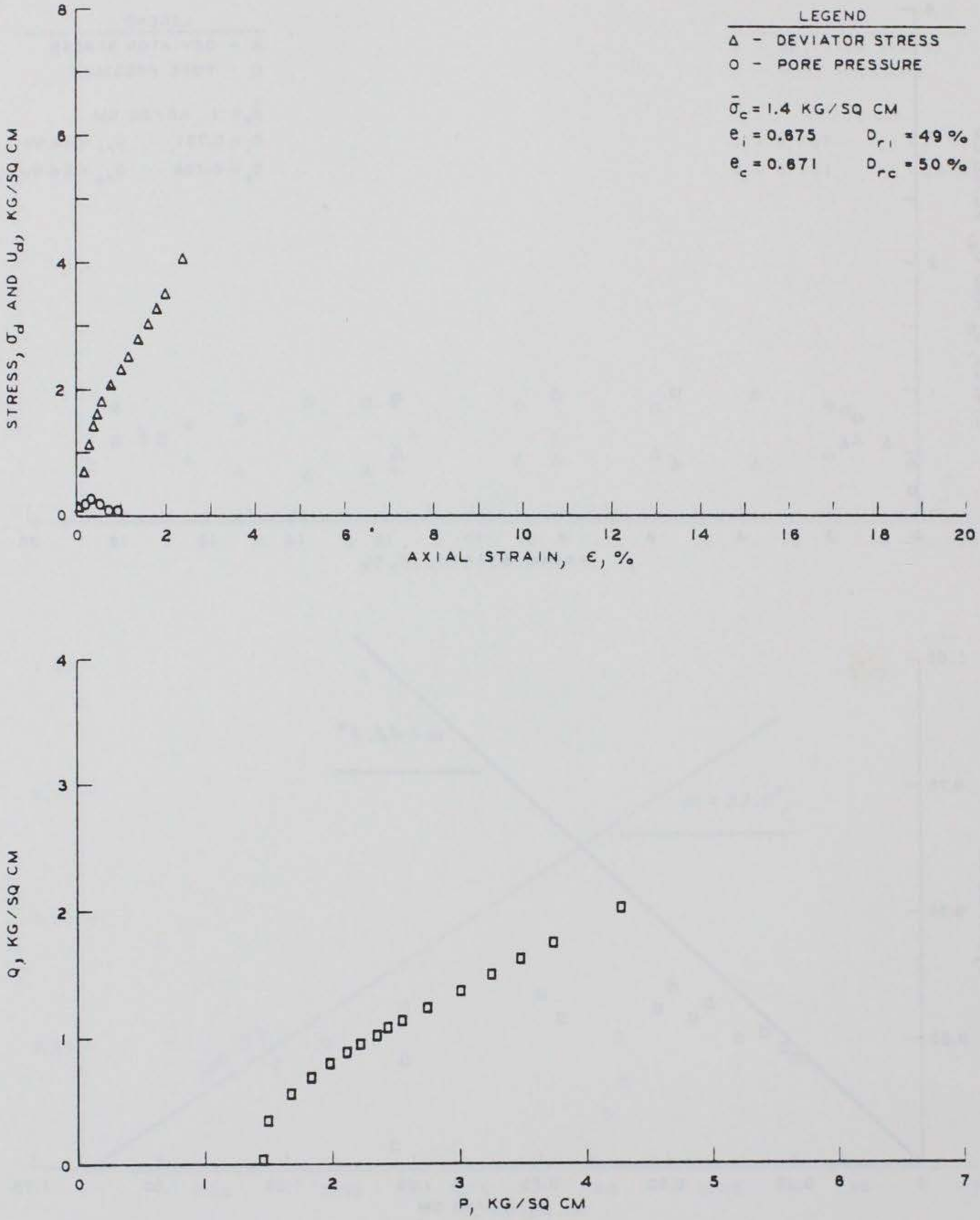

Figure C3. Results of $\bar{R}$ Test A3

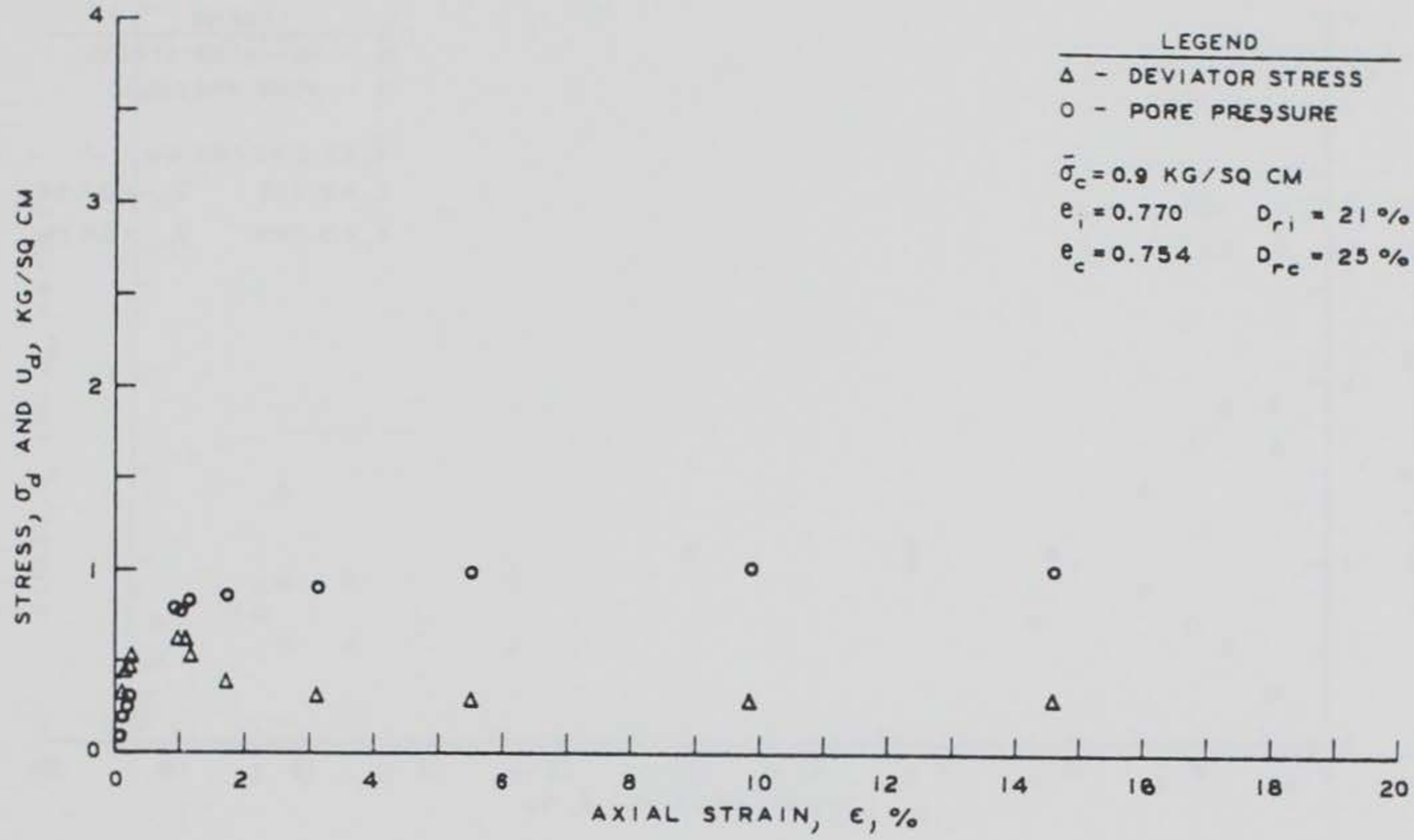

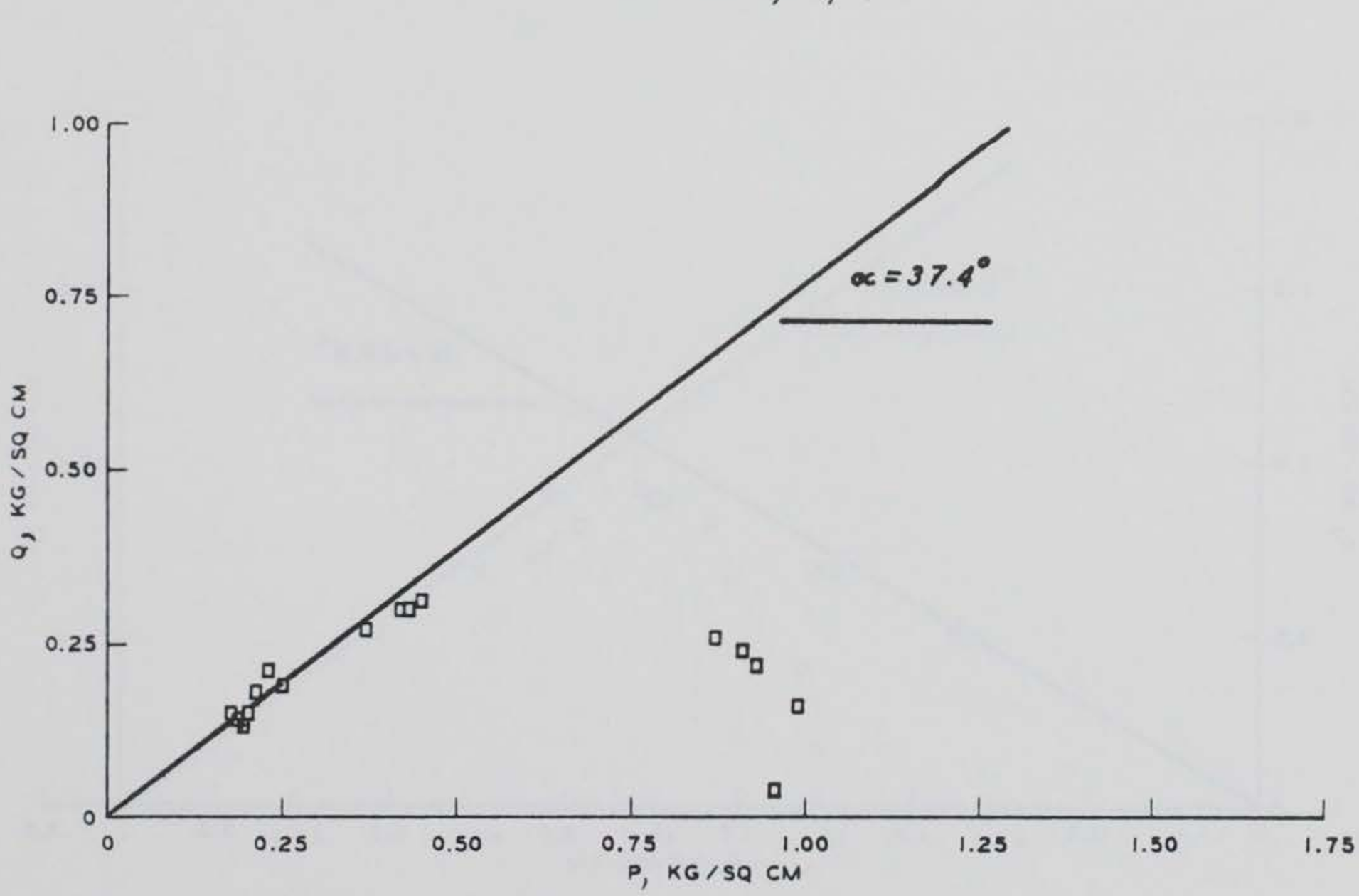

Figure C4. Results of $\bar{R}$ Test A4

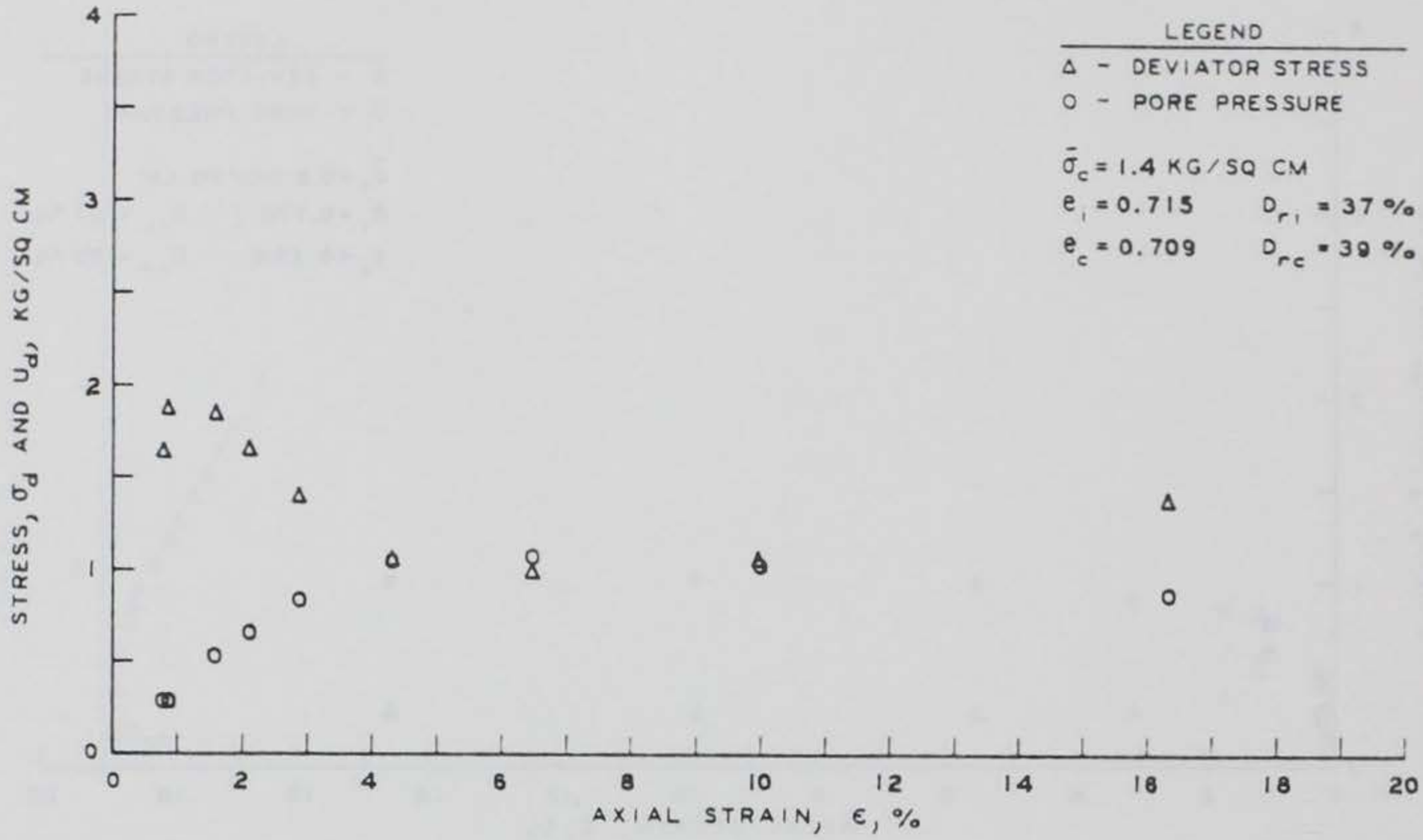

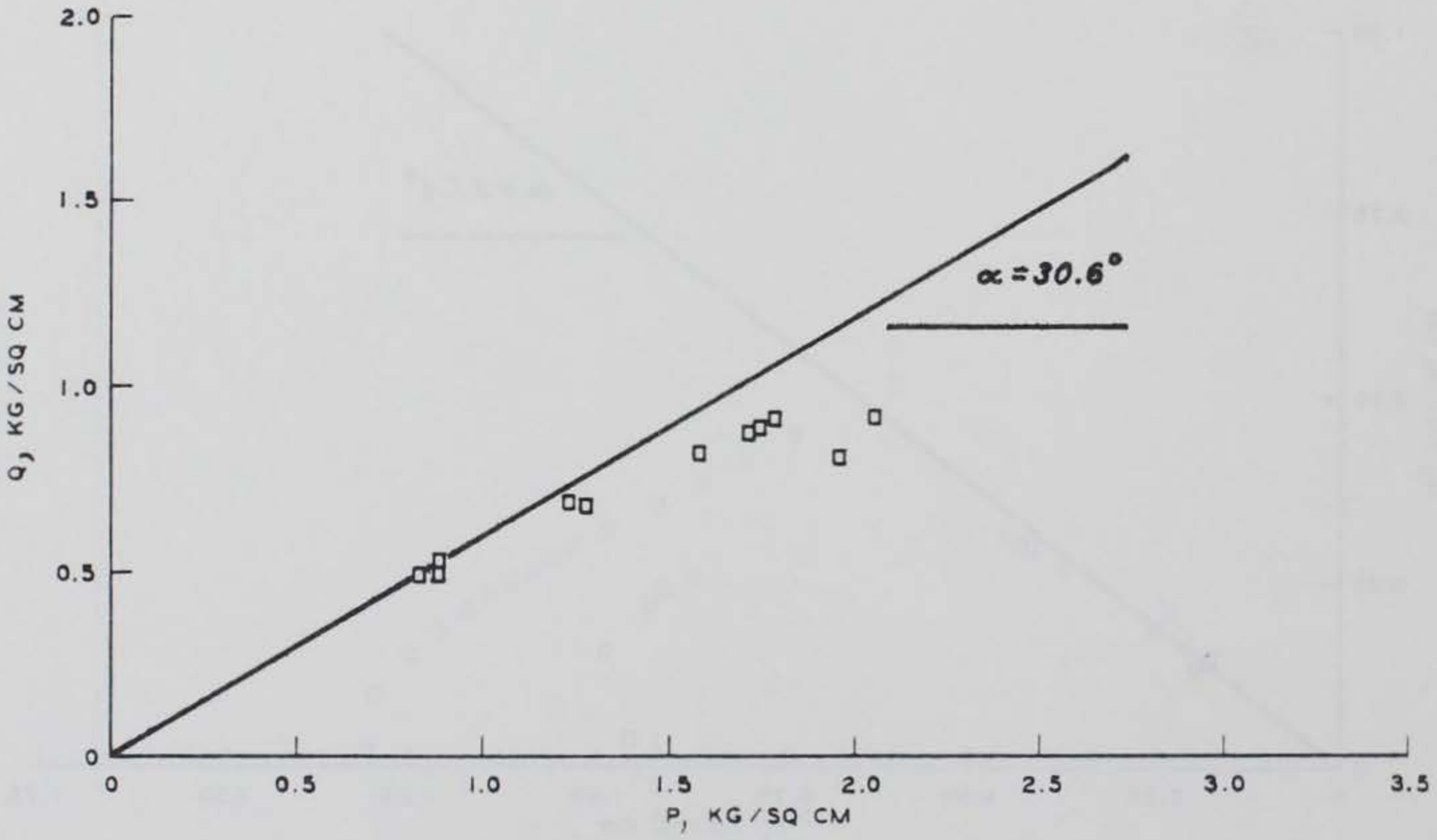

Figure C5. Results of $\bar{R}$ Test A5

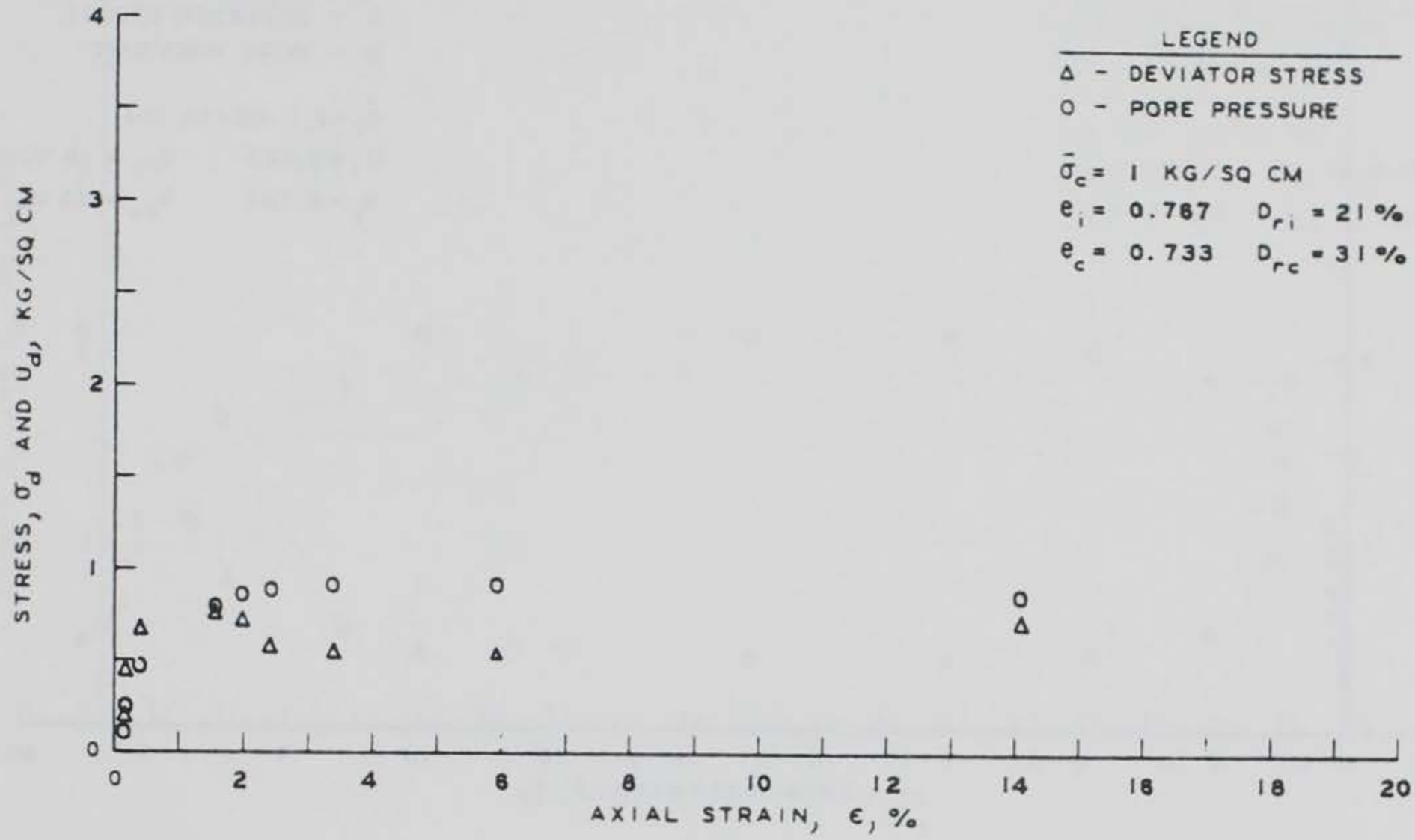

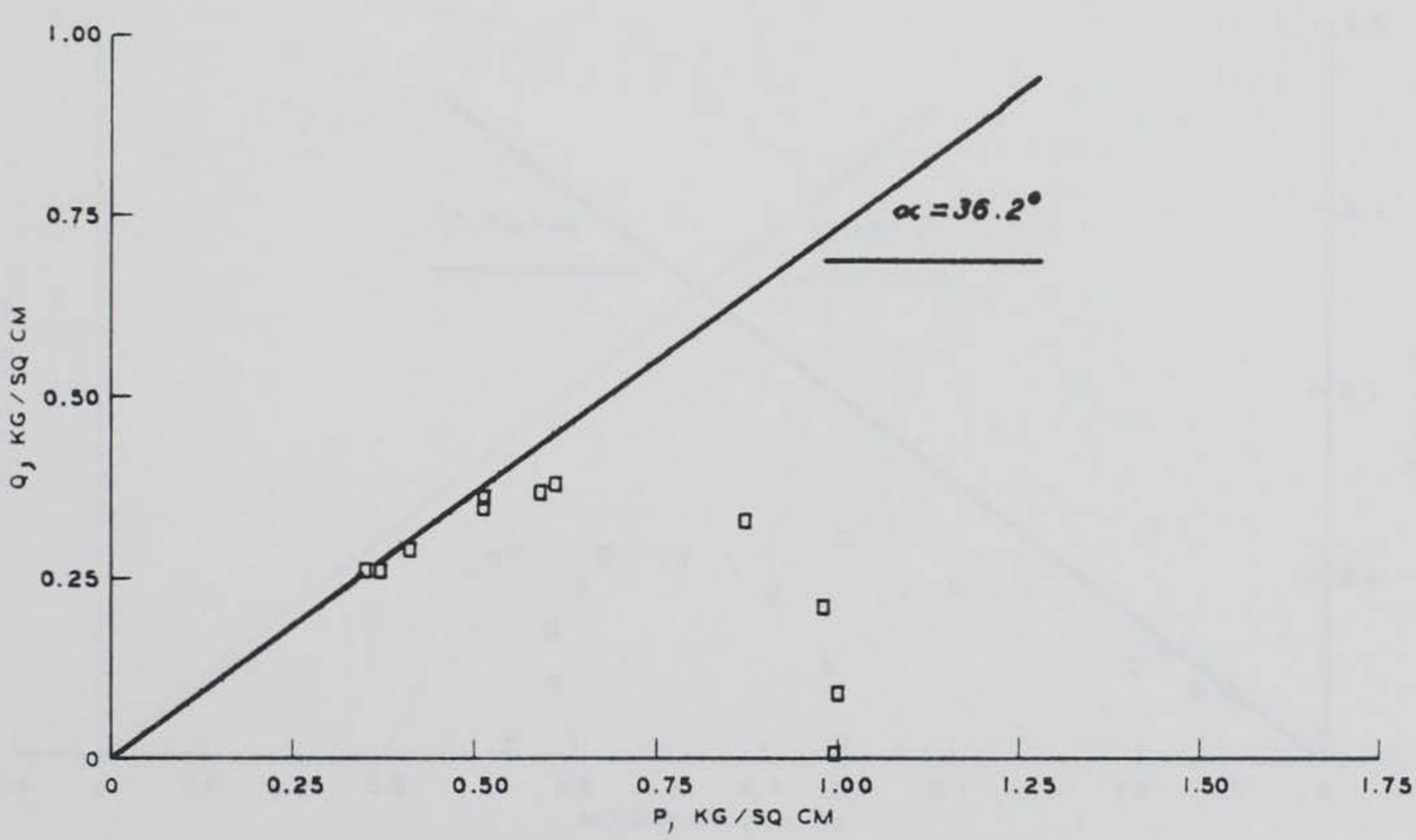

Figure C6. Results of $\bar{R}$ Test A6

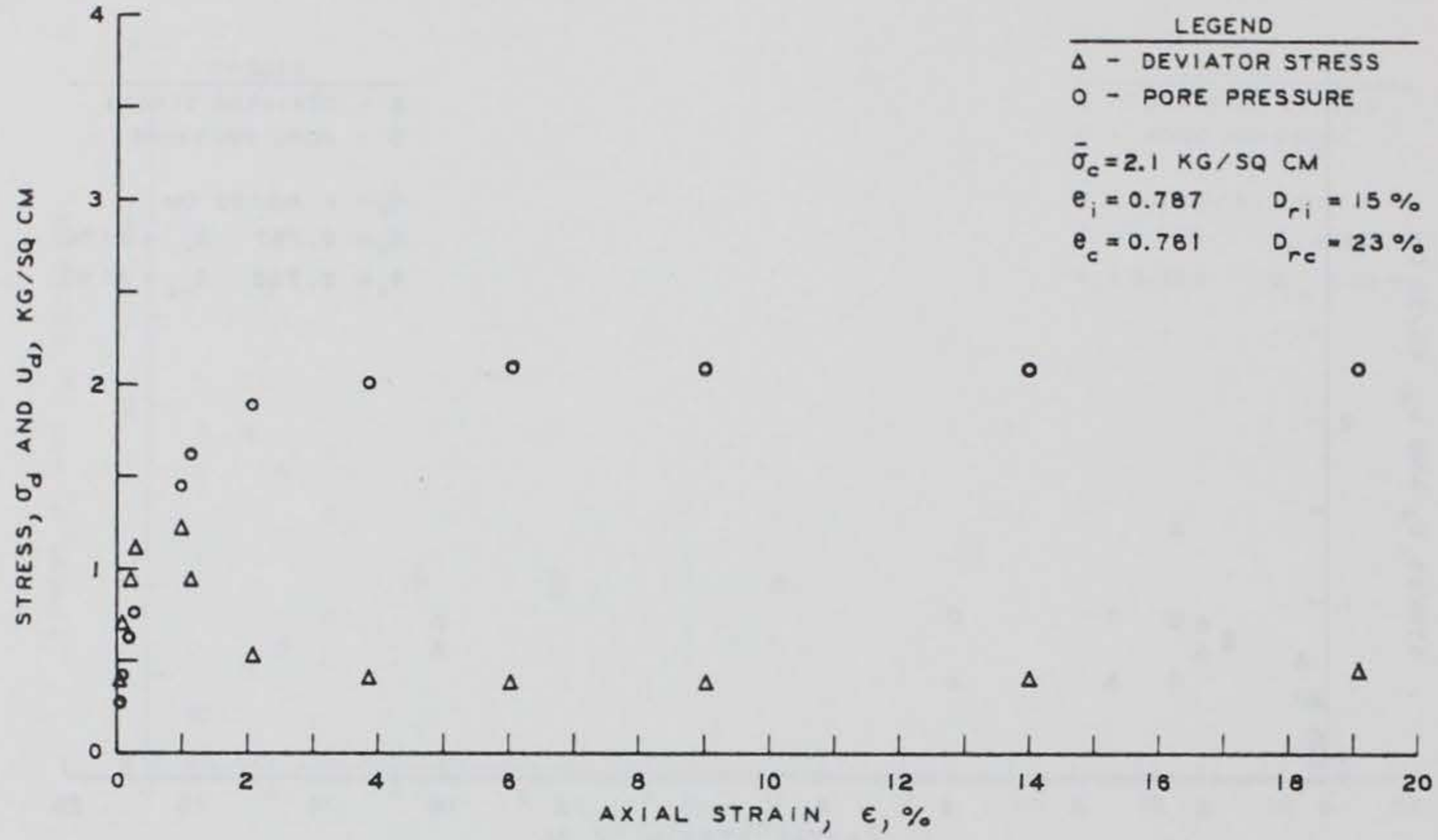

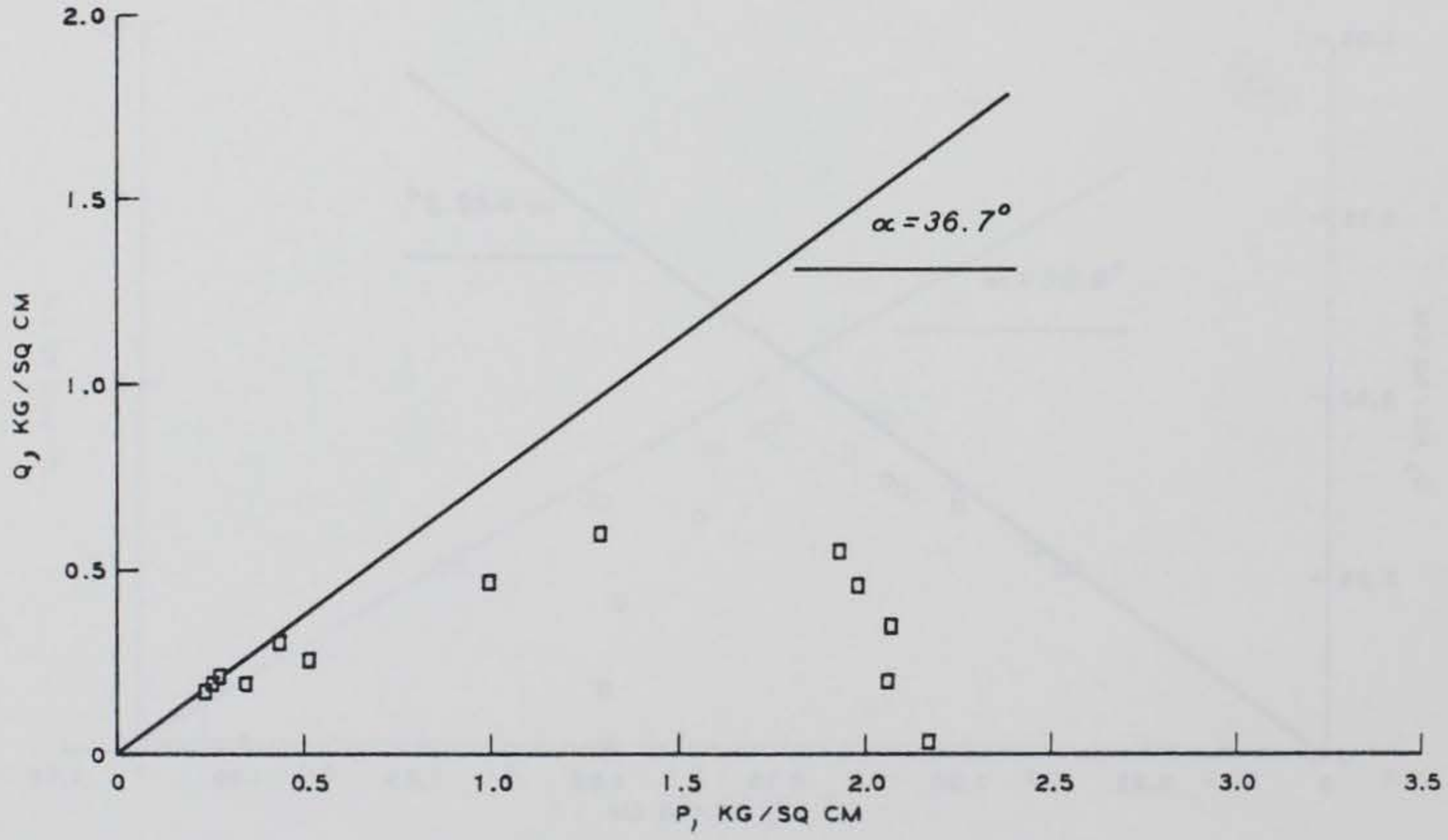

Figure C7. Results of $\bar{R}$ Test A7

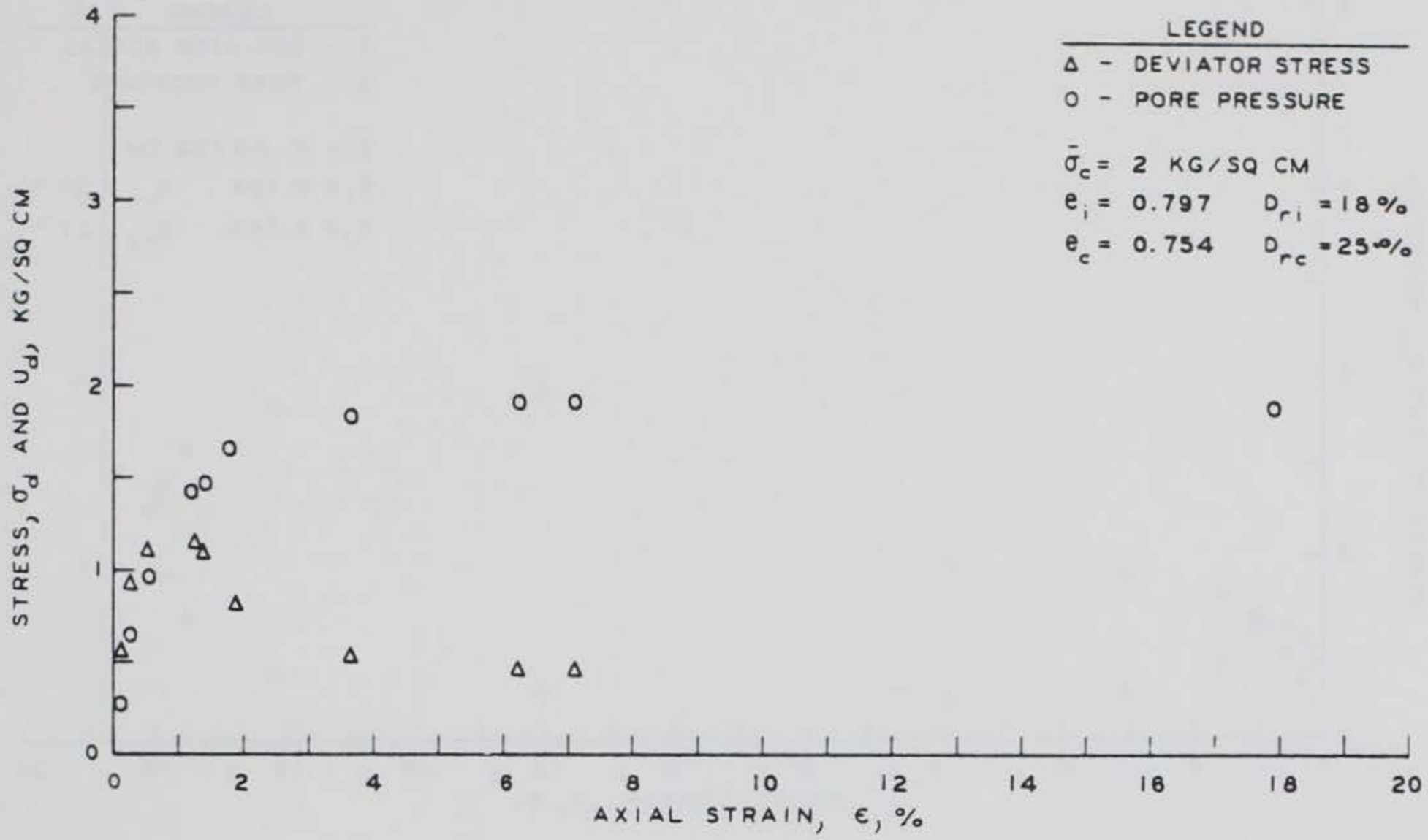

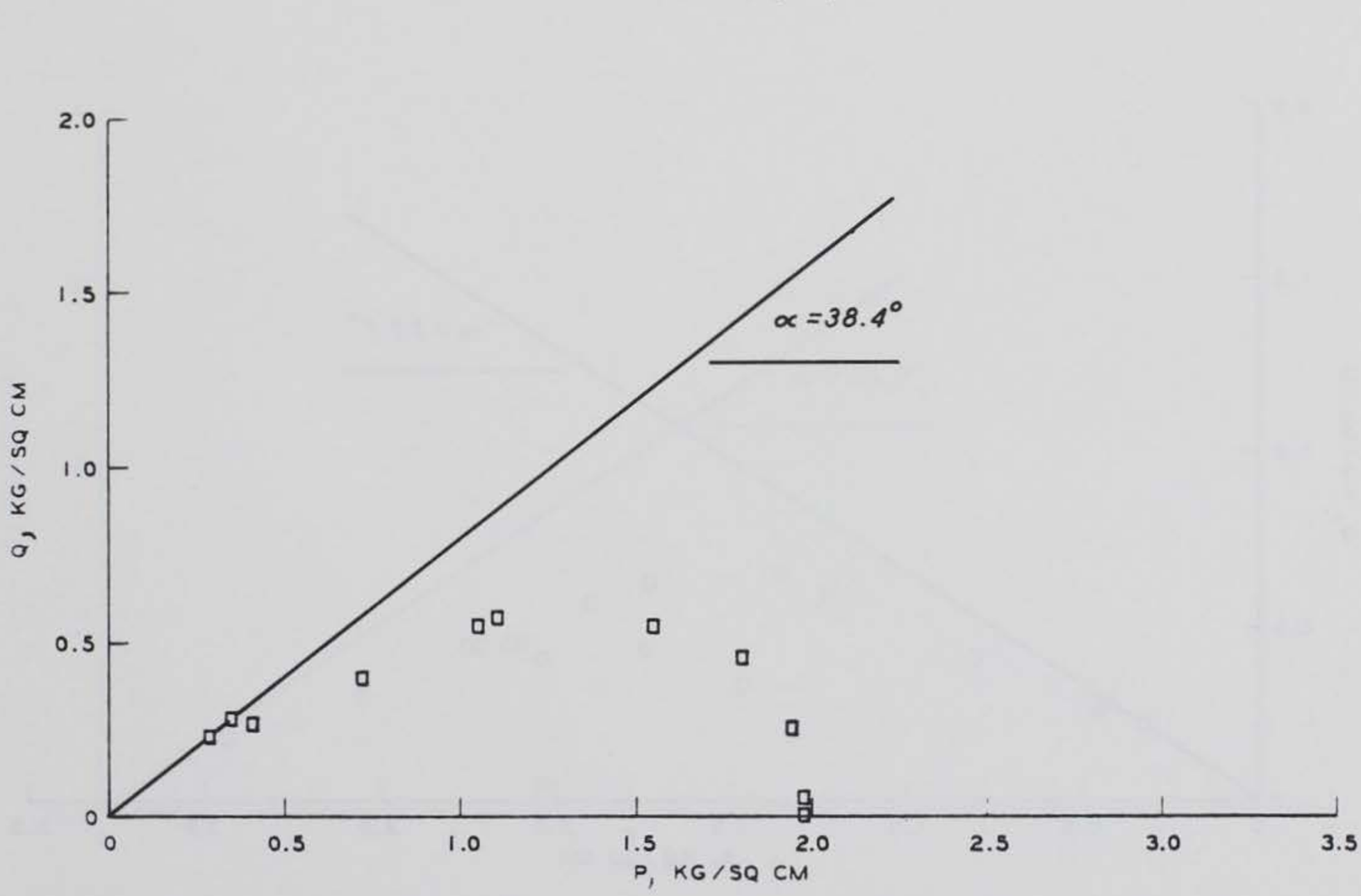

Figure C8. Results of $\bar{R}$ Test A8

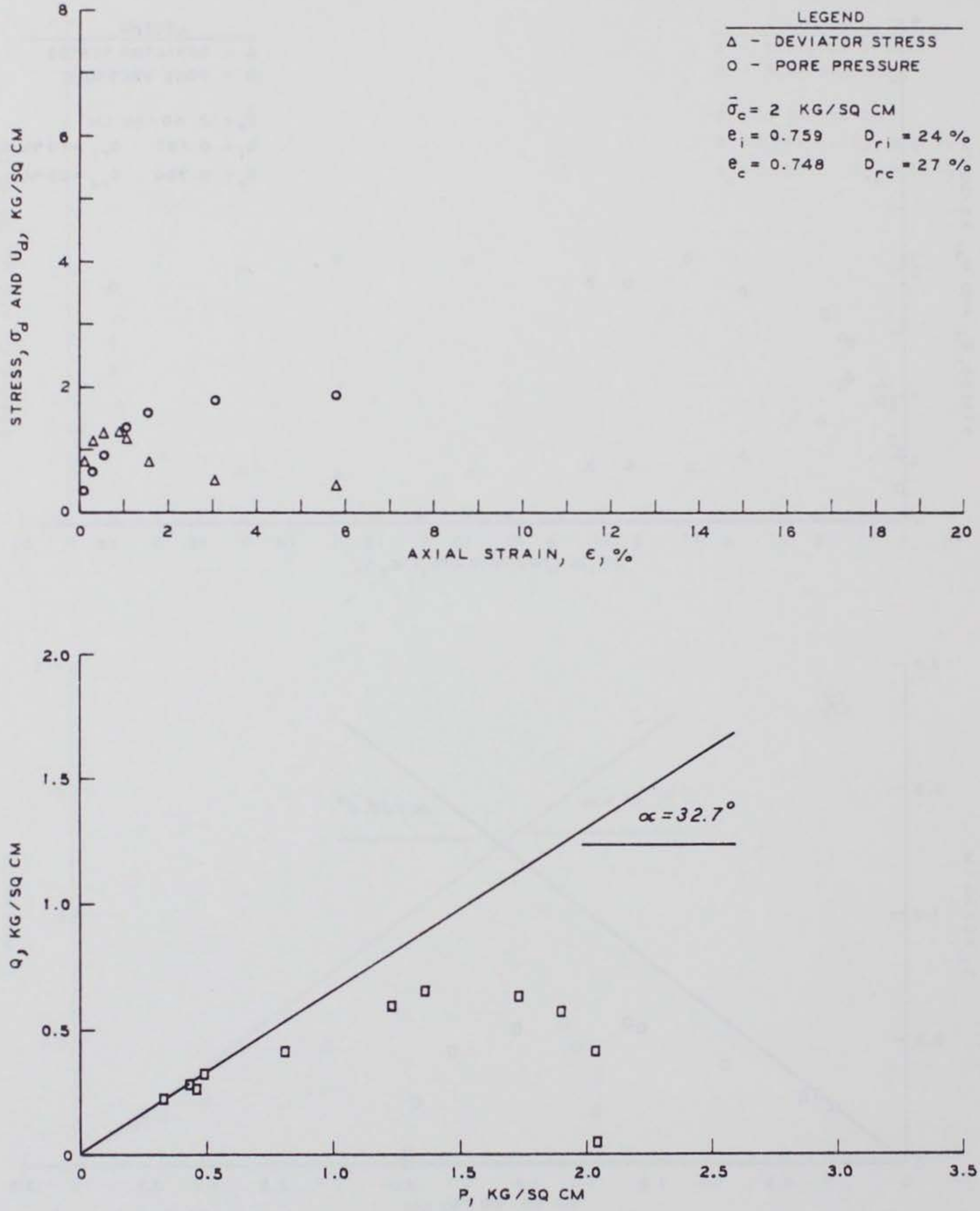

Figure C9. Results of $\bar{R}$ Test A9

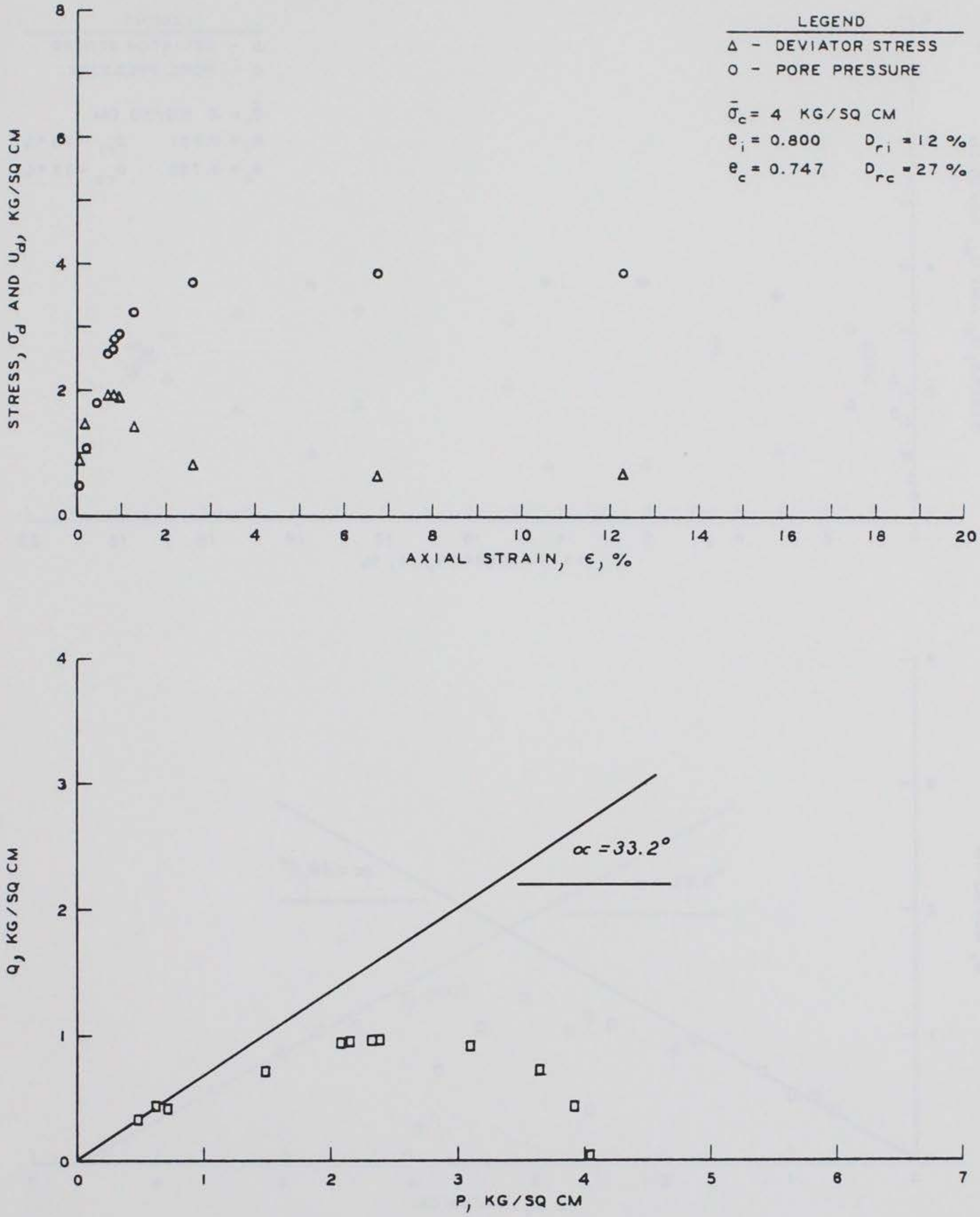

Figure C10. Results of $\bar{R}$ Test A10

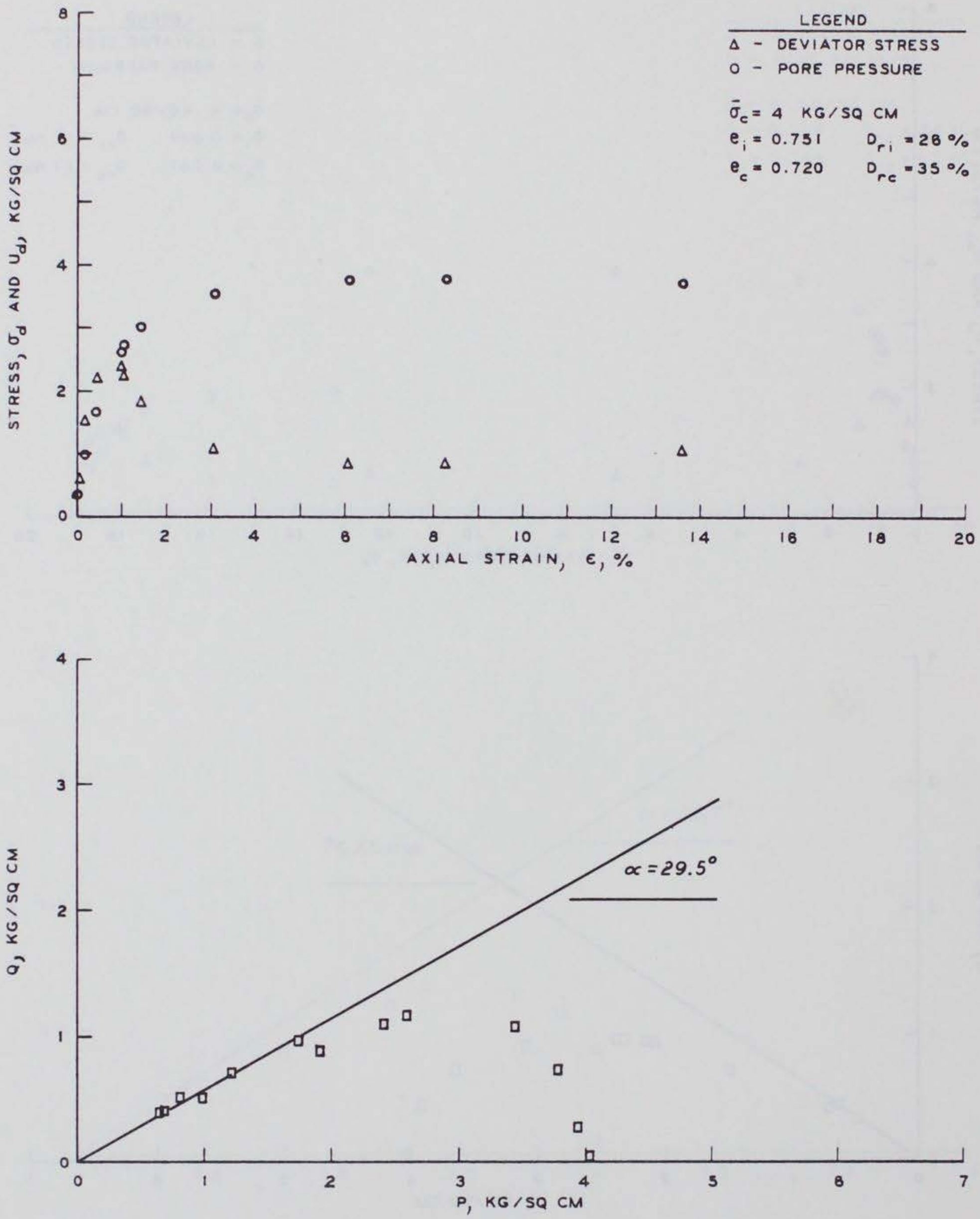

Figure C11. Results of $\bar{R}$ Test A11

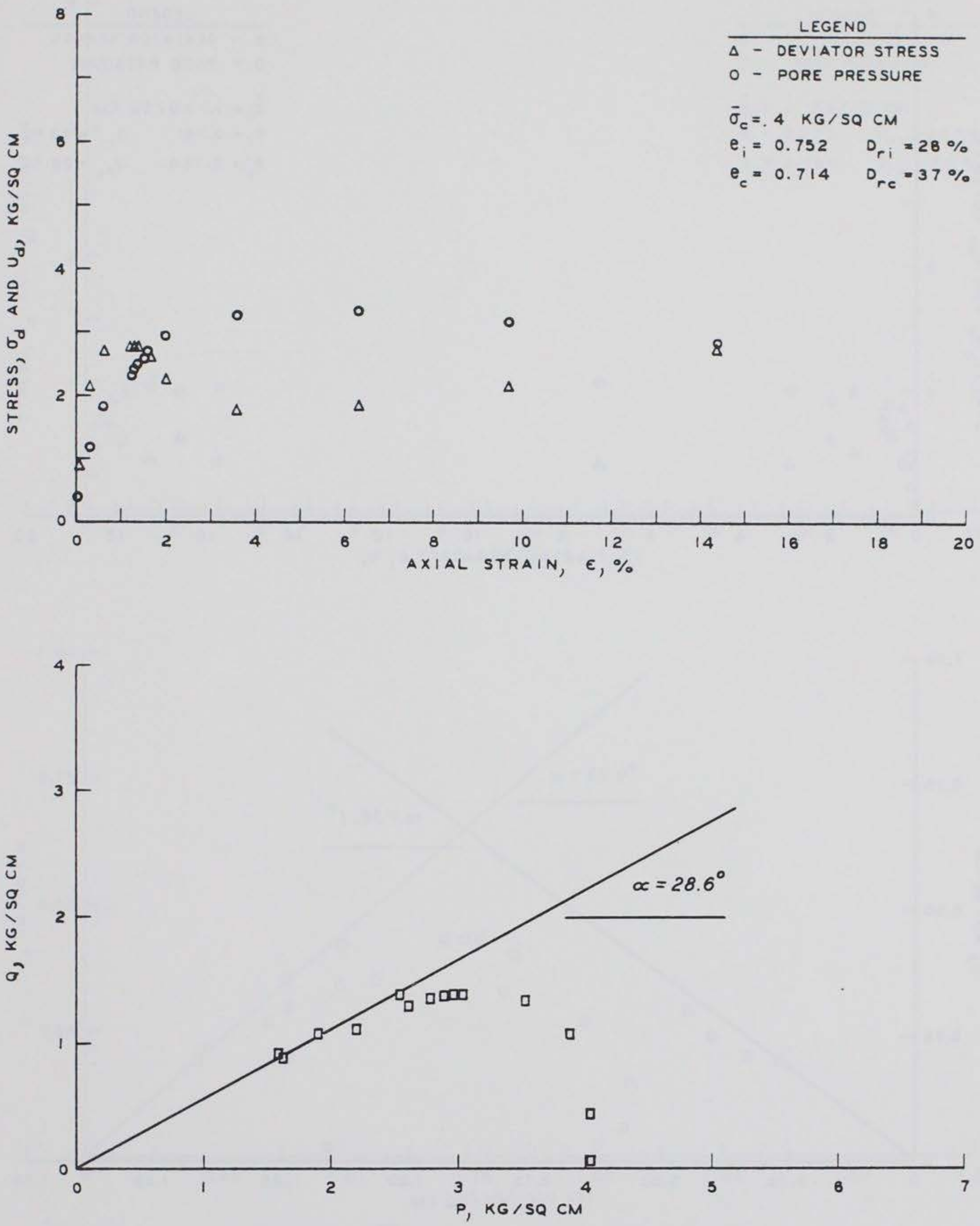

Figure C12. Results of $\overline{R}$ Test A12

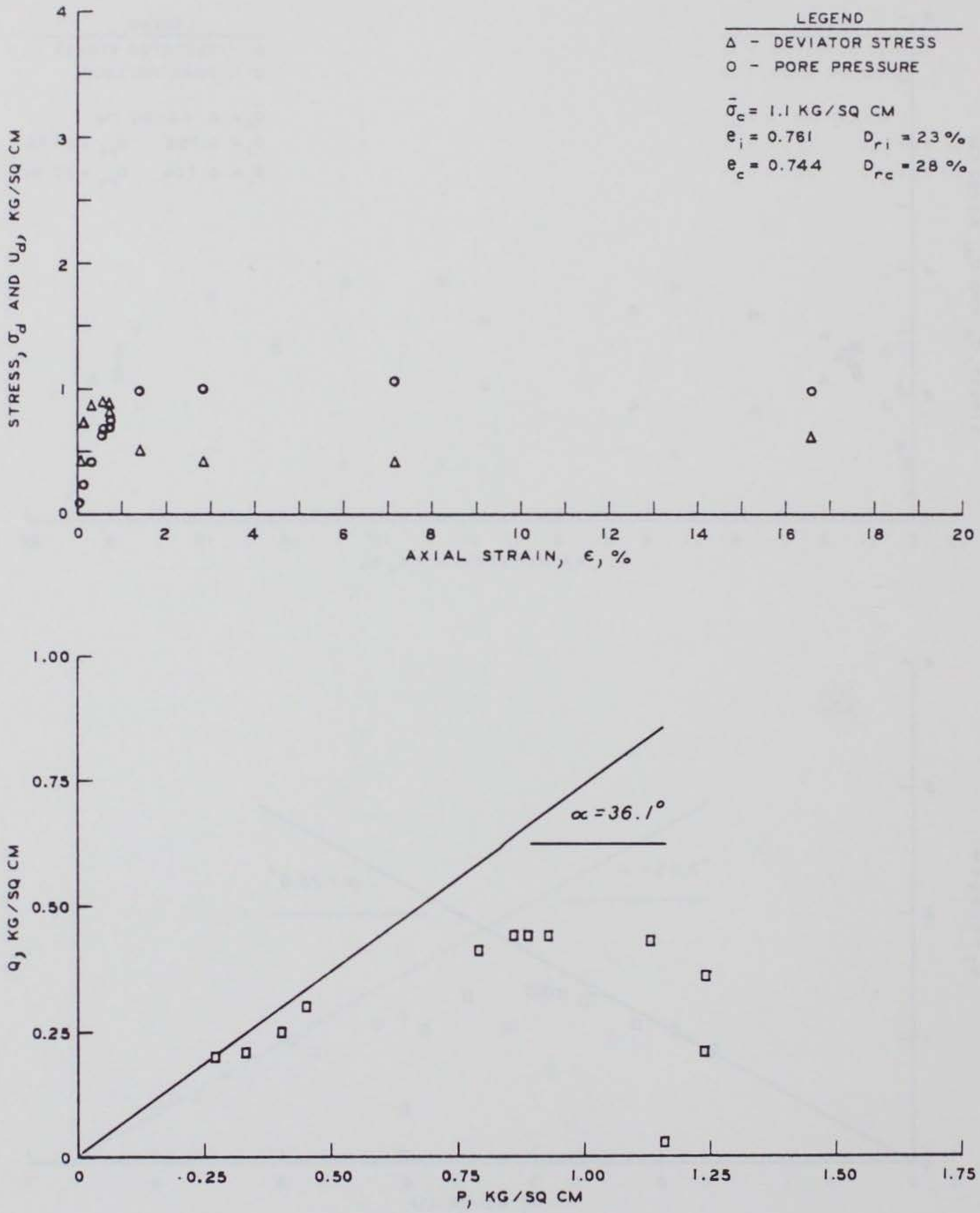

Figure C13. Results of $\bar{R}$ Test B1

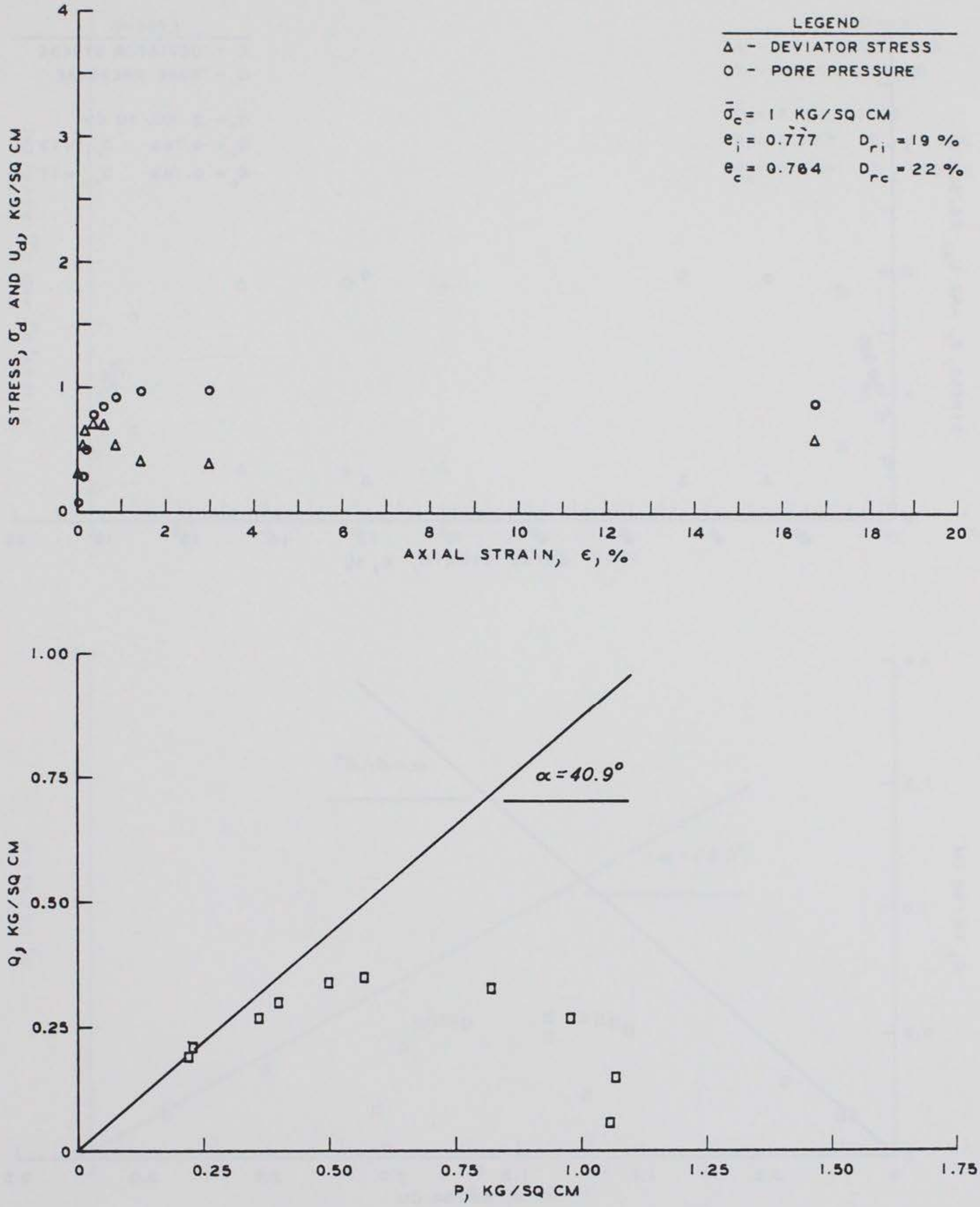

Figure C14. Results of $\bar{R}$ Test B2

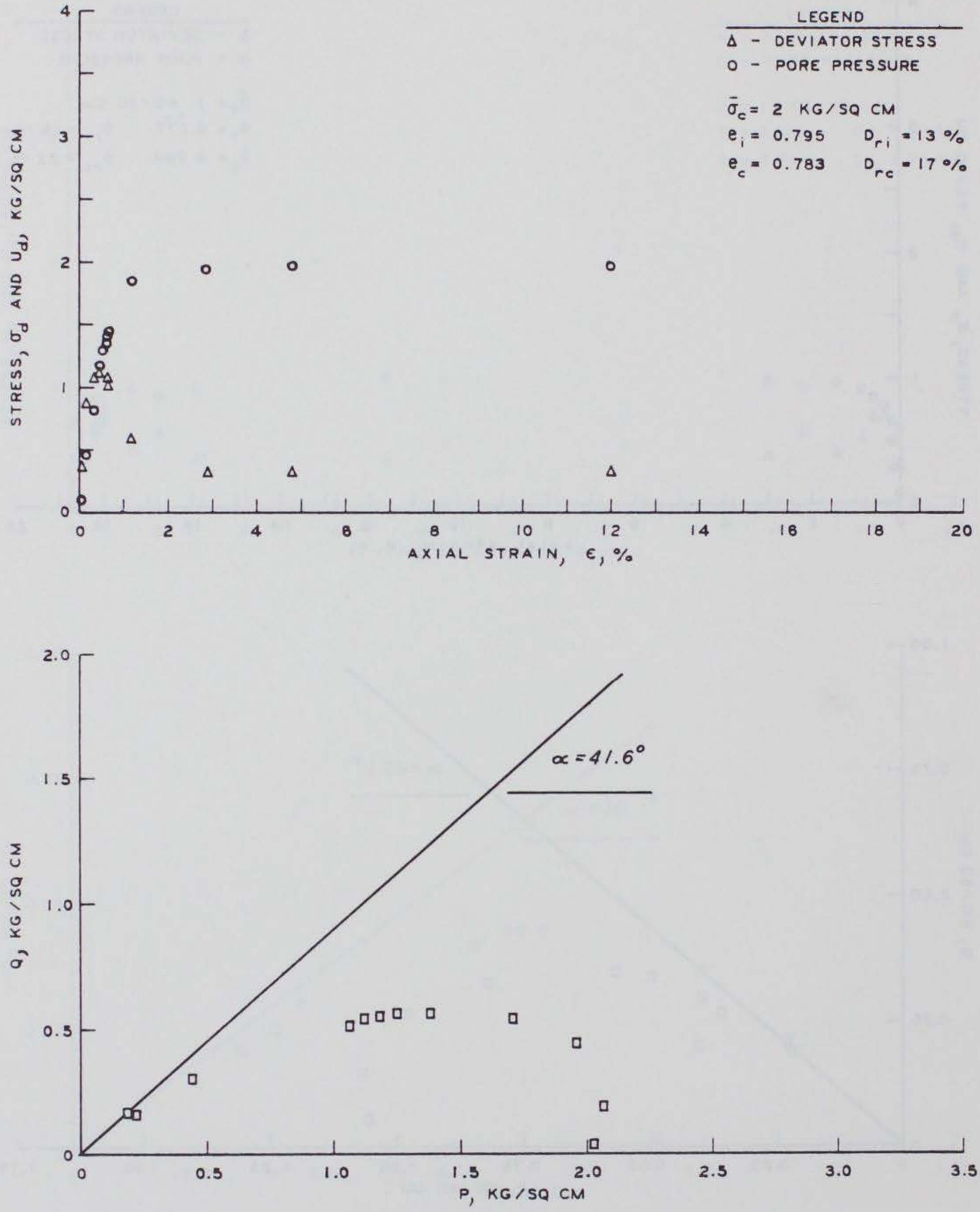

Figure C15. Results of $\bar{R}$ Test B3

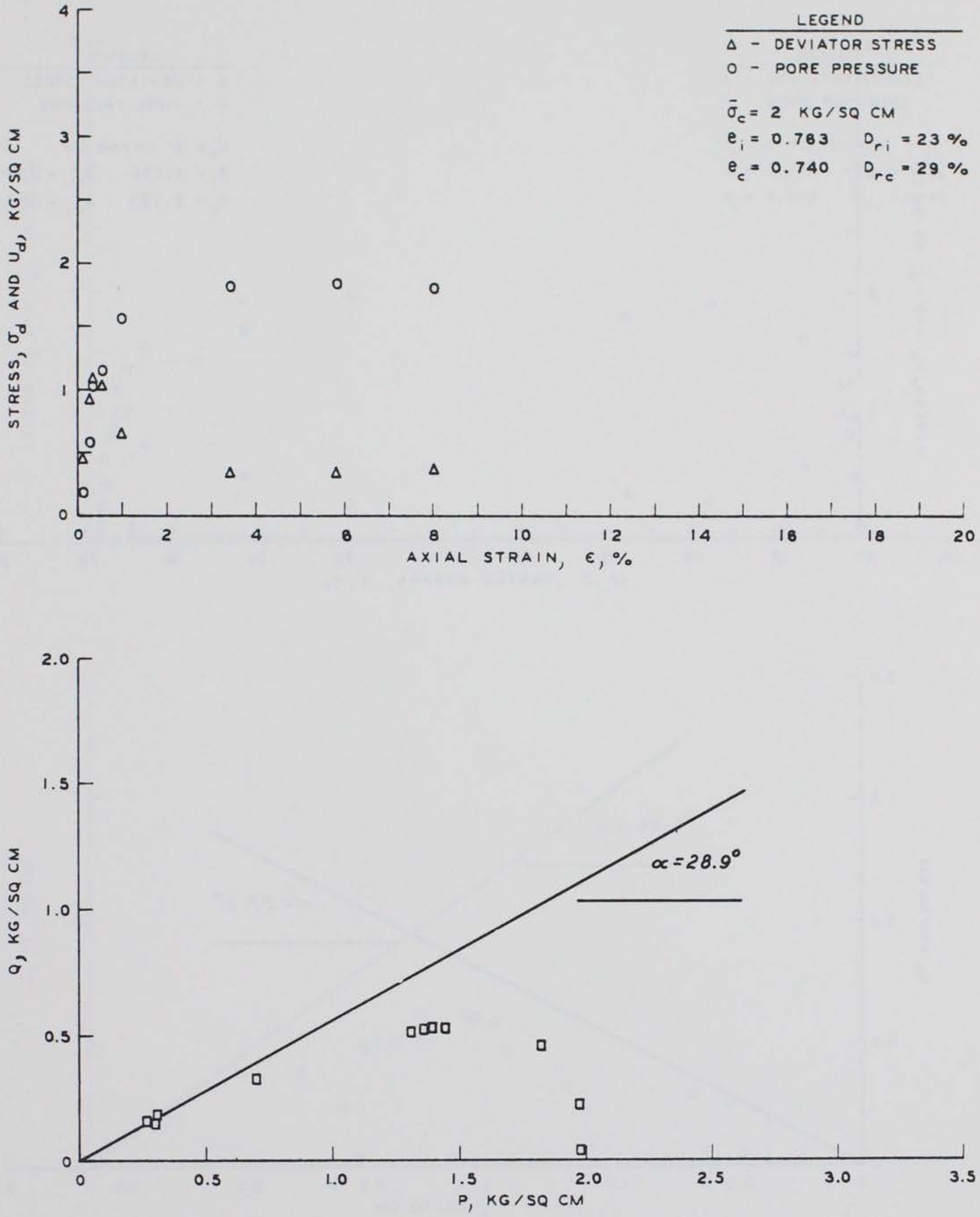

Figure C16. Results of $\bar{R}$ Test B4

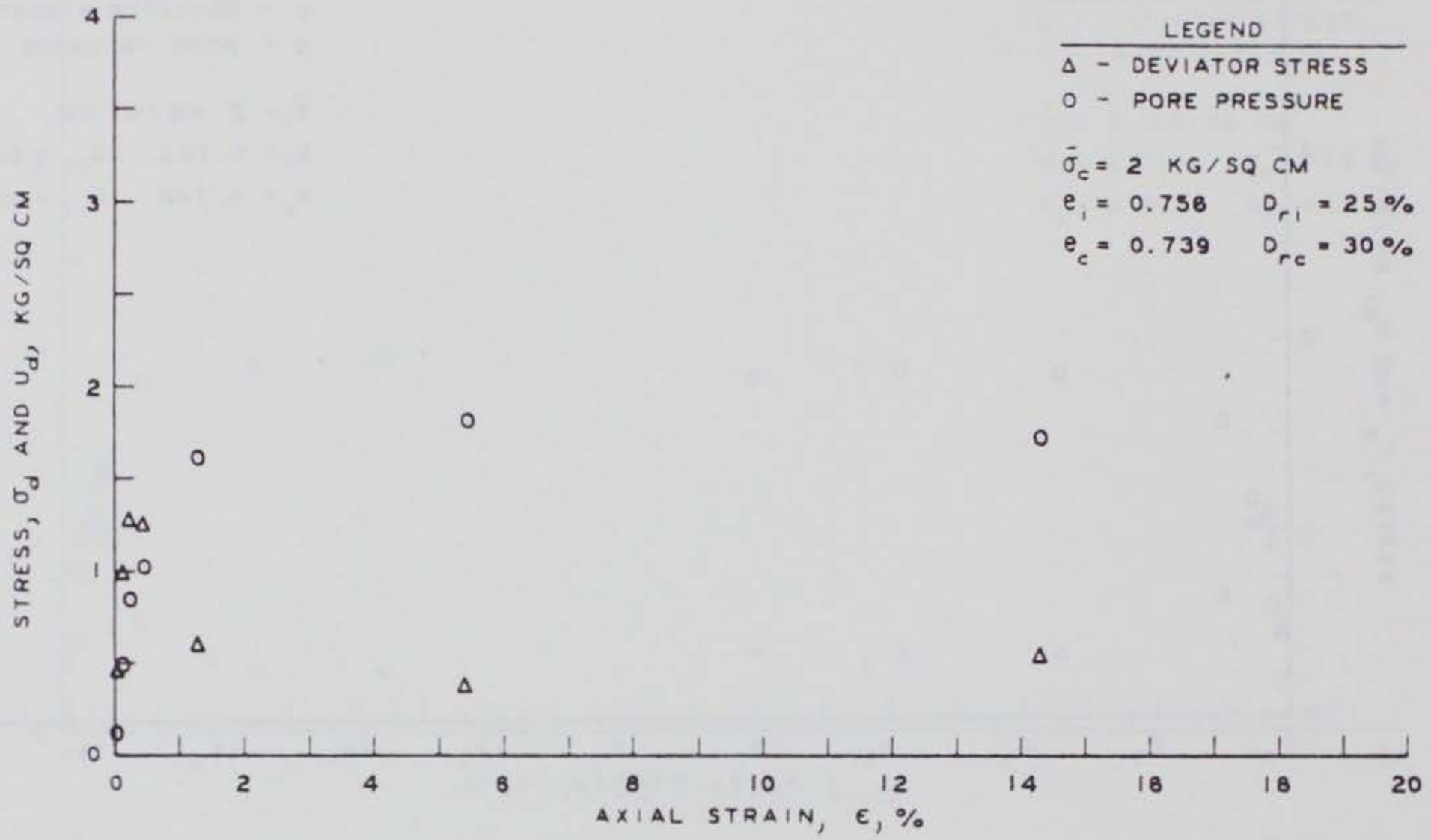

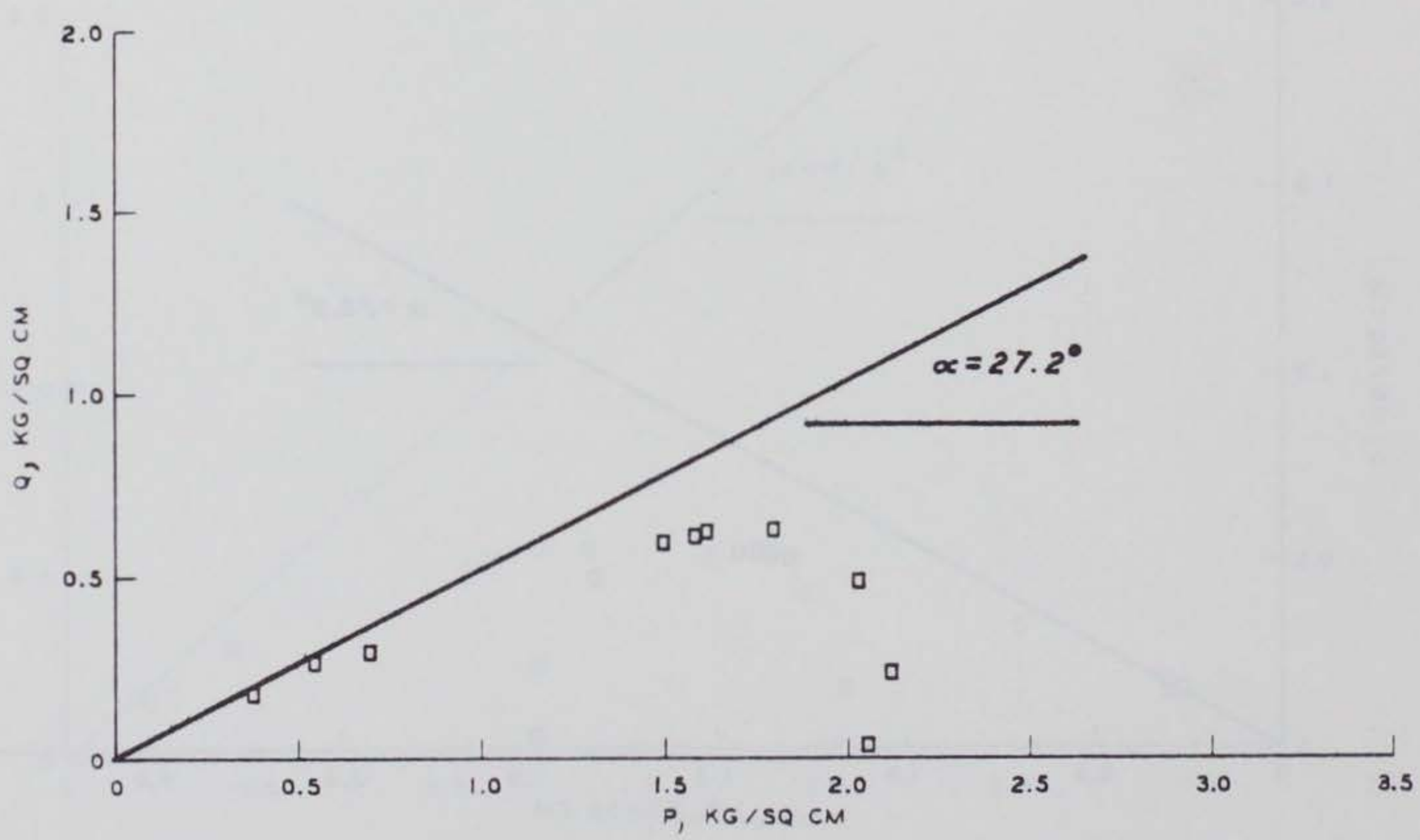

Figure C17. Results of $\bar{R}$ Test B5

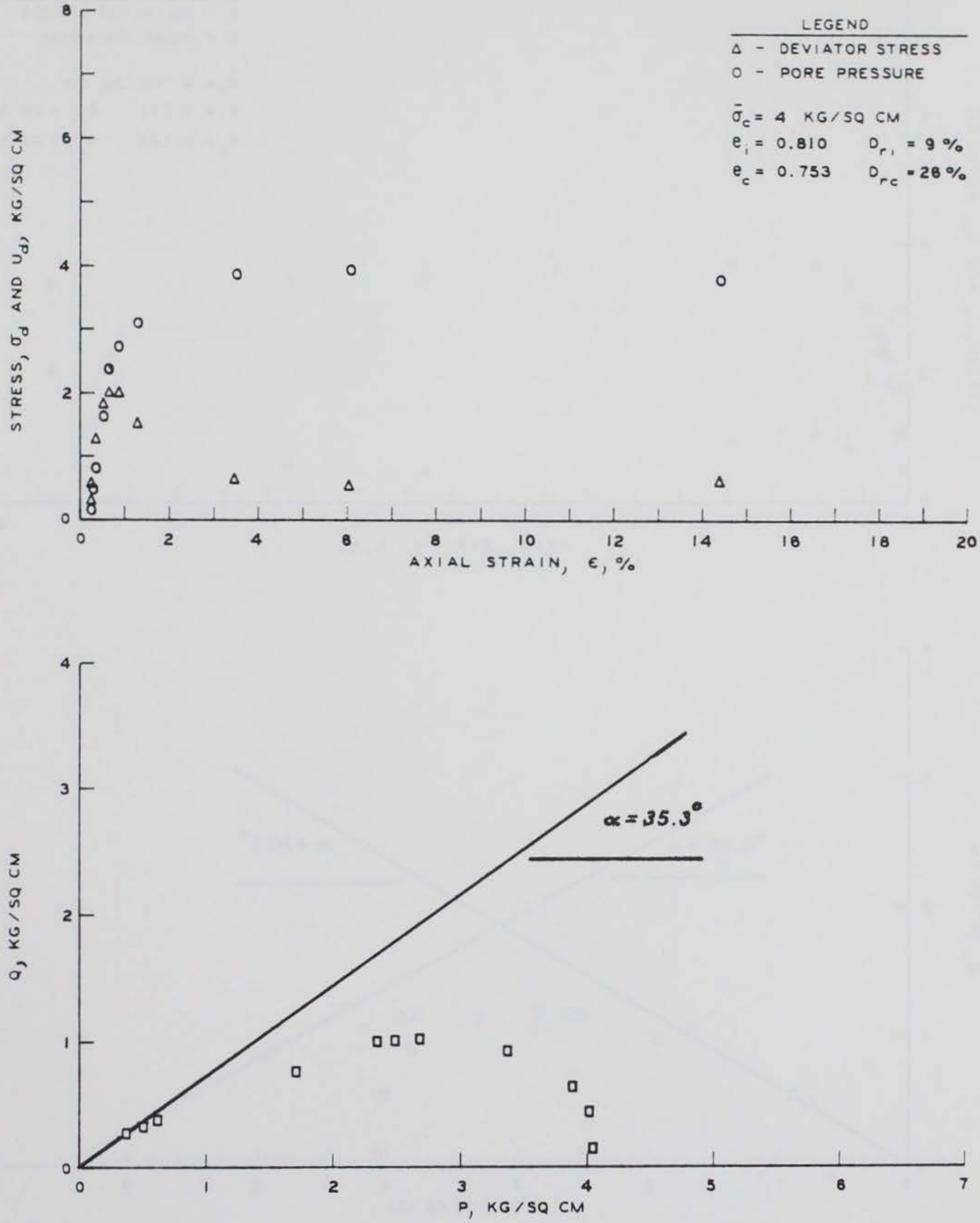

Figure C18. Results of $\bar{R}$ Test B6

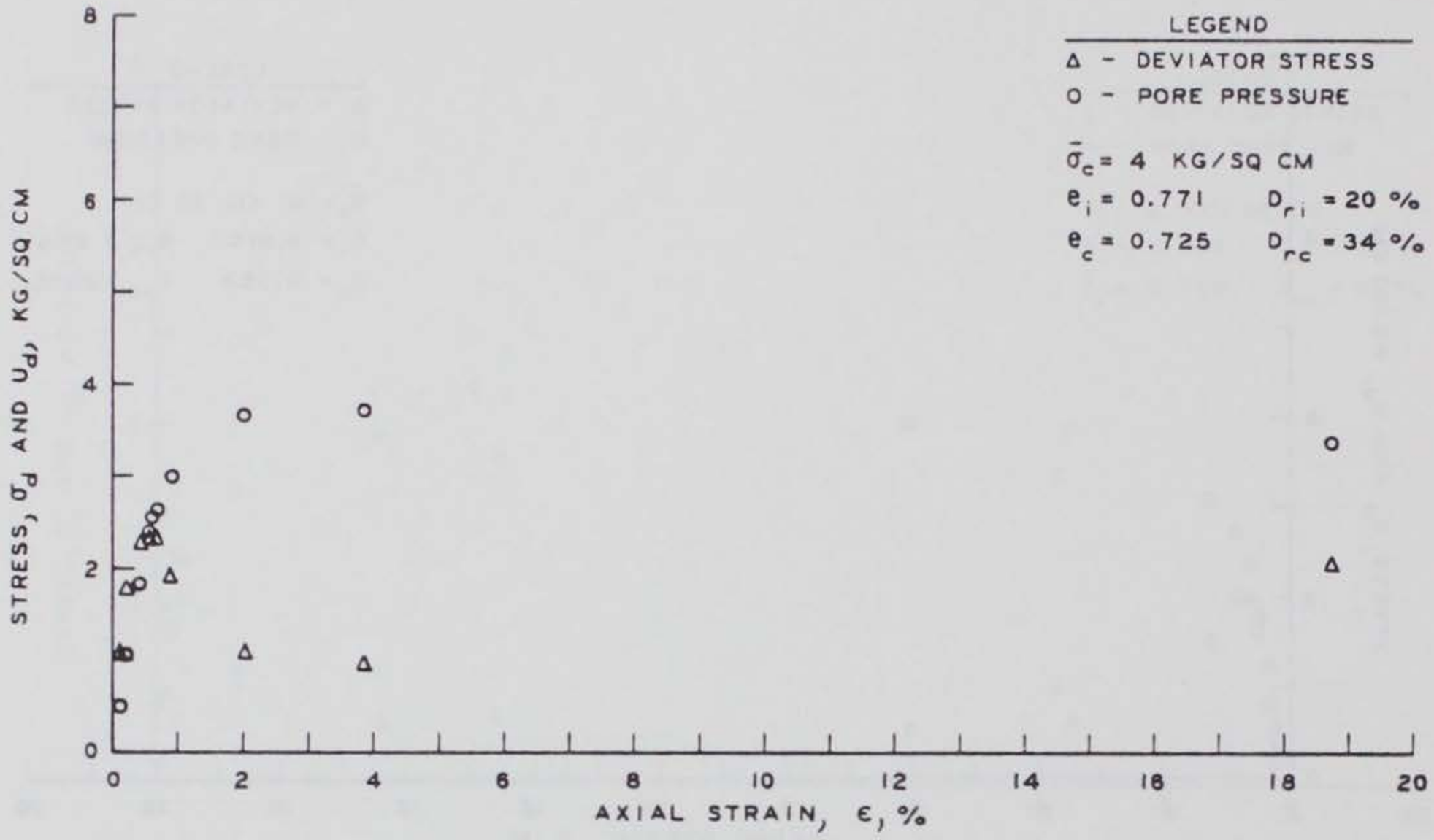

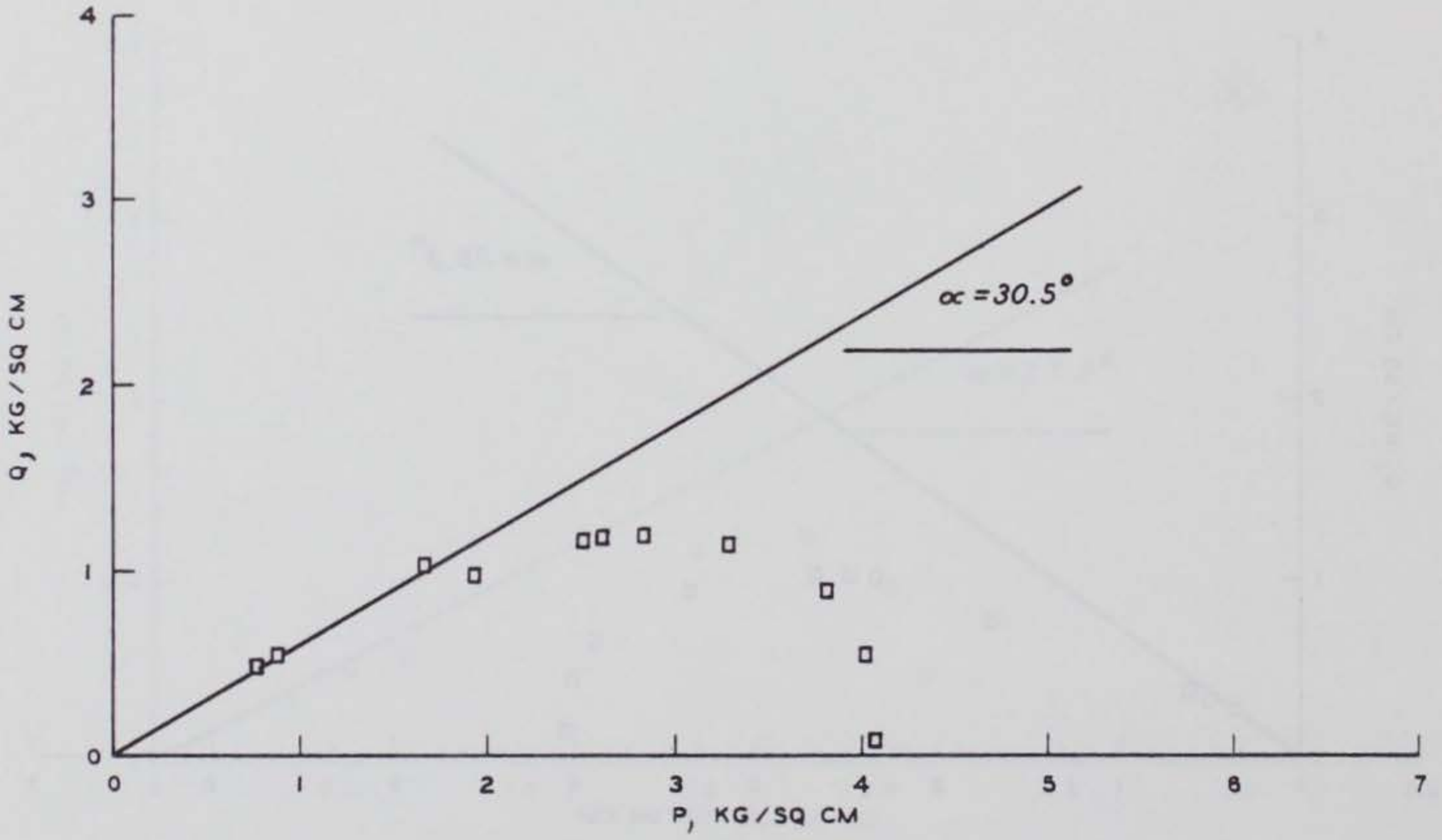

Figure C19. Results of $\bar{R}$ Test B7

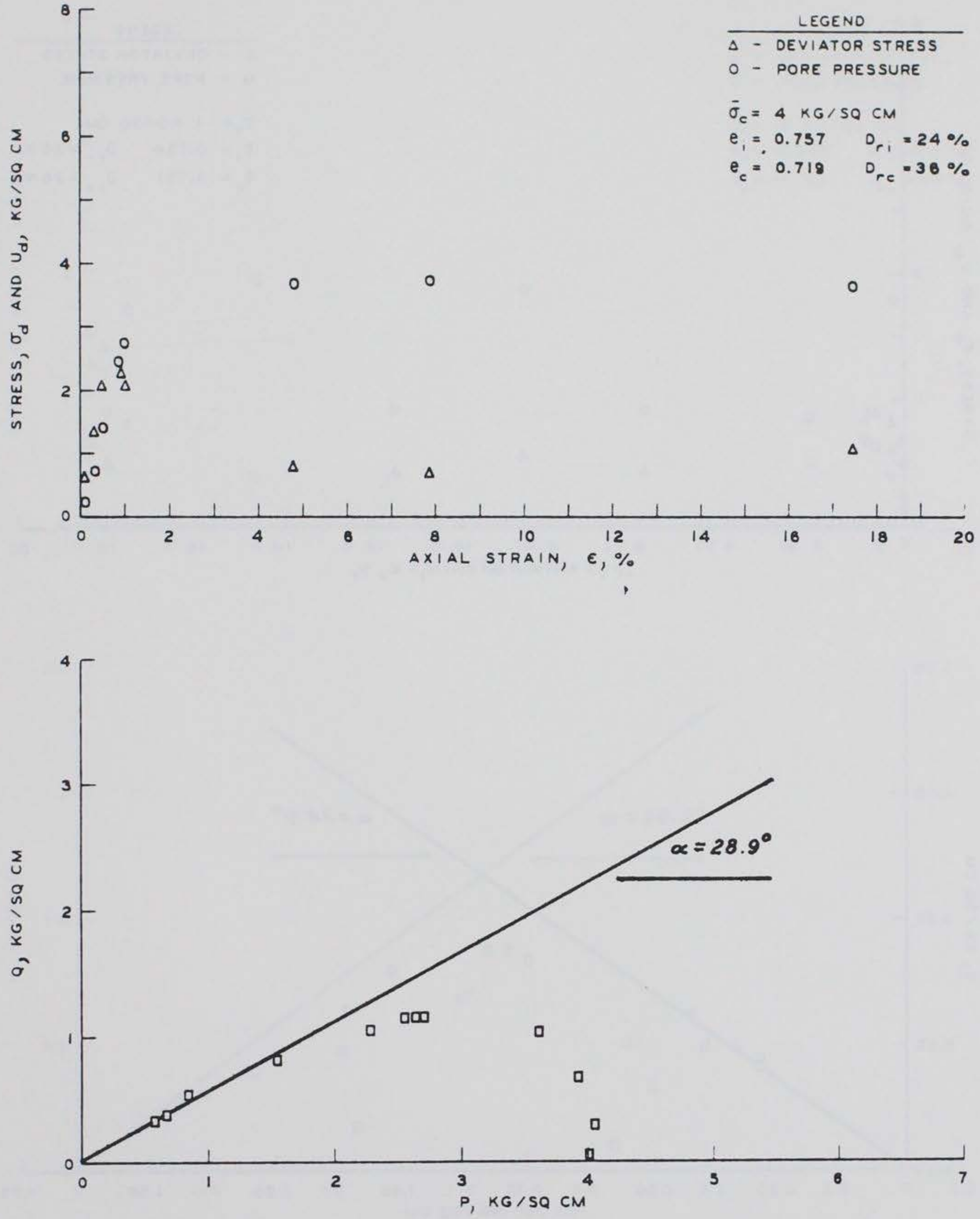

Figure C20. Results of $\bar{R}$ Test B8

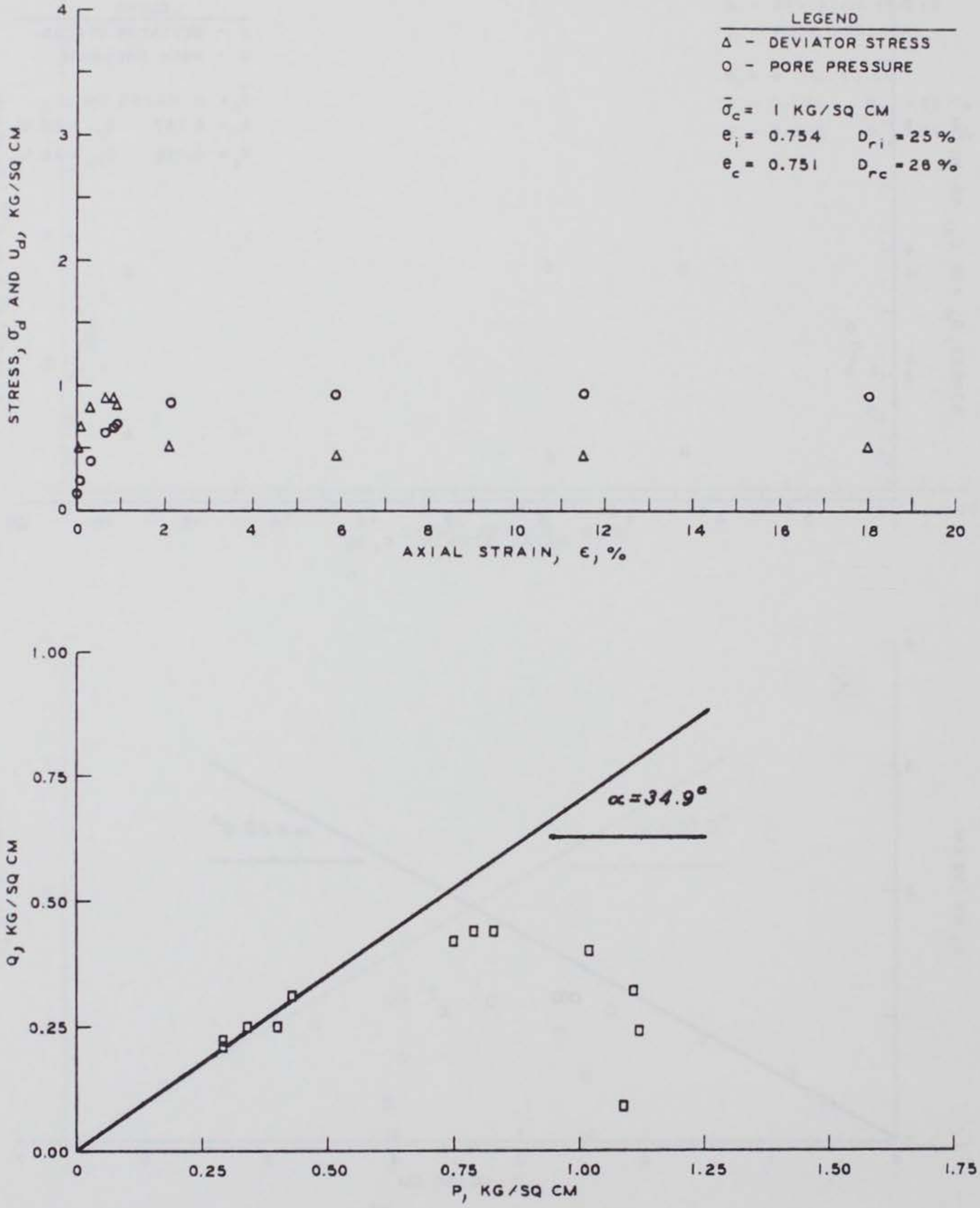

Figure C21. Results of $\bar{R}$ Test D1

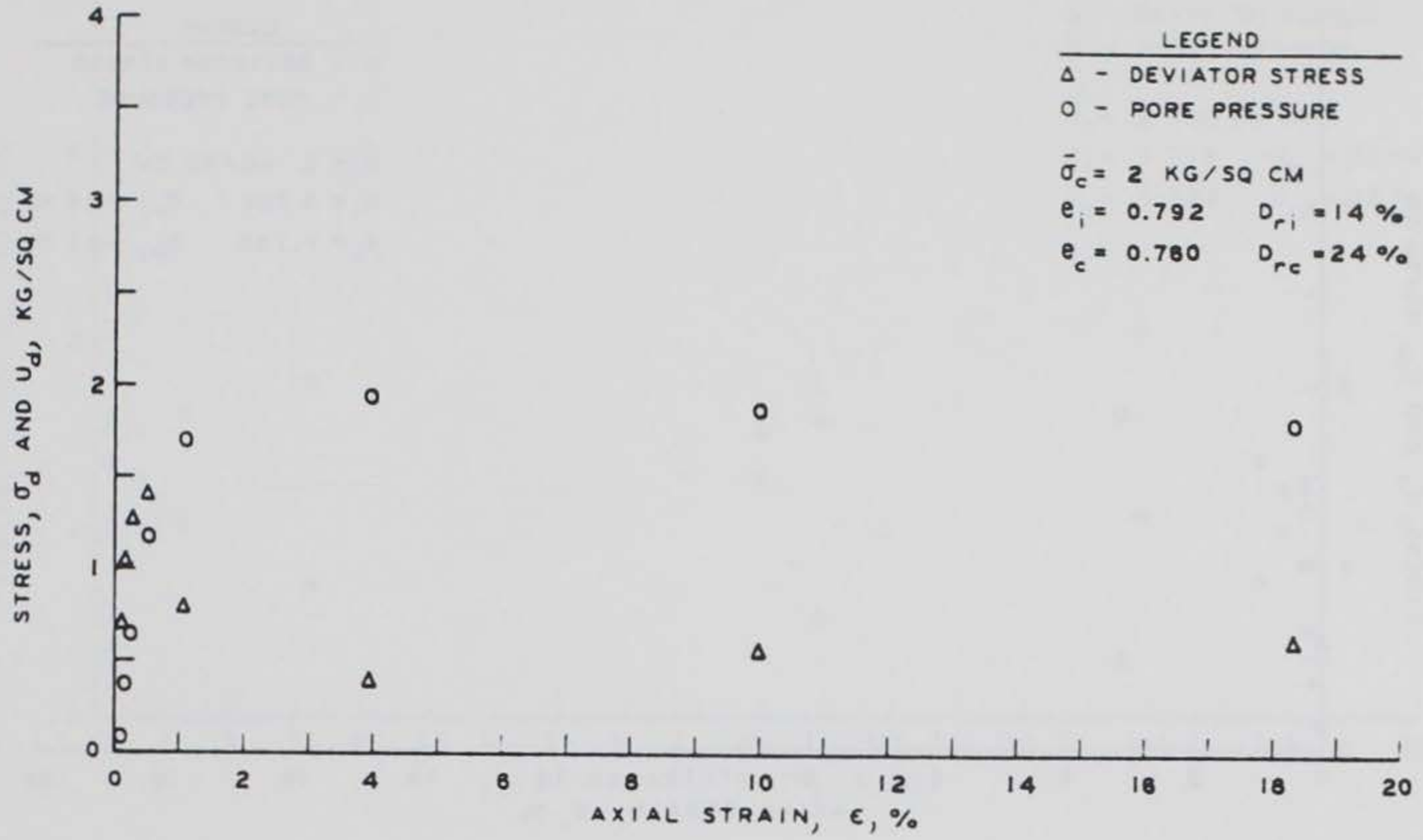

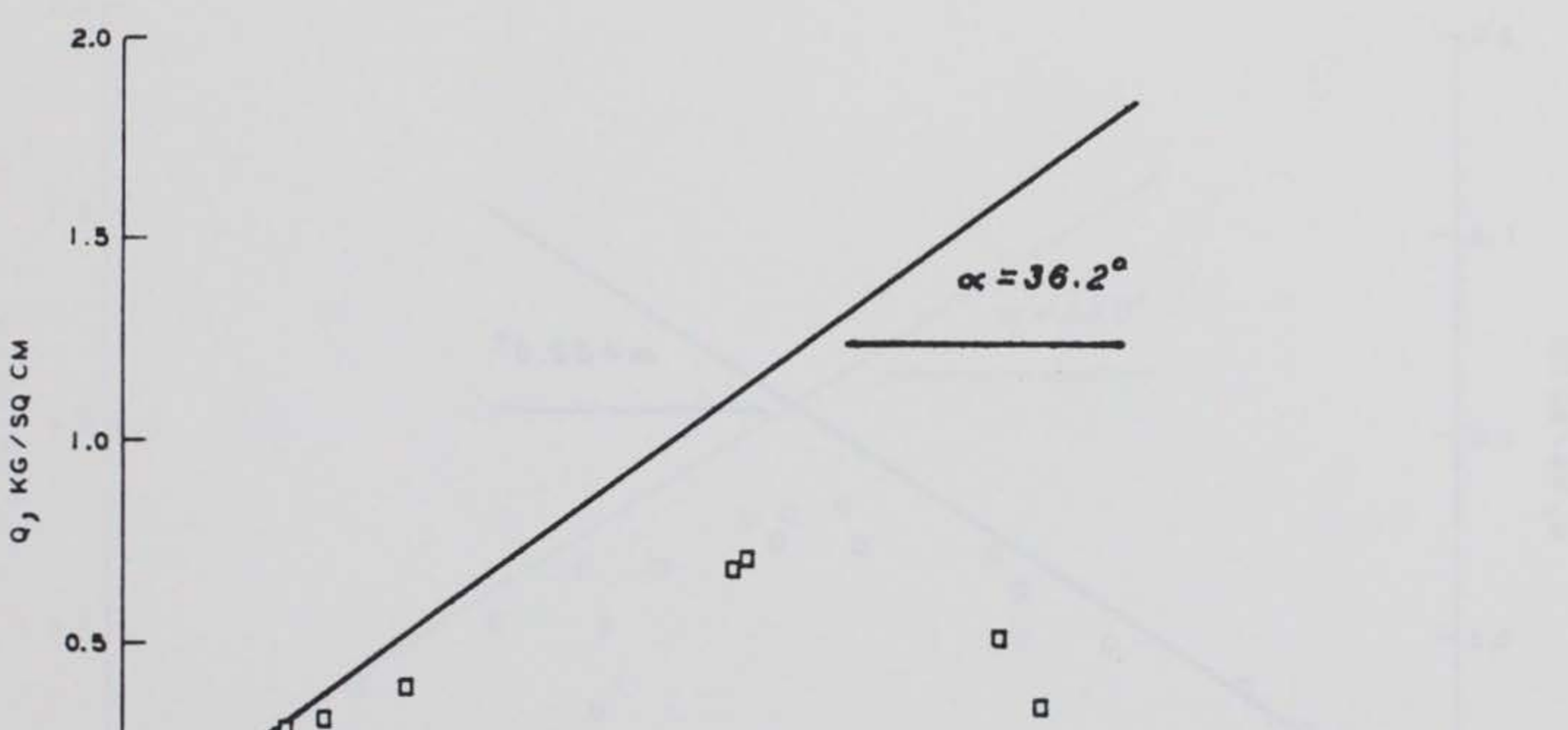

Figure B22. Results of $\bar{R}$ Test D2

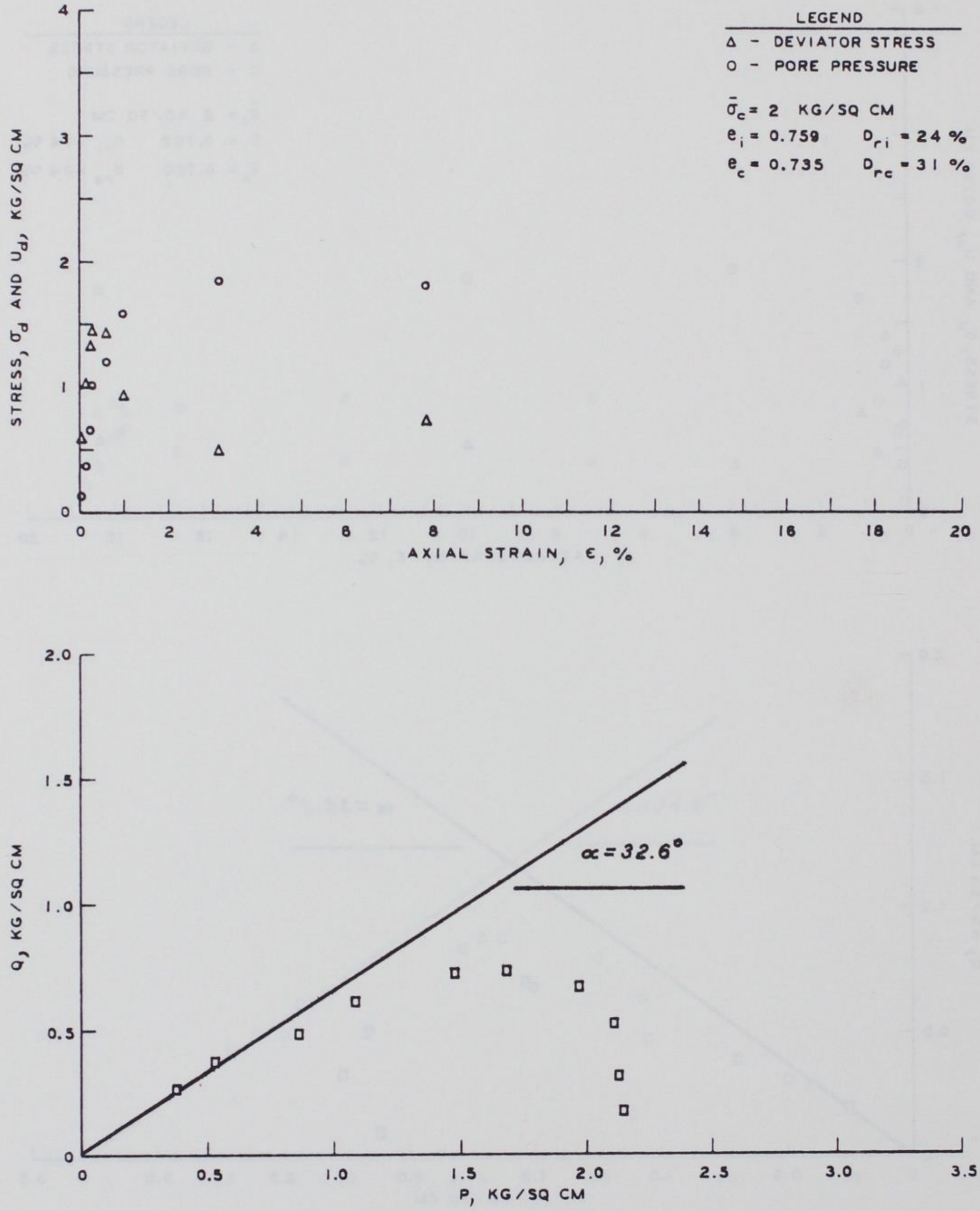

Figure B23. Results of $\bar{R}$ Test D3

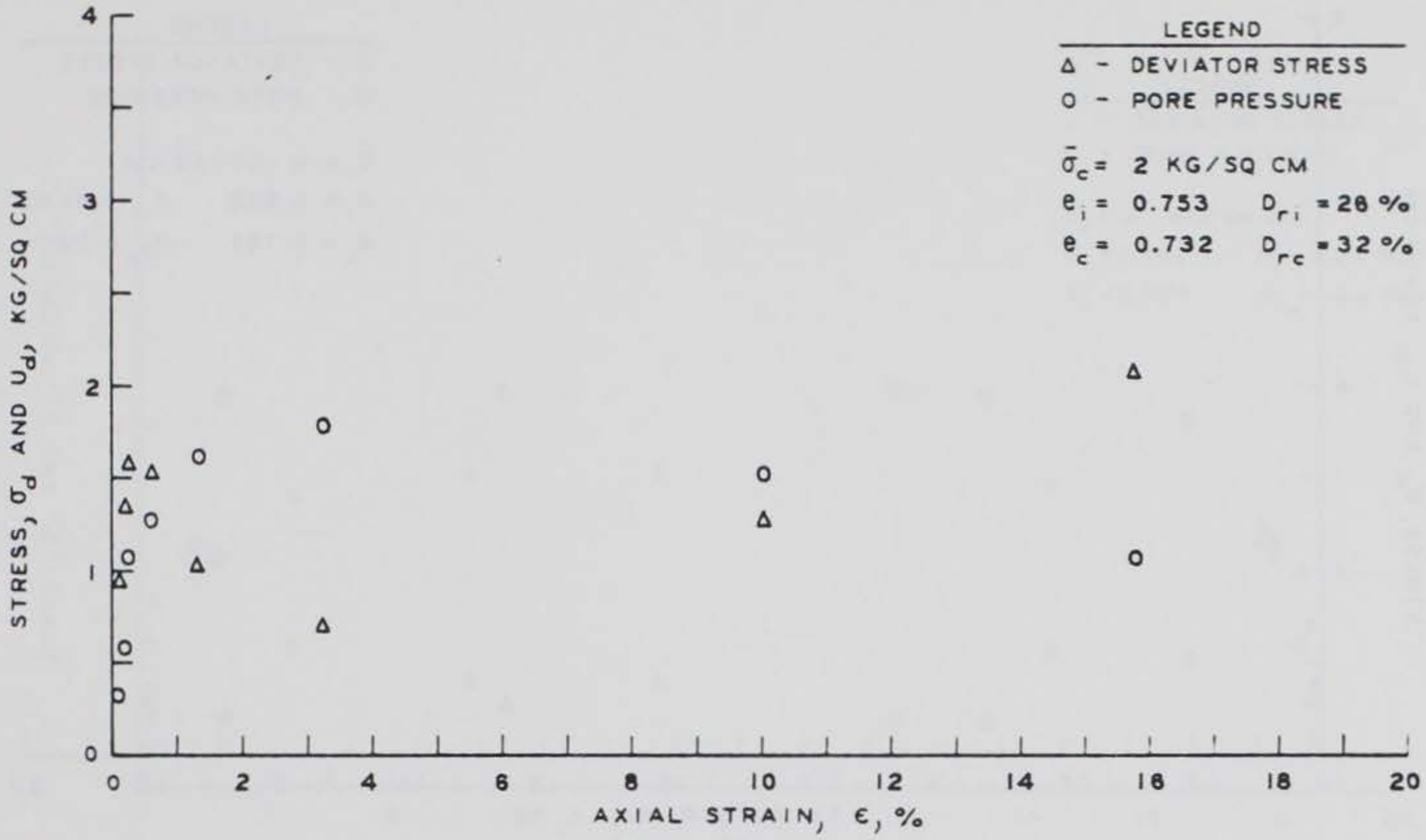

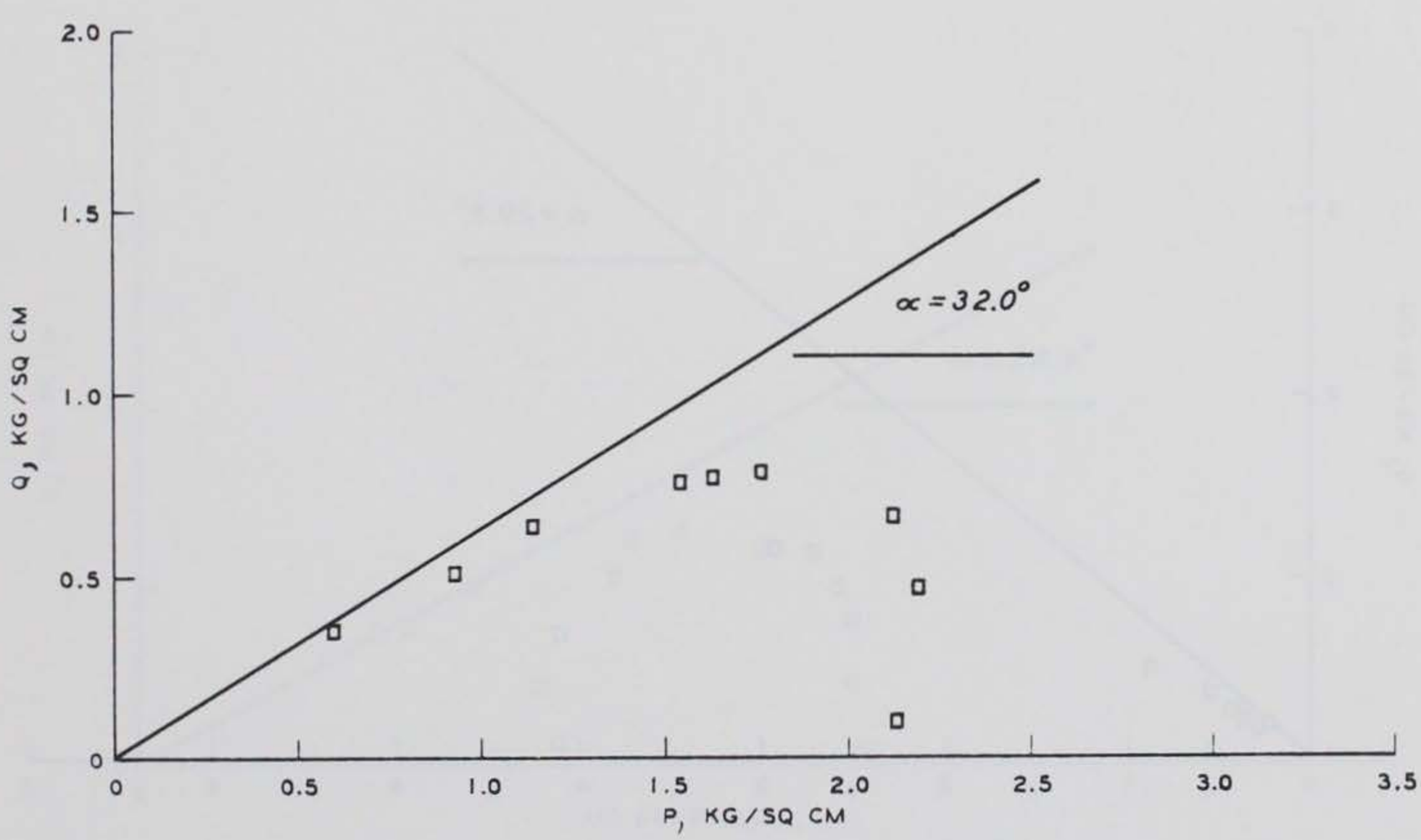

Figure B24. Results of $\bar{R}$ Test D4

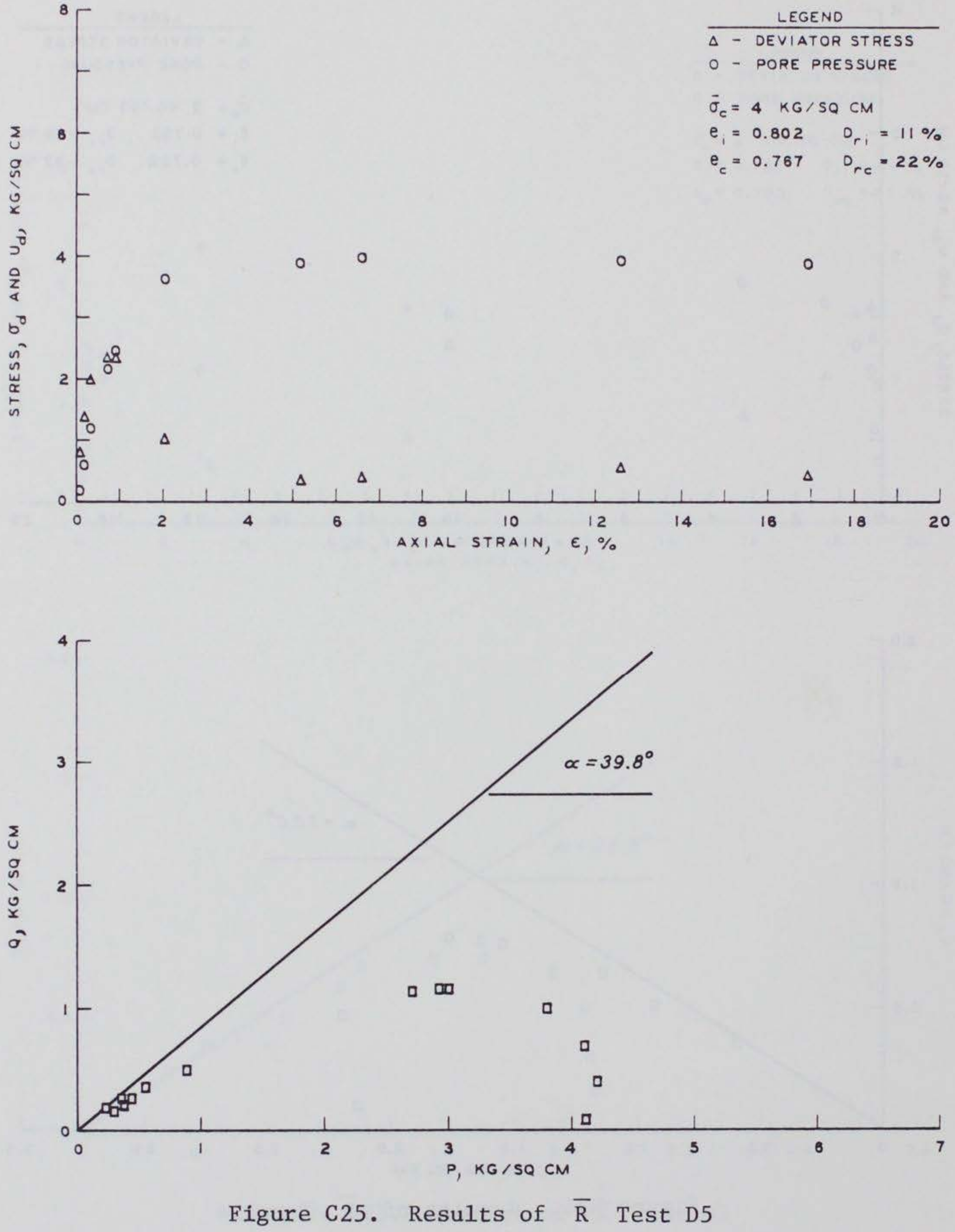

Figure C25. Results of $\bar{R}$ Test D5

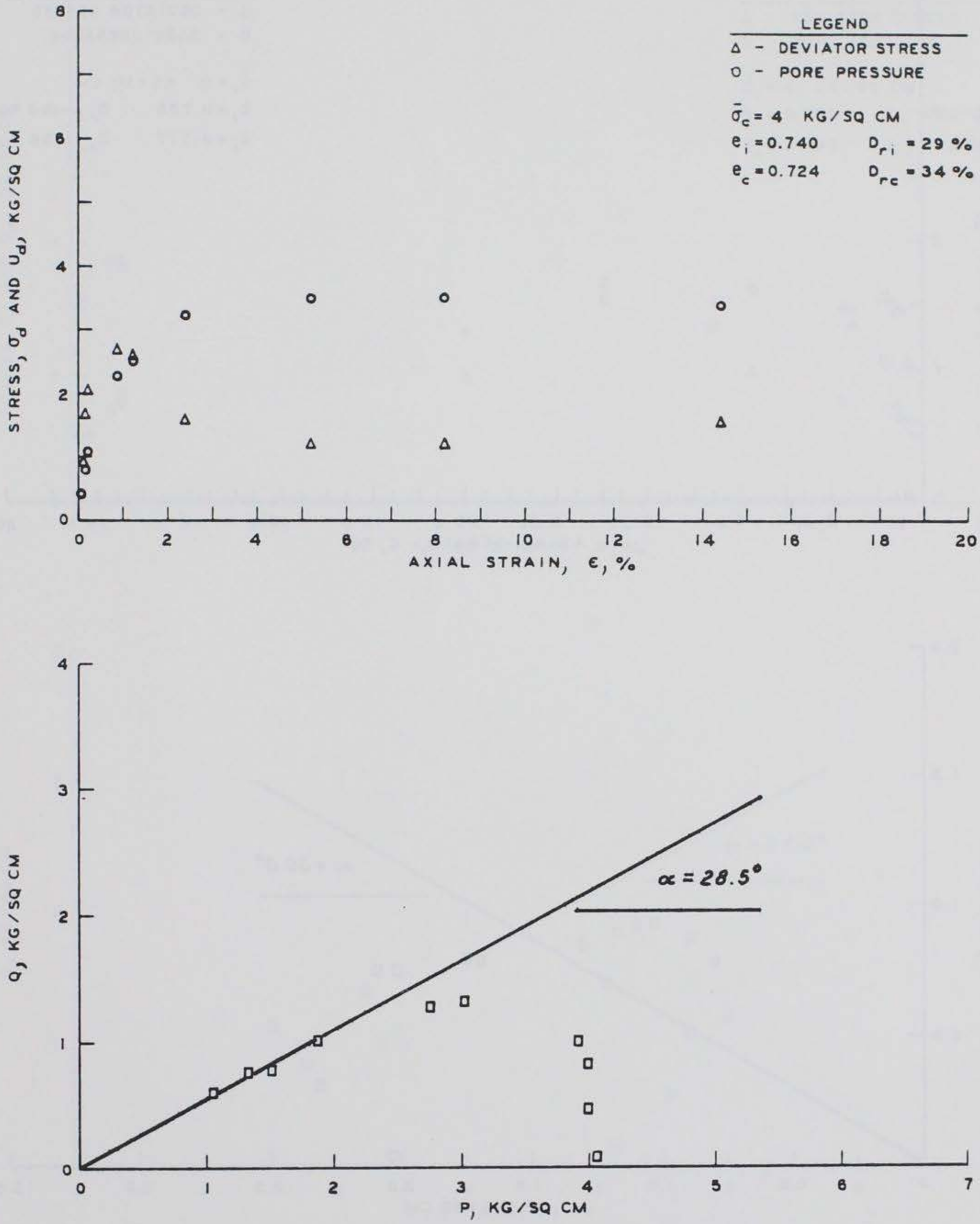

Figure C26. Results of $\bar{R}$ Test D6

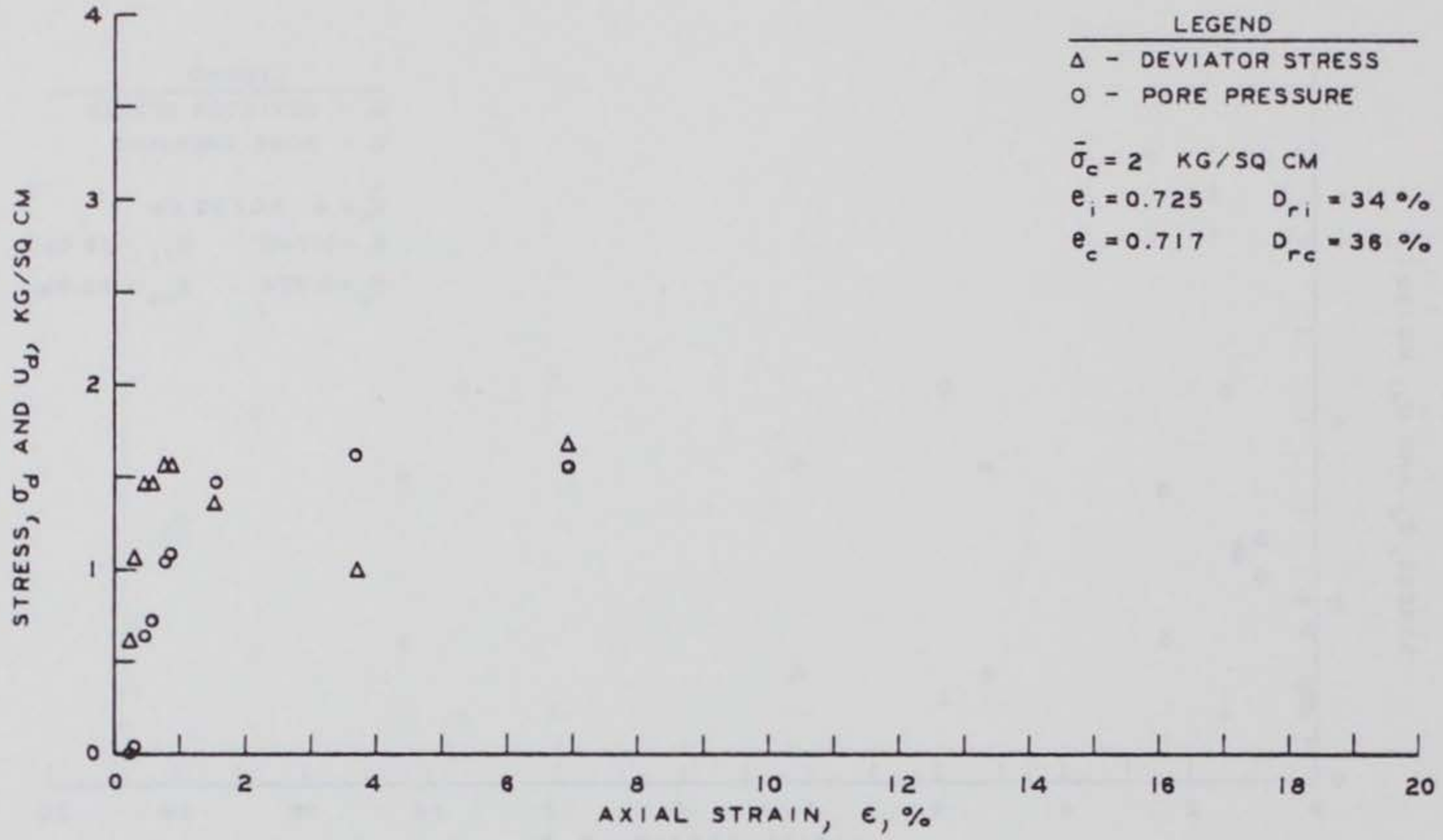

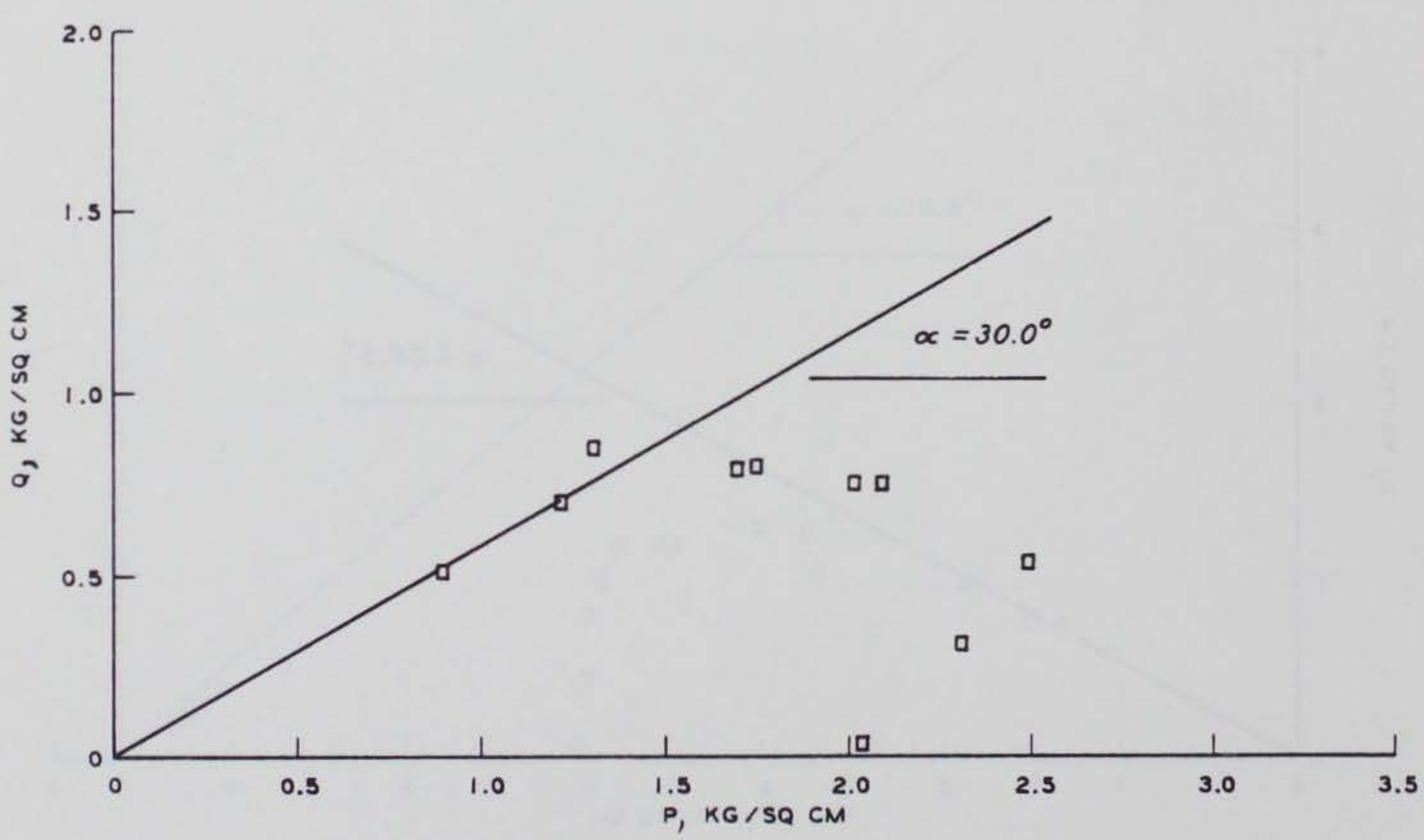

Figure C27. Results of $\bar{R}$ Test H1

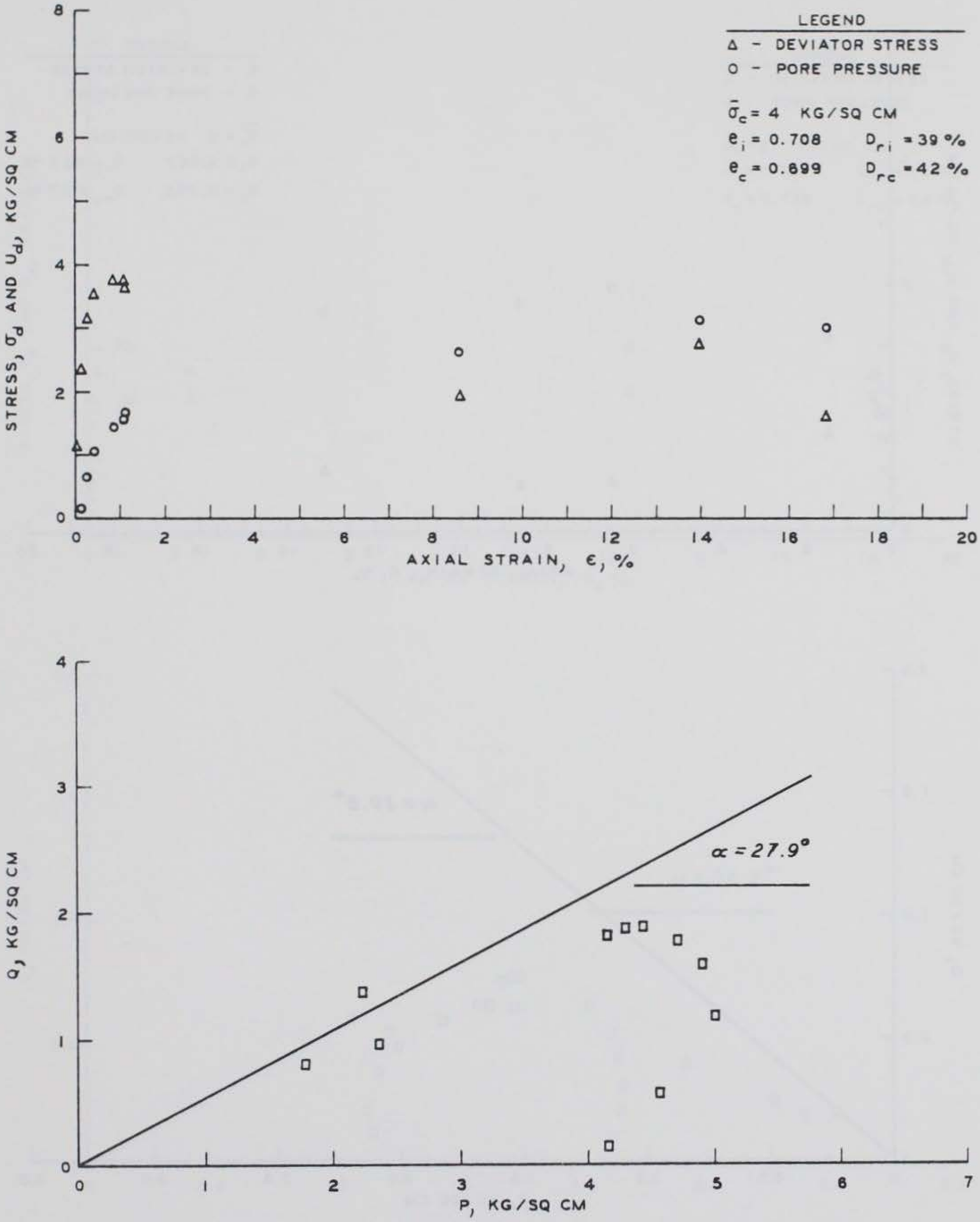

Figure C28. Results of $\bar{R}$ Test H2

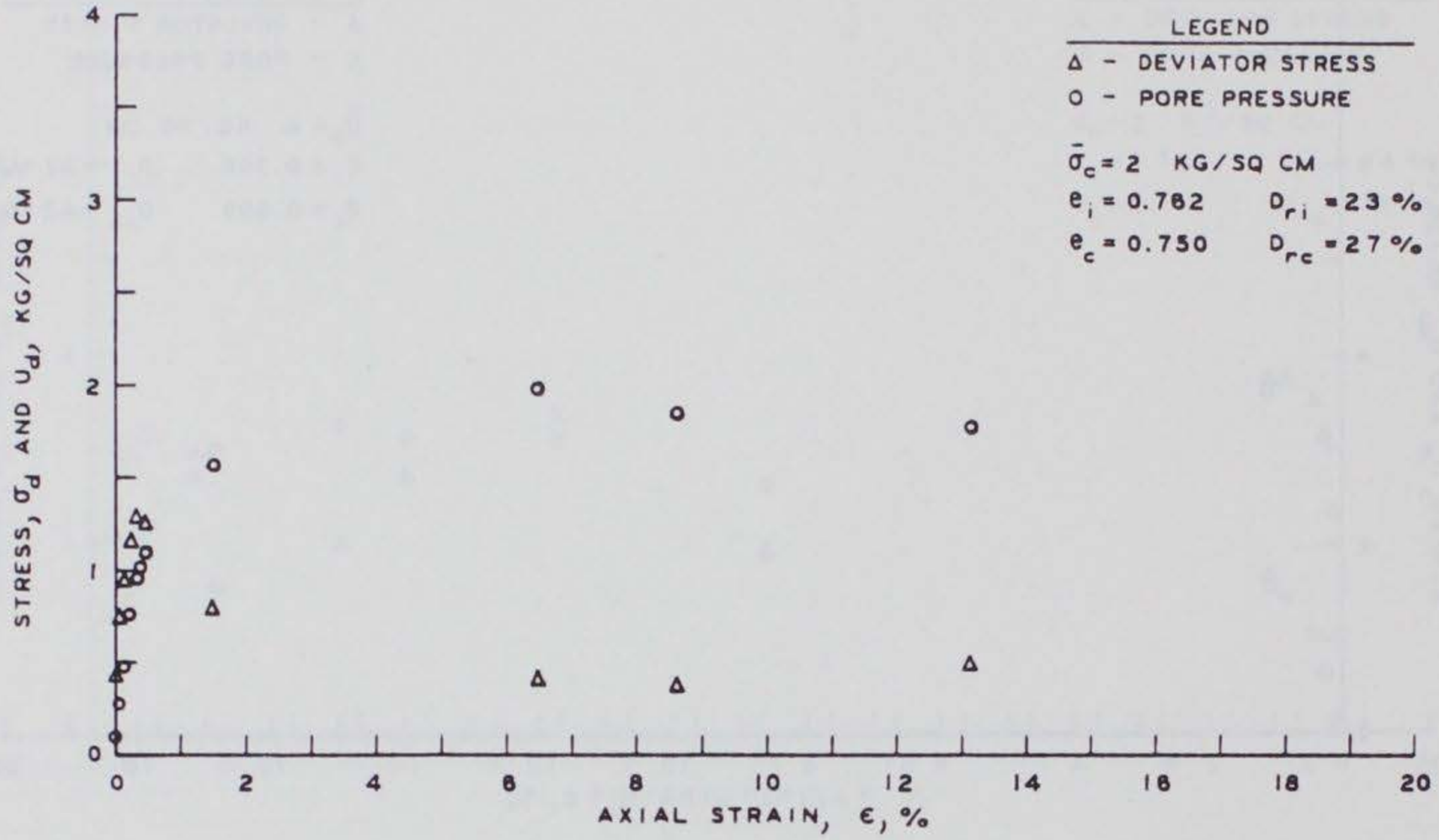

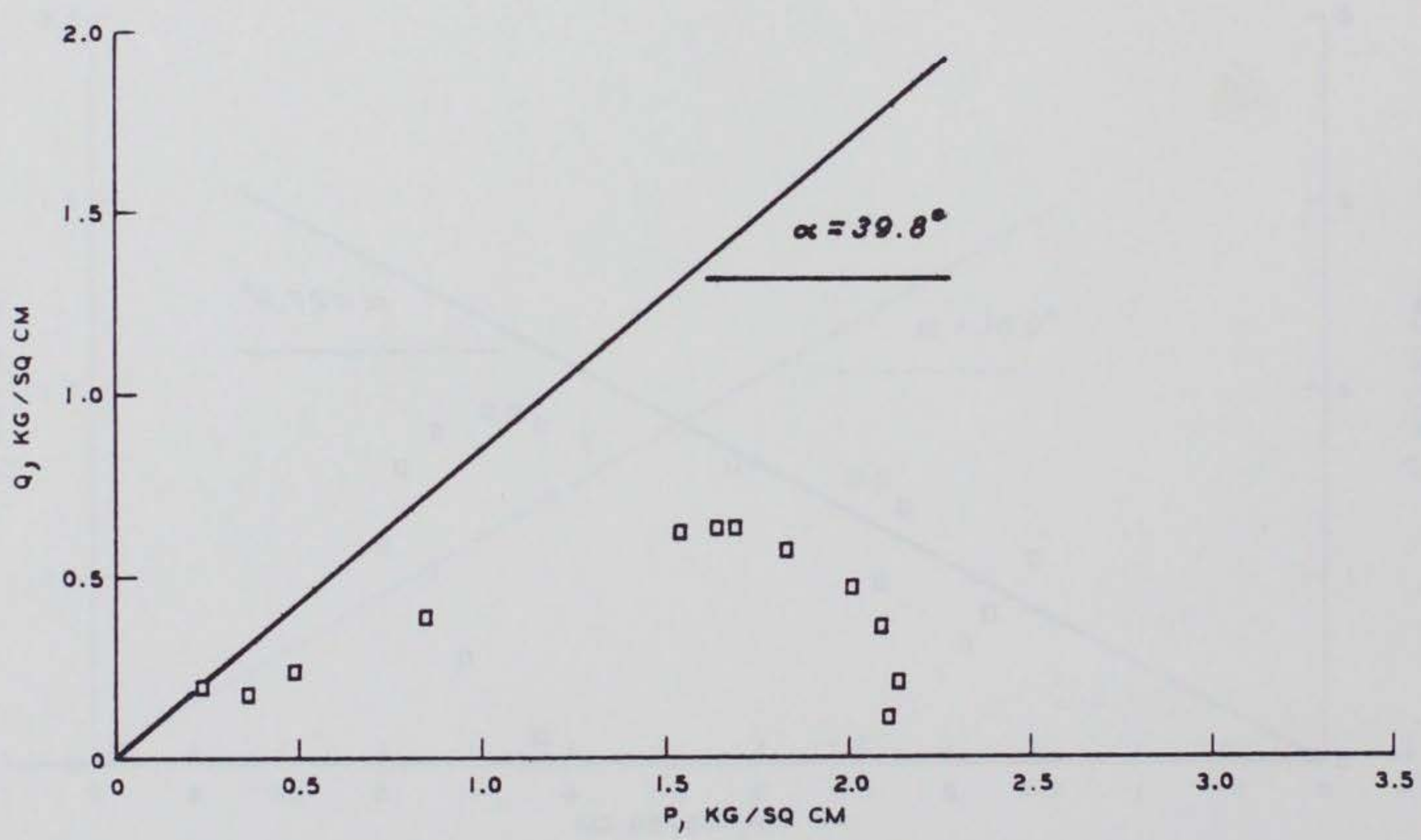

Figure C29. Results of $\bar{R}$ Test I1

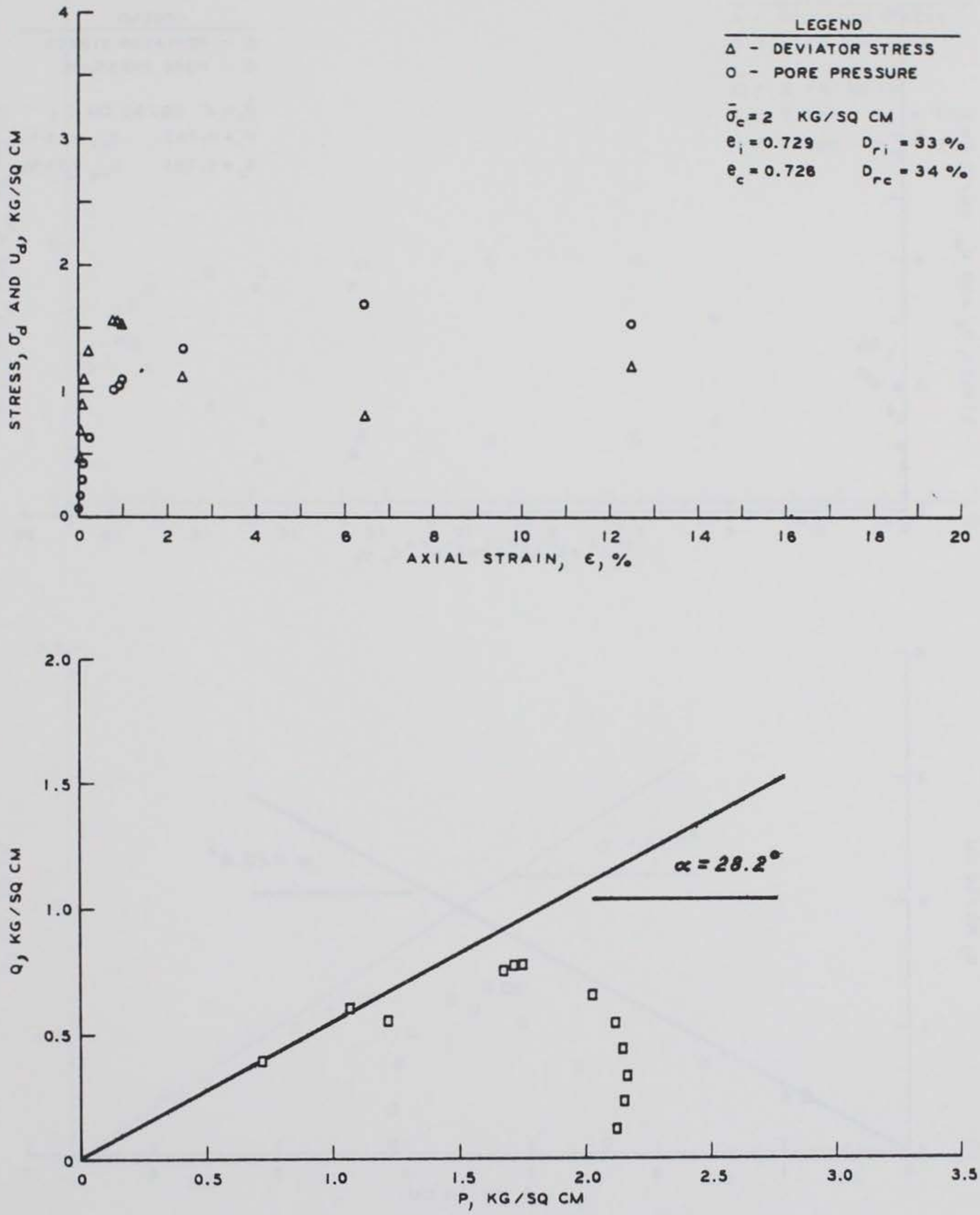

Figure C30. Results of $\bar{R}$ Test I2

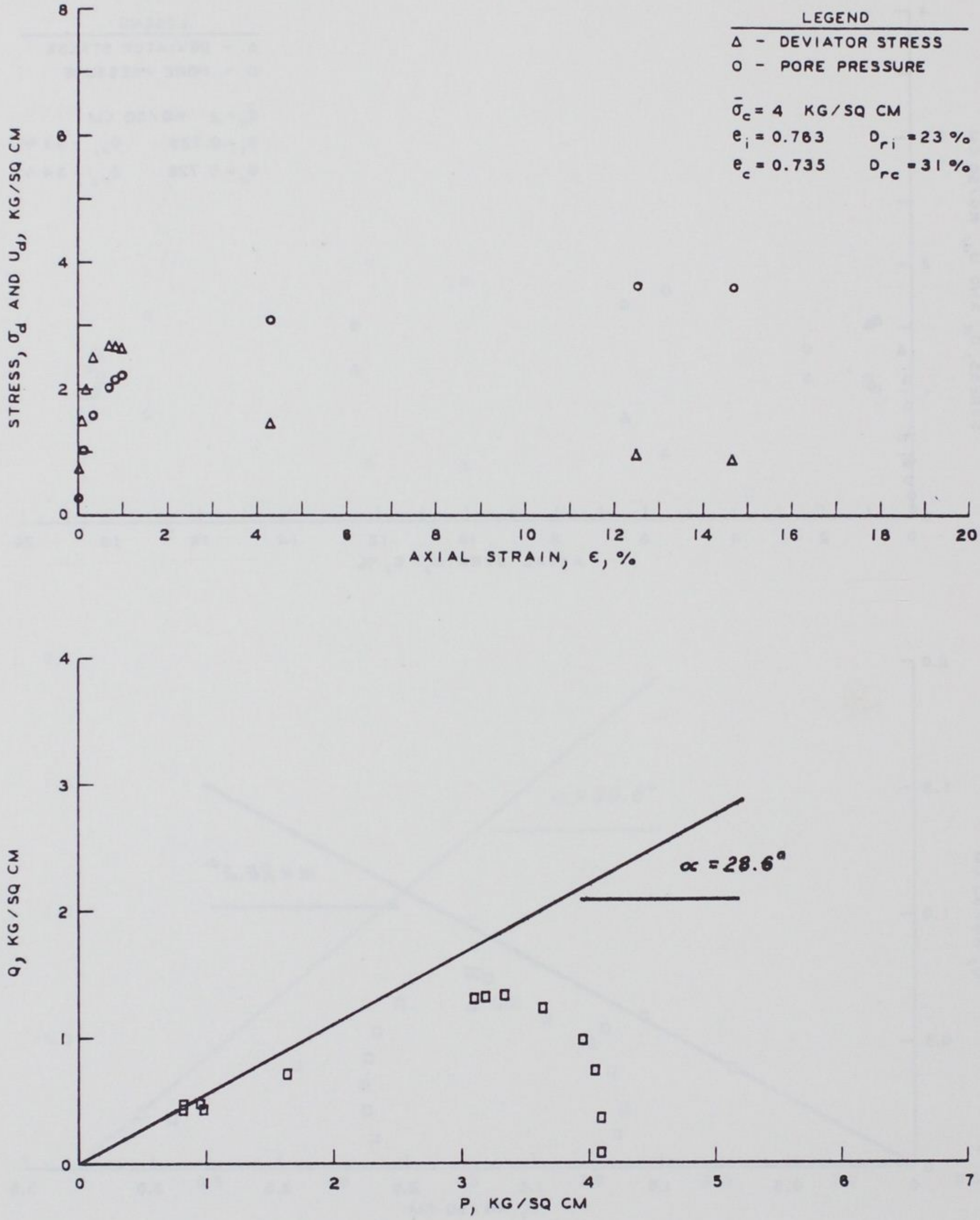

Figure C31. Results of $\bar{R}$ Test I3

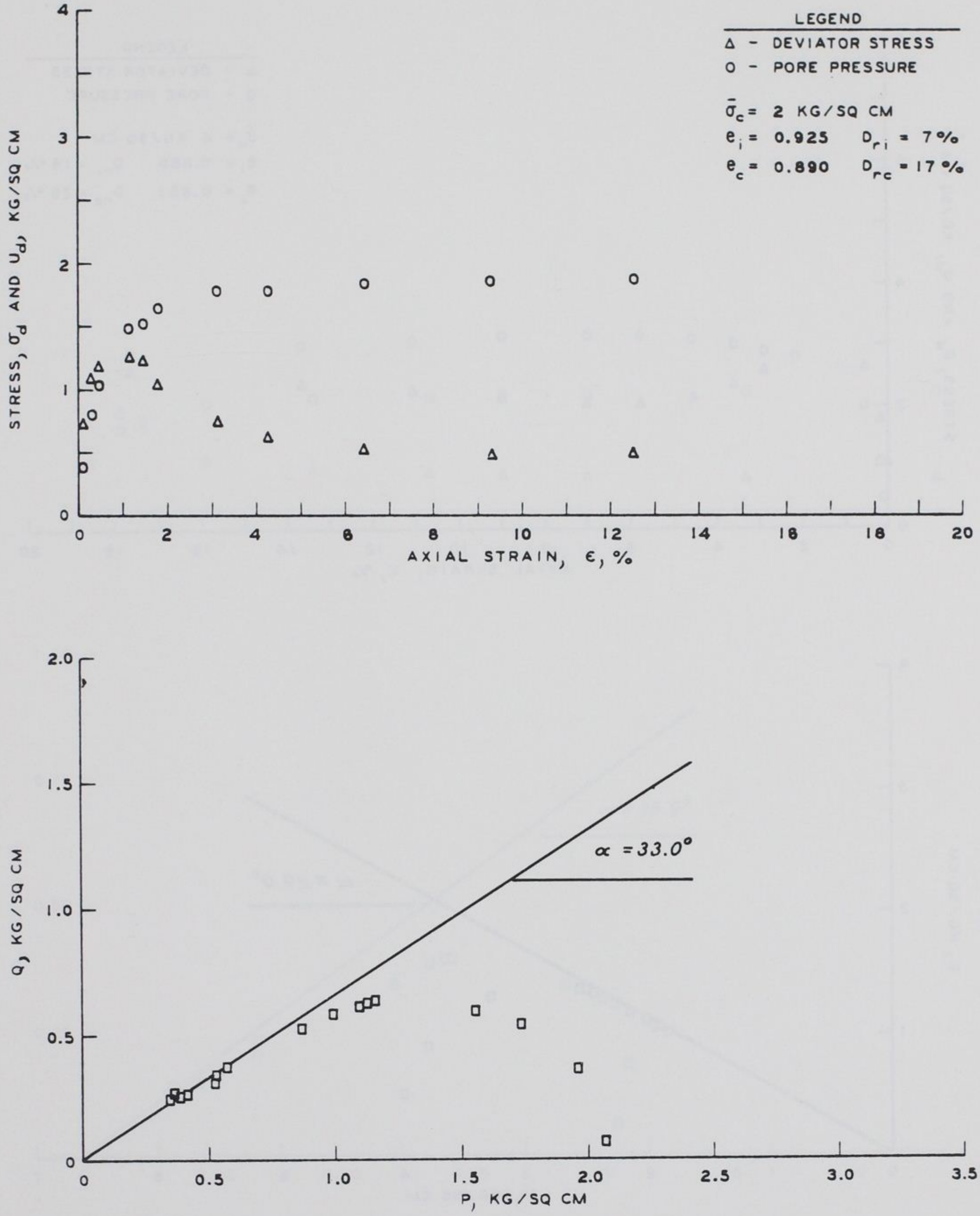

Figure C32. Results of $\bar{R}$ Test MB1

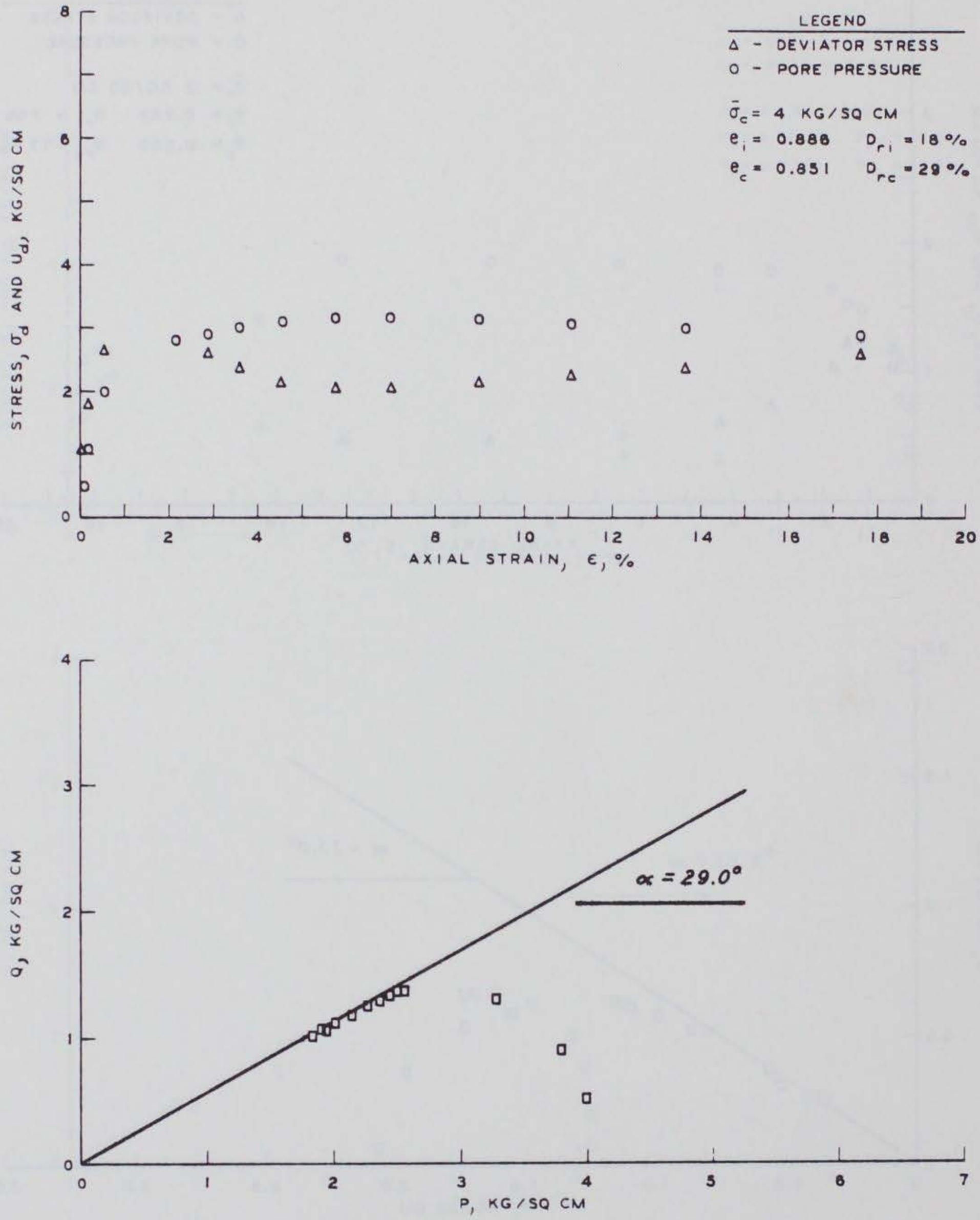

Figure C33. Results of $\bar{R}$ Test MB2

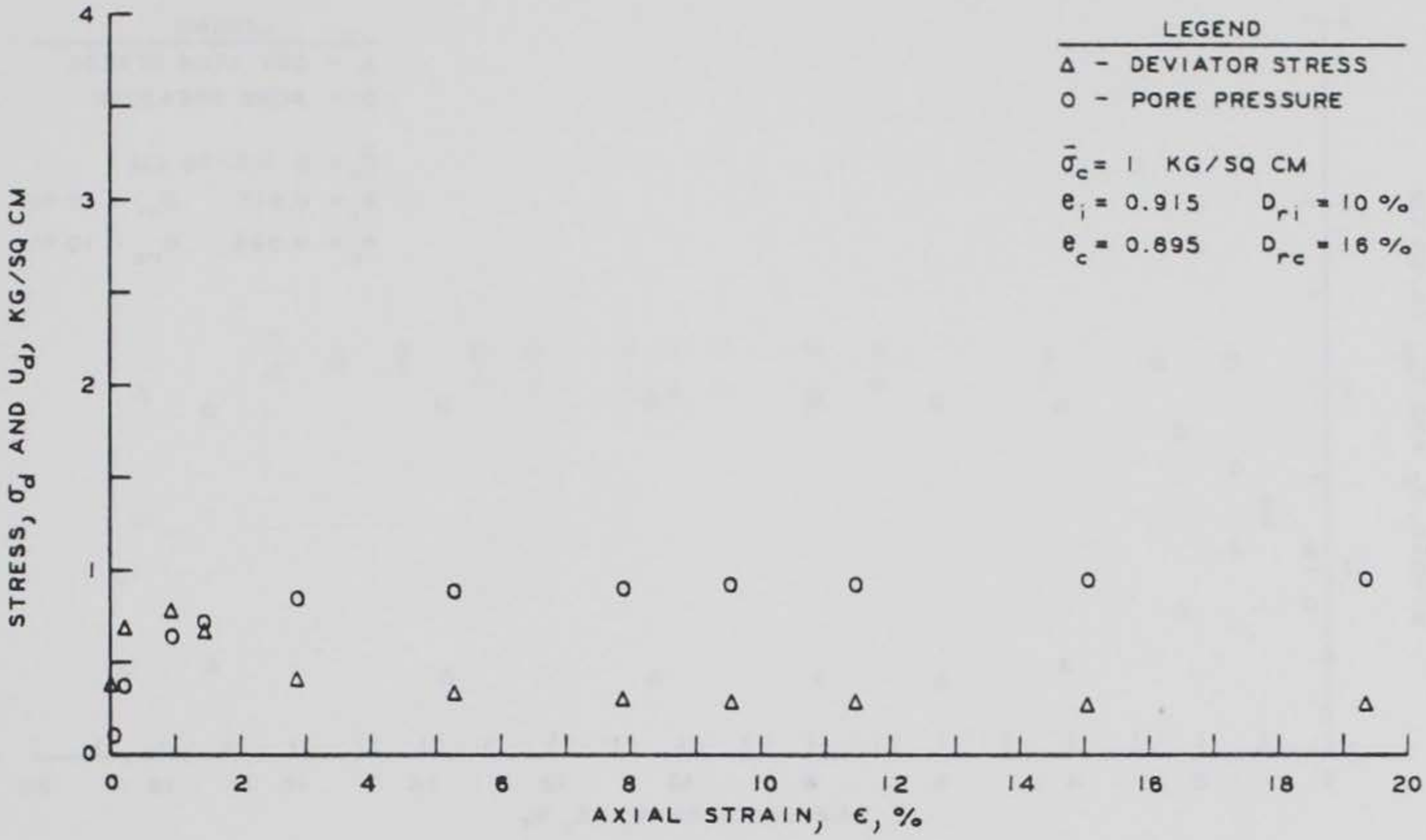

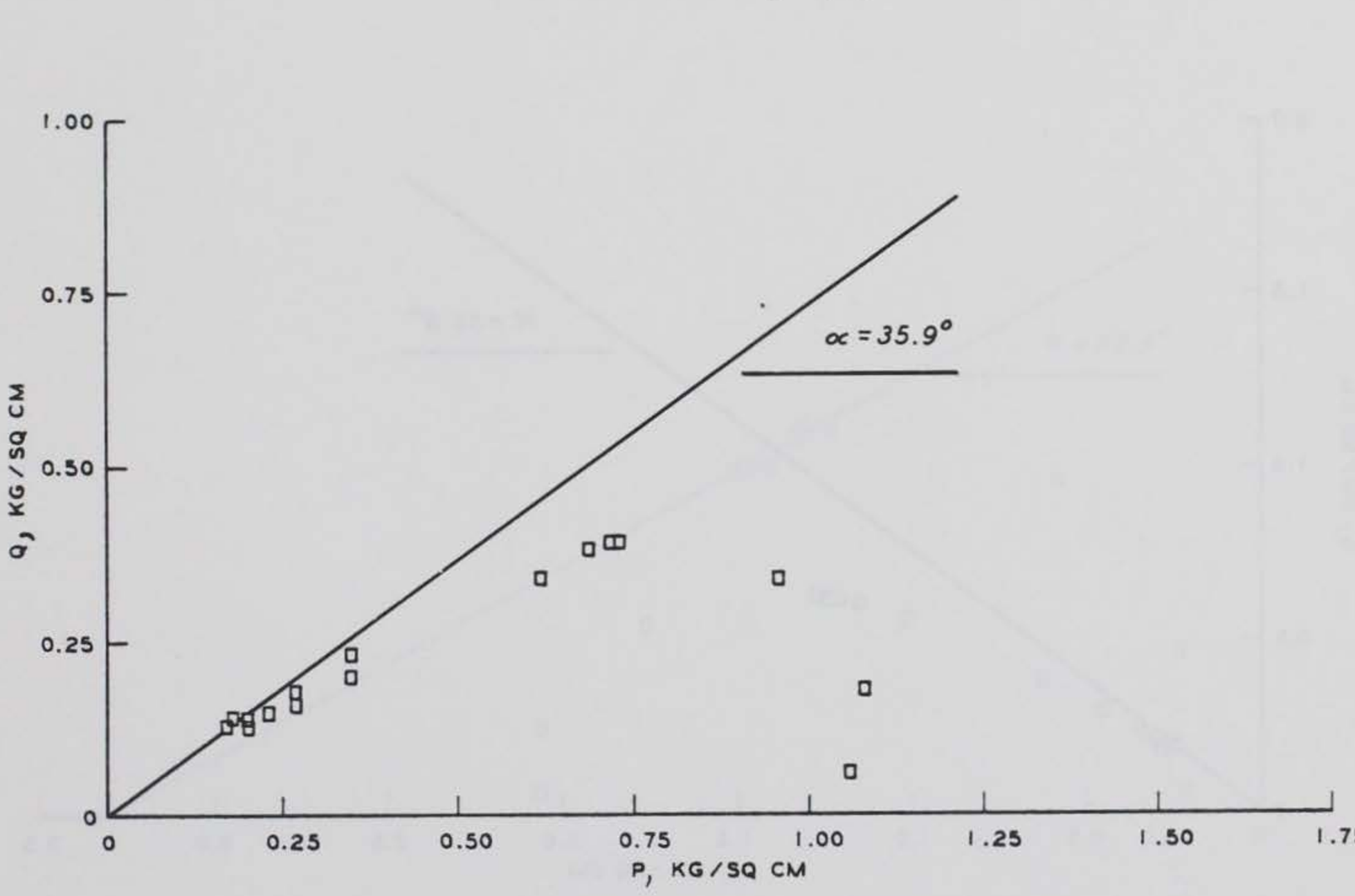

Figure C34. Results of $\bar{R}$ Test MD1

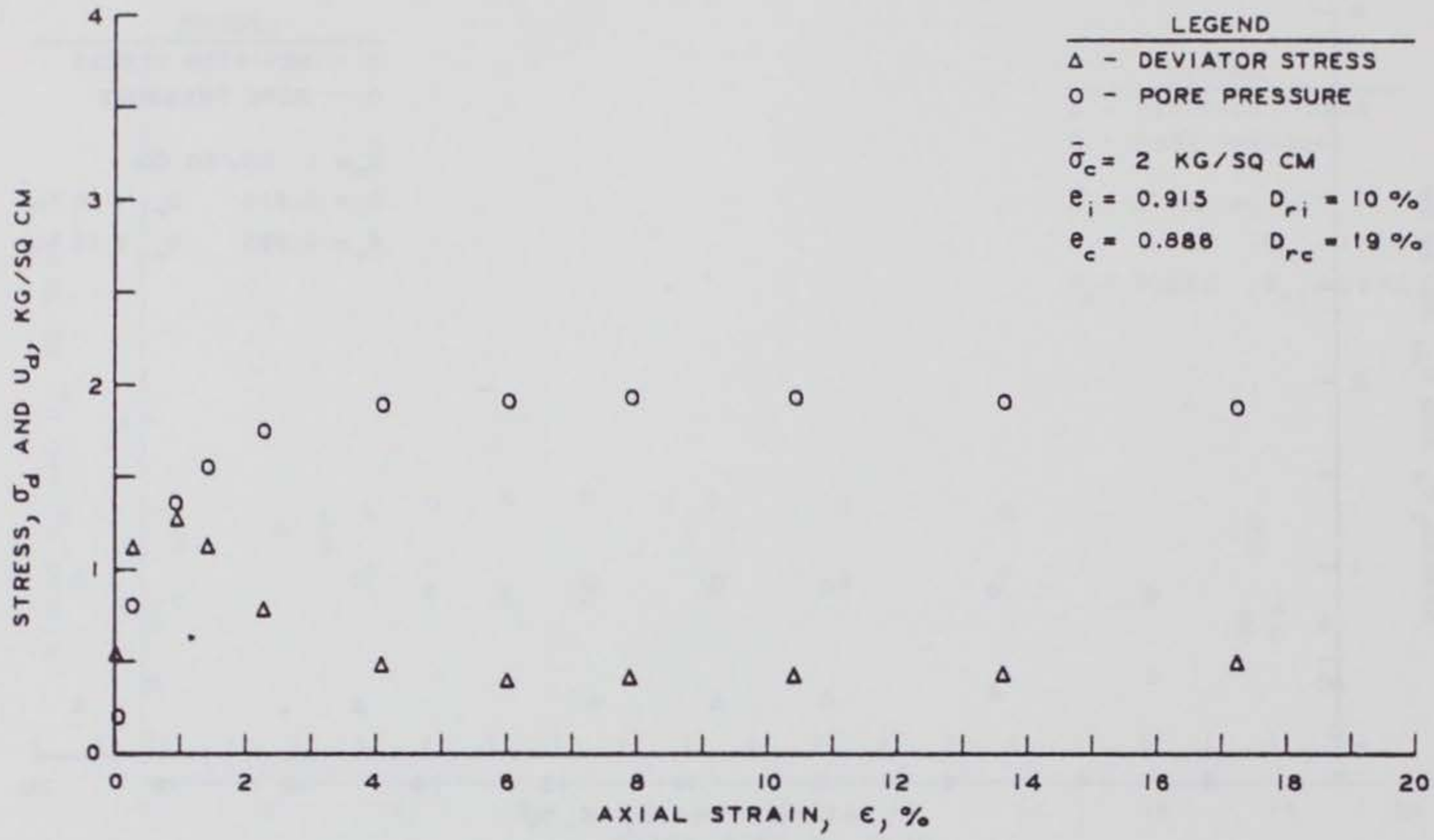

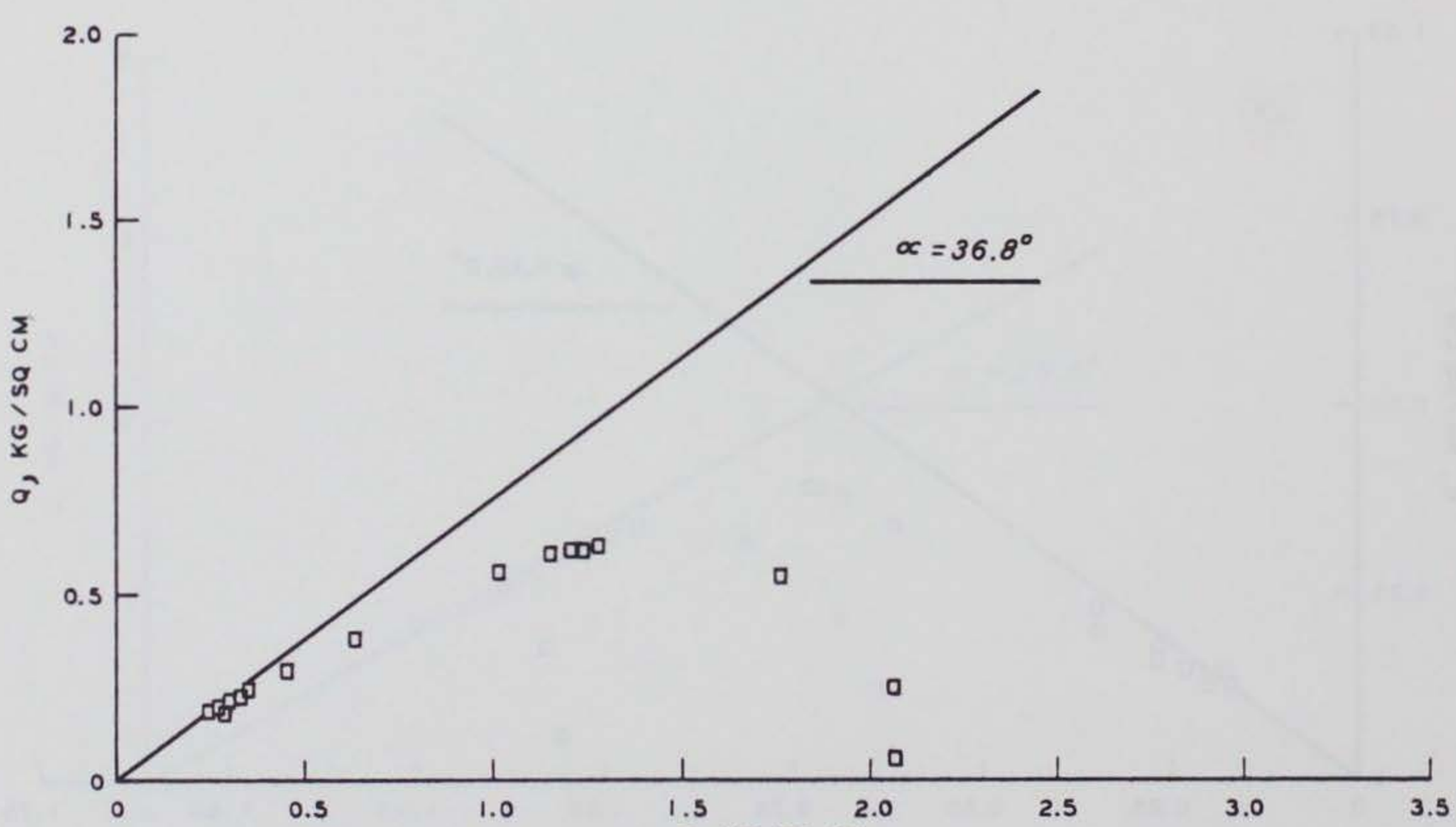

Figure C35. Results of $\bar{R}$ Test MD2

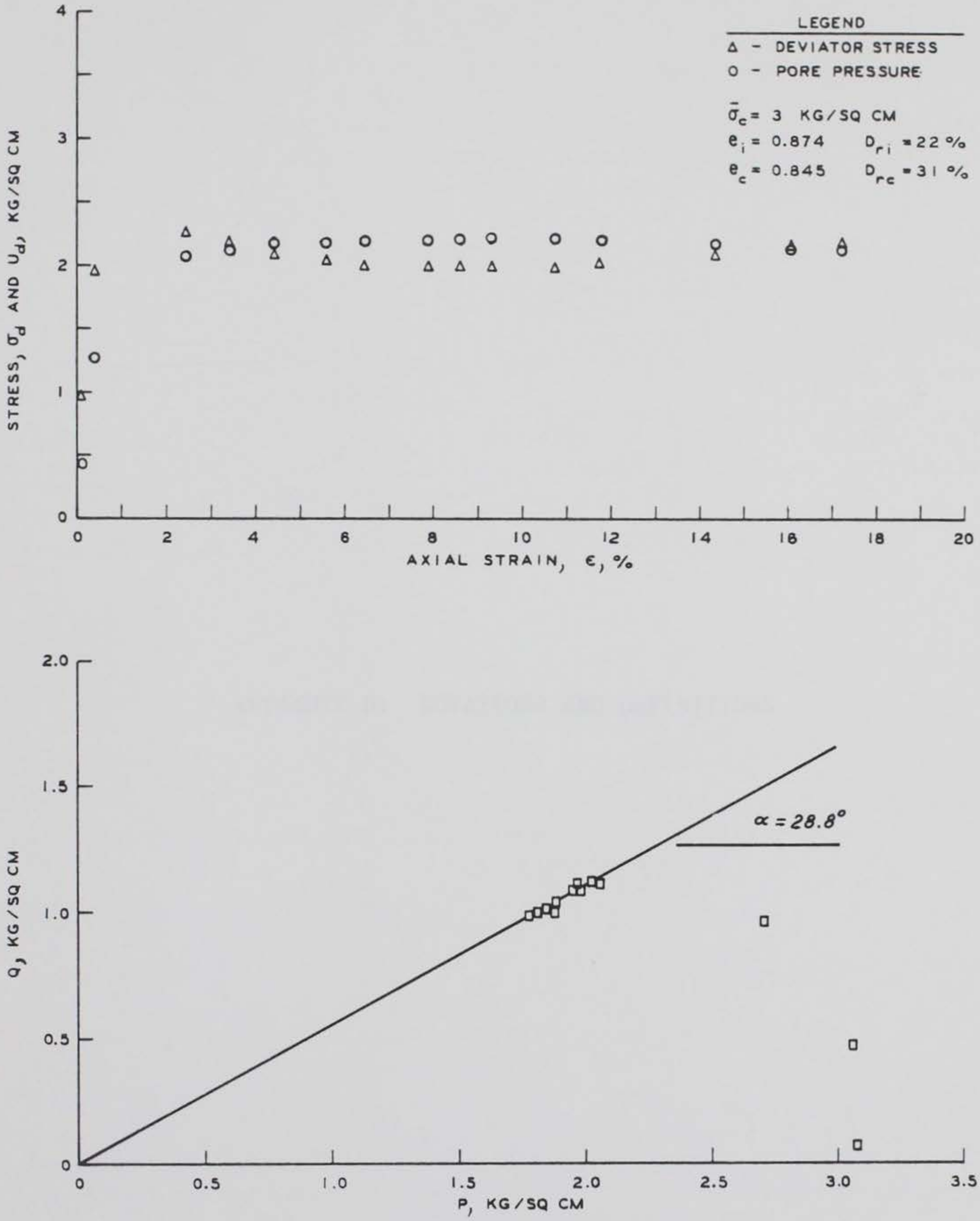

Figure C36. Results of $\bar{R}$ Test MD3

APPENDIX D: NOTATIONS AND DEFINITIONS

B-value — Skempton's pore pressure coefficient defined as the ratio of increase in pore pressure to increase in chamber pressure (i.e., $B = \Delta u/\Delta\sigma_3$)

Contractive — A specimen is said to be contractive if it tends to decrease in volume when subjected to an increase in shear stress. Depending on whether its volume is allowed to change or is kept constant while the deviator stress is increased, the volume will either decrease or the pore pressure will increase

C_c — Coefficient of curvature = $(D_{30})^2/D_{10} \times D_{60}$

C_u — Coefficient of uniformity = D_{60}/D_{10}

Critical void ratio — That void ratio at which a saturated cohesionless soil can undergo deformation or actual flow without volume change. This parameter is a function of the effective stress history of the sand

D_r — Relative density = $[(e_{max} - e)/(e_{max} - e_{min})] \times 100$, percent

D_{rc} — Relative density of a specimen after being consolidated to given effective stresses, percent

D_{ri} — Relative density of a test specimen as reconstituted, percent

D_{10} — Grain size for which 10 percent by weight of the grains is finer, mm

D_{30} — Grain size for which 30 percent by weight of the grains is finer, mm

D_{60} — Grain size for which 60 percent by weight of the grains is finer, mm

Dilative — A test specimen is dilative if it tends to increase in volume when subjected to an increase in shear stress. For a saturated specimen either the volume increases if drainage is allowed to change, or the pore pressure decreases if the volume is not allowed to change

e — Void ratio, the volume of voids (filled with gas and/or water) divided by the volume of solid particles

e_c — Void ratio of specimen after consolidation to a given effective stress

e_i — Initial void ratio of the reconstituted specimen

e_{max} Void ratio of soil in its loosest state as can be determined in the laboratory using a standard test

e_{min} Void ratio of soil in its densest state as can be determined in the laboratory using a standard test

$\bar{e}_f$ curve The critical void ratio curve obtained by plotting e_c versus $\bar{\sigma}_{3f}$, minor effective principal stress

G_s Specific gravity of solids

Liquefaction The act or process of transforming any substance into a liquid. In cohesionless soils, the transformation is from a solid state to a liquefied state as a consequence of increased pore pressure and reduced effective stress (Committee on Soil Dynamics 1978)

Monotonic Loading Loading in steadily increasing or decreasing manner. A step (incremental) or ramp (continuous) function, up or down

$\bar{P}$ Effective stress path parameter, $\bar{P} = (\bar{\sigma}_1 + \bar{\sigma}_3)/2$

P_e Hvorslev equivalent pressure parameter

$\bar{Q}$ Effective stress path parameter, $\bar{Q} = (\bar{\sigma}_1 - \bar{\sigma}_3)/2$

Ram speed The method in which monotonic load is applied, either incremental or continuous

$\bar{R}$ test A triaxial test with pore pressure measurements in which a specimen is first consolidated to a particular effective stress state, and then, without permitting any further change in water content, is loaded to failure

U_d Pore pressure change induced by application of a deviator stress

U_{dmax} Maximum pore pressure change induced by application of deviator stress

α The angle between the line from the origin in Q versus P space to the point that corresponds to the critical state for a cohesionless material and the P axis ; e.g., $\tan \alpha = \sin \phi'$

ε Axial strain, percent

ε_P Axial strain at peak deviator stress

ε_f Axial strain at minimum deviator stress

σ_c Consolidation pressure

$\bar{\sigma}_c$	Effective consolidation pressure = σ_c - back pressure
σ_d	Deviator stress = $\sigma_1 - \sigma_3$
σ_{df}	Minimum deviator stress
σ_{dP}	Peak deviator stress
$\bar{\sigma}_1$	Major effective principal stress (effective axial stress)
$\bar{\sigma}_3$	Minor effective principal stress (effective confining stress)
$\bar{\sigma}_{3f}$	Minor effective principal stress at failure, $\bar{\sigma}_{3f} = \bar{\sigma}_c - U_{dmax}$ as defined by Castro (1969)
$(\bar{\sigma}_1/\bar{\sigma}_3)_{max}$	Maximum effective principal stress ratio
ϕ'	Effective angle of internal friction
K_c	Ratio $\bar{\sigma}_1/\bar{\sigma}_3$ at rest